Development of Numerical Models for Water Resources Management of Dong Nai - Saigon River Basin in Context of Climate Change and Rural Development

チオ, アィン ゴック

https://doi.org/10.15017/1654992

出版情報：九州大学, 2015, 博士（農学）, 論文博士
バージョン：
権利関係：全文ファイル公表済

Development of Numerical Models for Water Resources Management of Dong Nai-Saigon River Basin in Context of Climate Change and Rural Development

TRIEU ANH NGOC

2016

CONTENTS

LIST OF FIGURES

LIST OF TABLES

LIST OF VARIABLES AND ABBREVIATION

MATHERMATICAL VARIABLES

τ_b	Bed shear stress (N/m^2)
τ_{cre}	Critical bed shear stress for erosion (N/m^2).
R	The water release (m$^{3/}$s)
W^{Dead}	Dead water storage at dead water level (m^3)
W^{Max}	Maximum water storage at maximum water level (m^3)
$f_{\text{ob}}(\text{w})$	Objective function
$p(\vec{\text{x}})$	Penalty function
K^z	Penalty weight of equality constraints
$p(\text{w})$	Sub penalty function
W^{Inflow}	The water volume by rainfall runoff (m^3)
W^{Upper}	Upper limit water storage at the upper water level (m^3)
W^{Release}	Water amount in reservoir released to downstream (m^3)
W^{Env}	Water demand for environmental flod requirement (m^3)
R^{Agr}	Water release for agriculture (m$^{3/}$s)
R^{Dom}	Water release for domestic (m$^{3/}$s)
R^{Env}	Water release for environmental flow requirement (m$^{3/}$s)
R^{Ind}	Water release for industry (m$^{3/}$s)
R^{Spil}	Water release via spillway (m$^{3/}$s)
W	Water storage (m^3)
BF_{u}	Base flow (m^3/s)
C_{A0}	Infiltration coefficient (1/h)

C_{A1}	Surface runoff coefficient (1/h)
C_{A2}	Sub-surface runoff coefficient (1/h)
C_{B0}	Infiltration coefficient (1/h)
C_{B1}	Intermediate runoff coefficient (1/h)
C_{C0}	Infiltration coefficient (1/h)
C_{C1}	Sub-base runoff coefficient (1/h)
C_{D1}	Base runoff coefficient (1/h)
CK_1	The time constant for routing interflow (hour)
CK_2	The time constant for routing overland flow (hour)
CK_{BF}	Time constant for routing base-flow (hour)
CQ_{IF}	Time constant for routing interflow (hour)
CQ_{OF}	Overland flow runoff coefficient
D(TL)	The decimal of part of TL
D_{A1}	Height of surface outlet (mm)
D_{A2}	Height of sub-surface outlet (mm)
D_B	Height of intermediate outlet (mm)
D_C	Height of sub-base outlet (mm)
D_{damage}	Damage caused by flooding
DDR	1-month deficit rate
DL	A portion of amount of infiltration (mm)
DYi	Number of 1-month periods in a year
E	Erodibility of the bed (kg/m^2/s)
E_2	Nash-Sutcliffe coefficient
E_{expose}	The condition of being exposed without protection to the effects of harsh weather
E_{pan}	Pan evaporation (mm/day)
E_{piche}	Piche evaporation (mm/day)
ET_p	Potential evaporanspiration
G	Percolation (mm)

GSI	The generalized shortage index
H	Water storage level (mm)
H_{hazard}	something causing unavoidable danger, peril, risk, or difficulty
I	Infiltration through the vertical outlet into the tank (mm/day)
K	Empirical coefficient, K depend on the crop seasons
K_p	Pan evaporation coefficient.
L	Actual possible moisture contents in lower zone storage (mm)
L_{max}	Maximum possible moisture contents in lower zone storage (mm)
MAE	Mean absolute error
MSE	Mean square error
NDC	Number of 1-month in a continuous deficit
P	Rainfall (mm)
P_n	Infiltration (mm)
Q	Discharge (mm/day)
Q_{IF}	Interflow (m^3/s)
Q_{OF}	Overland flow (m^3/s)
R_2	Coefficient of correlation
RE	Relative error
$RMSE$	Root mean square error
R_{risk}	Risk, exposure to the chance of injury or loss
SA	Initial storage of Tank A (mm)
SB	Initial storage of Tank B (mm)
SC	Initial storage of Tank C (mm)
SD	Initial storage of Tank D (mm)
SM	Limit moisture threshold (mm)
SSC	Suspended Sediment Concentration (mg/L)
SSD	Suspended Sediment Discharge (m^3/s)
T_G	Root zone threshold value for groundwater
T_{IF}	Root zone threshold value for interflow

TL	Lag time (hour)
T_{OF}	Root zone threshold value for overland flow
U	Water content in surface storage (mm)
U_{max}	Maximum water content in surface storage (mm)
$V_{vulnerable}$	Capable or susceptible to being wounded or hurt due to a natural phenomenon of certain intensity
α	Erosion coefficient ($m/N^{1/2}$)

ABBREVIATION

BL	Baseline scenarios
BL2050	Baseline scenarios + Climate Change upto 2050s
BL2100	Baseline scenarios + Climate Change upto 2100s
CC	Climate Change
CC2050	Climate Change scenarios upto 2050s
CC2100	Climate Change scenarios upto 2100s
CWL	the Critical Water Level
DP	Dynamic Program
DT	Dautieng Reservoir
DTF	Dam faifure of Dautieng Reservoir
DTM	Dong Thap Muoi area
DTOR	The Dautieng Reservoir operating rule curve
GA	Genetic Algorithem
GA-NAM	The hydrological NAM Model using a genetic algorithm
GA-Tank	The hydrological Tank Model using a genetic algorithm
HCMC	Ho Chi Minh City
HDD	High Development Dam scenarios in the Mekong River Basin
HT	Condition of Infrastructure in 2010 + JICA 2001
ICEM	International Centre for Environmental Management

IPCC	International Panel on Climate Change
JICA	Japan International Cooperation Agency
LDD	Low Development Dam scenarios in the Mekong River Basin
LMD	the Lower Mekong Delta
LP	Linear Program
LWL	the Lower Water Level
MARD	Ministry of Agriculture and Rural Development
MONRE	Ministry of Natural Resources and Environment
MRC	Mekong River Commission
MRD	the Mekong River Delta
RWL	the Retarding Water Level
SIWRR	Southern Institute of Water Resources Research
SLR	Sea Level Rise
SS	Suspended Sediment
T1547	Condition of Infrastructure in 2010+ Project 1547/QĐ-TTg for constructions of low rings
T2	Condition of Infrastructure in 2010+ Sea Dyke Project for constructing the super dyke connecting the Gocong to the Vungtau
TA	Trian Reservoir
TAF	Dam faifure of TriAn Reservoir
UWL	the Upper Water Level
WB	World Bank
Xayaburi	Xayaburi hydropower dam (in construction)
XDD	Xayaburi Hydropower Dam scenarios in the Mekong River Basin

CHAPTER I

INTRODUCTION

1.1. Overview

1.1.1. Introduction to Dong Nai-Saigon Basin

In general, the terrain of the Dong Nai – Saigon River Basin gradually slopes from northeast to southwest with 4.6% average slope of the entire basin. Top of this basin is the Lang Bian Plateau (with an altitude of about 2,000m) and this basin is expanded until it meets the Vamco River (altitude from 1 to 2.5 m). The downstream the Dong Nai River is coastal vicinity, including the estuary from the Gocong to the Vungtau, so the hydrological flow characteristic is mostly influenced by rain, river flooding from upstream of the Dong Nai, Saigon, the Vam Co River and tidal regime from the East Vietnam Sea (see **Figure 1-1**).

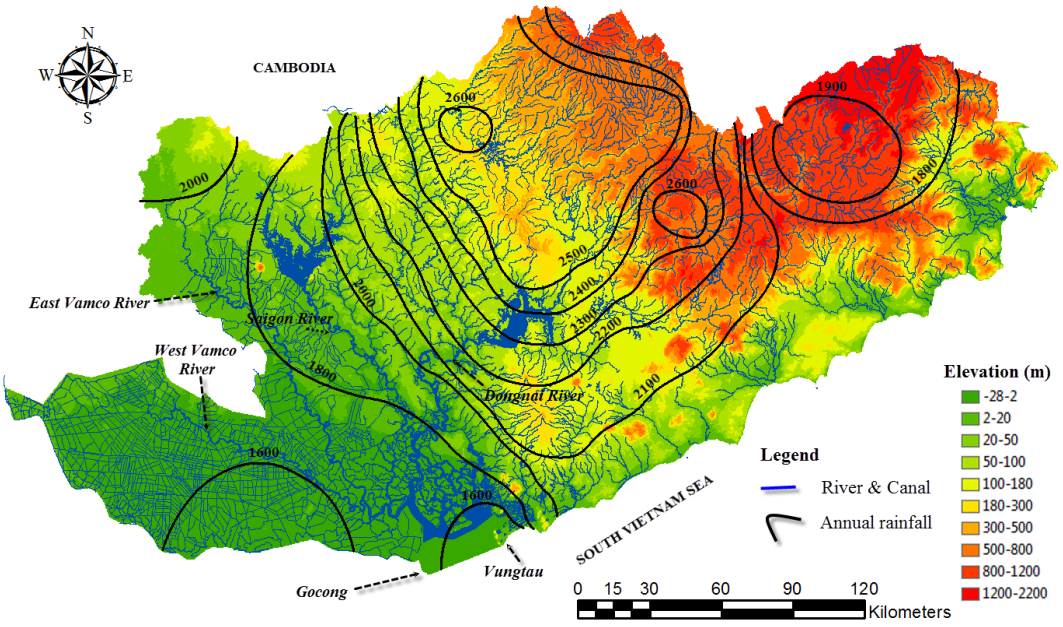

Figure 1-1: Location of the study area and upstream hydraulic construction

The climate of the study area is driven by the tropical monsoon climate. There are two seasons in a year, the rainy season is from June to November and the dry season is from December to May. In the dry season, the northeast wind dominates, while the main wind direction is southwest in the rainy season. In early dry season from December to January, the winds mainly blow from north, after that period it changes from southeast. However, in rainy season, winds only blow from west - southwest. In the study area, the average temperature is 27°C, the highest temperature of 40°C, and the lowest temperature of 13.8°C. Besides, the oscillation of the air temperature is quite large in a day; it can be over 6 - 7°C.

About 85% of the annual rainfall is within the rainy season. The average annual rainfall is about 2,100mm/year, but the spatial variation within the basin is quite large, ranging from about 700mm/year of rain per year (Phanrang and Phanri) through 1,500 – 2,000mm/year in the downstream of the Dong Nai–Saigon River to the wettest upstream areas where the annual rainfall is between 2,500 and 3,000mm/year. The humidity is high, about 90%, especially in the areas directly facing the monsoon. The humidity difference is also influenced by seasonal monsoon and the characteristics of the terrain. Direct evaporation in the basin is from 600 to 1,350mm/year depending on location.

The river systems in the study area include a part of the Mekong River Basin (Dong Thap Muoi area, so-called the “Plain of Reeds”), the Vamco River System, the Saigon River, and the Dong Nai River.

The Mekong River flowing into Vietnam is divided into two distributaries, the Tien River and the Hau River. These two rivers germinate into a dense river network on the low plain of southern Vietnam. While the Hau River flows straight to the East Vietnam Sea through two estuaries, the Tien River’s flow is oscillatory and tortuous through Vietnam’s geology. The Tien River finally empties into the East Vietnam Sea through six estuaries.

The West Vamco River originates from Cambodia, flowing through Longan Province, while the East Vamco River rises also from Cambodia, but

flows through Tayninh Province. These two rivers flow together into the Vamco River in Tantru, and then it flows into the East Vietnam Sea through Soairap Estuary. Both rivers have characteristics as the tidal river and very small slope, so the tidal current can penetrate very deep inland, over 190 km in the East Vamco River and 170 km in the West Vamco River from Tantru, which is about 240 km and 220 km from the sea.

The Saigon River is composed of two main branches, the Saigon River and the Sanhdoi River. The Saigon River also has the characteristics of the tidal river. Due to the small slope of the river in the total length of 280 km, the tide can affect until the downstream of the Dautieng reservoir far 206 km from the sea. The Saigon River flows across the Ho Chi Minh City (HCMC, hereafter) located about 15 km from the river mouth and then dumps into the Nhabe River. Because of flat low-lying terrain with average elevation of 0-15m, this area is severely influenced by tide.

The Dong Nai River starts from the Trian hydropower reservoir to the Soairap Estuary, with a length of about 150 km. The mainstream of the Dong Nai River is large width; depth and small slope, therefore tide regime also strongly influences on flow hydrograph of the Dong Nai River. The Be River is a major tributary in the right bank of the Dong Nai River. The Be River flows into the Dong Nai mainstream at the downstream of Trian Dam.

1.1.2. The cascade of reservoirs in upstream of Dong Nai-Saigon Basin

In past decades, a number of hydraulic constructions have been built in the Dong Nai – Saigon River System, such as Trian hydropower reservoir, the Dautieng Reservoir, the Thacmo Reservoir, Phuochoa Reservoir, and the Hamthuan Reservoir (**Figure 1-2**). Those constructions significantly regulate the flows from the upstream, taking in water during flood season and releasing during dry season. However, this regulator flows through cascades of reservoir are quite small if compared with tidal flow caused by high tide. Consequently,

hydrodynamic river in the downstream of the Dong Nai – Saigon River are primarily depended on tidal flow.

Currently, there are many plans to construct a number of reservoirs in the upstream of the Dong Nai – Saigon River Basin. This may lead the downstream of the Dong Nai – Saigon River Basin to serious inundation and salt intrusion by impact of tide. The following is the detail descriptions of the existing, constructing and planed reservoirs in each sub-basin: the Dong Nai Basin, Be Basin, La Nga Basin, Saigon Basin, and East Vamco Basin.

The Dong Nai Basin has total area of around 28,200 km^2, if last point is at the Trian Reservoir, this basin is so-called Trian Watershed with total area of 14,800 km^2. The cascade system of hydropower construction with total capacity of electreic generator about 2,010MW, is arranged in descending order from upstream to downstream (**Figure 1-3**), including:

- Danhim Hydropower Dam (existing);
- Daininh Hydropower Dam (existing);
- Dongnai 1 Hydropower Dam (planning);
- Dongnai 2 Hydropower Dam (planning);
- Dongnai 3 Hydropower Dam (in construction);
- Dongnai 4 Hydropower Dam (in construction);
- Dongnai 5 Hydropower Dam (in construction);
- Dongnai 6 and 6A Hydropower Dam (in planning)
- Trian Hydropower Dam (existing);

The Be Basin has total area of 5,193 km^2, located upstream and among the Dong Nai Basin and the Saigon Basin, with downstream boundary at the Phuochoa Reservoir. In the Be Basin, four reservoirs had constructed in cascade, with total capacity of electric generator is about 270MW, in descending order (**Figure 1-2** and **1-3**):

- Thacmo Hydropower Dam (existing);
- Candon Hydropower Dam (existing);

- Srockphumieng Hydropower Dam (existing);
- Phuochoa Irrigation Dam (existing).

As a sub basin of Dongnai River Basin, the Langa River Basin has total erea about of 4,093 km^2. The upper stream of Langa river originates from a high hill (El. 700 to 1,000m) in Lam Dong province. Initially, it takes the NorthWestward direction for its flow course. After joining Dariam River coming from the East, the Langa River flows westwardly with lots of meanderings. The downstream of Langa River merges into Dong Nai river (the third largest river in VietNam) at TriAn reservoir.

Total area of the Saigon Basin is around 5,934 km^2, if end point of downstream boundary is put at Dautieng Reservoir, this basin is so-called Dautieng Watershed, has total of 2,700km^2. This basin has only the Dautieng Reservoir served for mainly agriculture. This is an important water regulatrion construction for not only this basin but also the downstream area – HCMC. This matter will mention later in next part.

The East Vamco Basin has total area of 6,156 km^2, with river length about 283 km. This basin is a part of Vamco Basin (including East Vamco and West Vamco) and significantly influenced by tidal regime. Although East Vamco and West Vamco enter into Vamco at downstream, they has quite different characteristics about hydrodynamic. The West Vamco tributary lies in flat low-lying, belonged to Mekong delta and strongly inundated by tide and flooding, whereas East Vamco tributary located on the southeastern region is in the Dong Nai-Saigon Basin. It has no hydraulic construction along this river. Flow regime in East Vamco tributary is partly influenced from regulation operation of the Dautieng Reservoir.

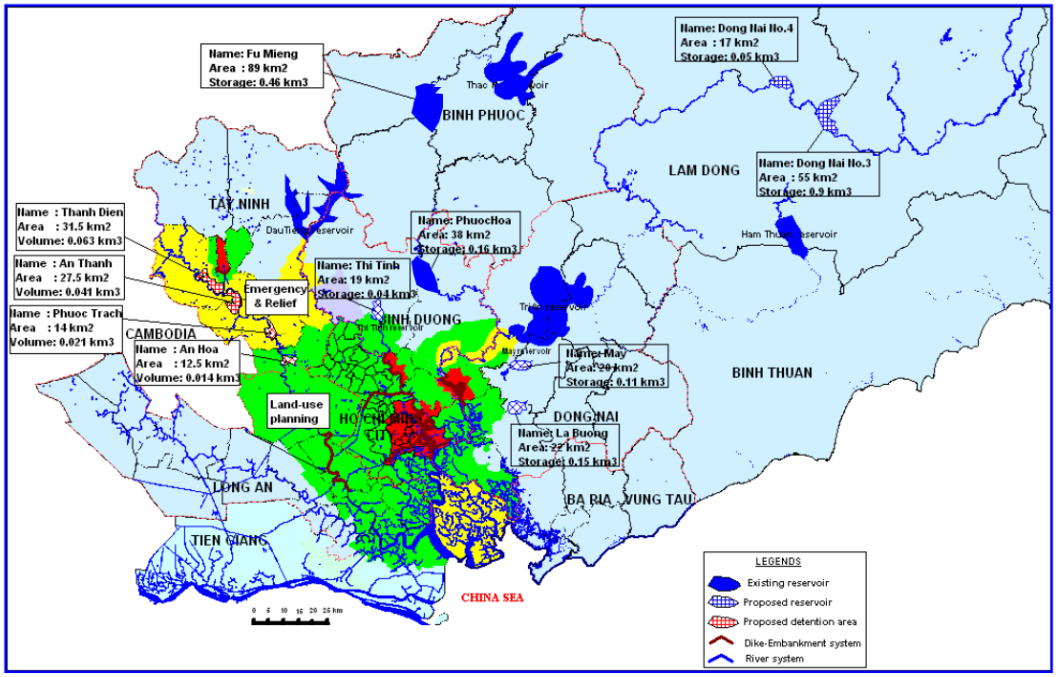

Figure 1-2: Existing and planing dams in study area

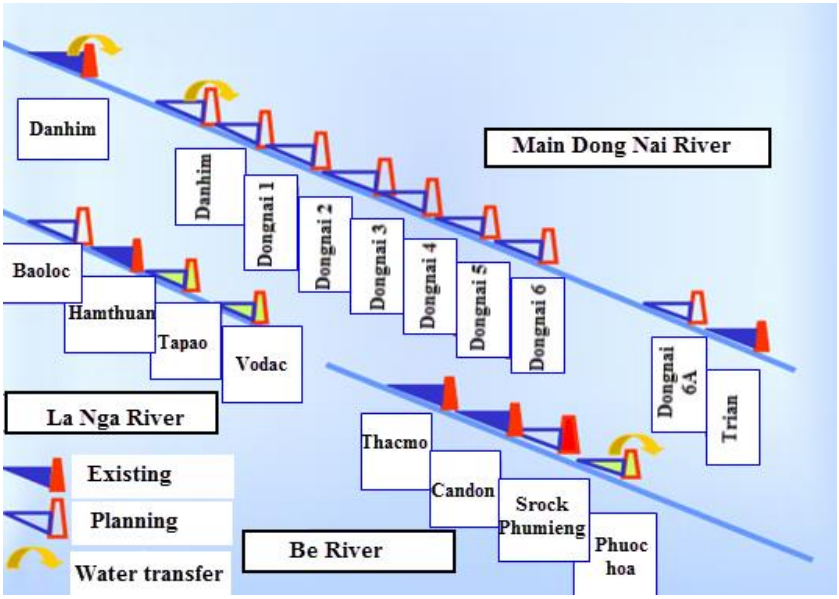

Figure 1-3: Flowchart of existing and planing cascades of reservoir

1.1.3. Introduction to Dautieng Reservoir

One of the biggest irrigation construction systems in south of Vietnam, the Dautieng reservoir, was constructed in 1980 and completed in 1983 by the support under credit fund of World Bank (WB). It is in Tay Ninh Province,

approximately 90km from HCMC, in southeastern Vietnam (**Figure 1-4**). Dautieng River Watershed has the shape as a leaf with the river density of 0.39km/km^2. The effective water conversation of Dautieng reservoir is 1.57×10^9 m^3 with water surface area of 270km^2. The design of Dautieng reservoir goals: (1) water supply for agriculture, industry, and human activities, (2) flood control in wet season, (3) pushing saltwater intrusion in downstream reach, and (4) improving water quality in downstream area of HCMC.

During 20 years operation and management, the Dautieng Reservoir has greatly contributed to social economic fields including environmental quality in downstream watershed:

- A total direct irrigation area of about 640km^2 for four provinces: Tay Ninh, Binh Duong, Long An and HCMC.
- A total area of 410km^2 of source creation for riverside lands along the Saigon and the East Vamco Rivers.
- Water supply for domestic and industrial demands.
- Decreasing salinity in downstream reachs below 4‰ and improving the water quality in downstream area of HCMC.

For past decades, water shortages have been seriously getting worse due to the influence of the impacts of climate change and global warming. Therefore, predicting rainfall-runoff process and operating optimal multi-use reservoirs for sustainable development become essential in order to increase water storage of reservoir as well as maintain its safety for flood control.

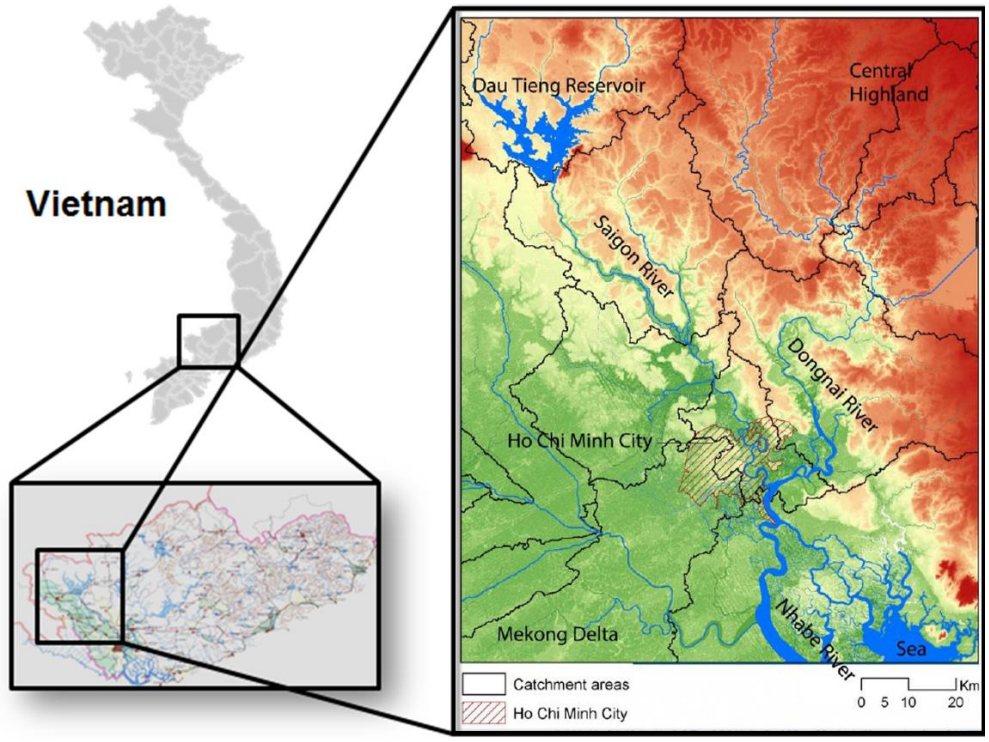

Figure 1-4: Location of Saigon Basin and Dautieng reservoir

1.2. Climate change and Global warming

An emerging challenge facing the world is global warming, and thus climate change (CC). The evidence for global warming is compelling, with records showing that the global-average surface air temperature has risen by around 0.6^{o}C since the beginning of the twentieth century (**Figure 1-5**), with about 0.4^{o}C of this warming occurring since the 1970s. 1998 was the warmest year on record, and 11 of the 12 years from 1995 to 2006 rank among the 12 warmest years (IPCC, 2007).

According to the Intergovernmental Panel on Climate Change (IPCC, 2007), the coastal countries of Southeast Asia are highly vulnerable to climate change. Of these, Vietnam has been ranked first in terms of population among ten countries and territories that could be impacted by sea level rise (SLR). In the past 50 years, the sea level has risen by 20cm at Hondau station in Hai Phong province. The data between 1979 and 2006 of Vung Tau gauge station pointed

out that the avarage sea level at this station has risen by 13 cm (**Figure 1-6**). Global climate change and SLR could alter the hydrodynamic characteristics of low-lying coastal areas such as the the Mekong River Delta (MRD). Hence, the morphological evolution of the Mekong River Estuaries is related to urgent challenges of sustainable development and protection of human society.

Additionally, the results of global climate change scenarios studies show that the global average annual precipitation will increase despite various changes from region to region (referenve). One of these regions, rainfall intensity will rise in tropical and high latitude localities that experience in overall increases in precipitation.

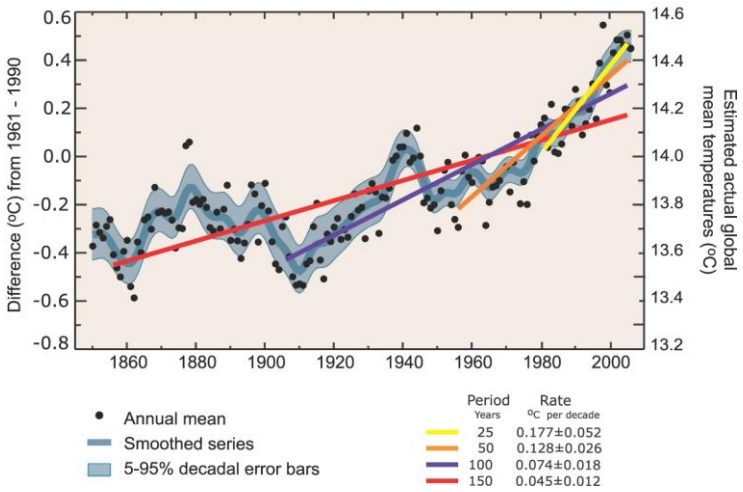

Figure 1-5: Global average temperature changes (IPCC/2007)

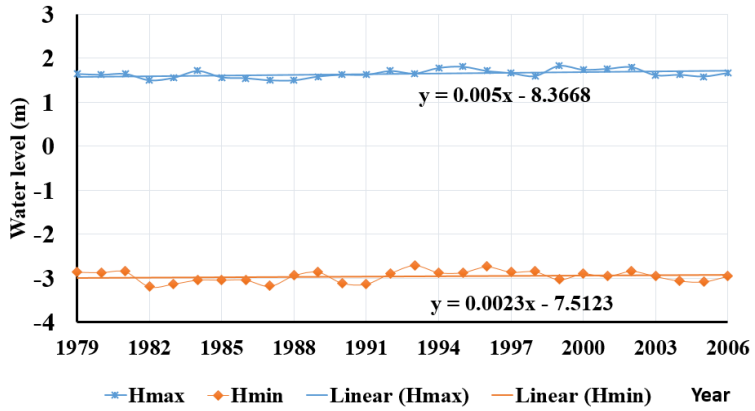

Figure 1-6: Water level changes in 1979-2006 at Vungtau station

Particularly, the relevance to flooding, the expectation is that precipitation will be more variable and with greater extremes. Taking the Dong Nai-Saigon River Basin as an example of southern Vietnam, the climate will become warmer. The average annual temperature is expected to rise between 2.5ºC to 3.7ºC by 2100s (**Figure 1-7**). Temperature rise will lead to changes in precipitation patterns, although, little change is predicted in the annual amount of precipitation. Most of the Dong Nai-Saigon River Basin is expected to be drier in the summer, with the greatest decreases in rainfall (up to 39%) in the south-east. Heavy rainfall will become more frequent, with intensities that are currently experienced around once every two years becoming between 5% and 20% heavier by the 2100s (**Figure 1-8**, **Figure 1-9**). Storm events in the summer will become more intense and more frequent.

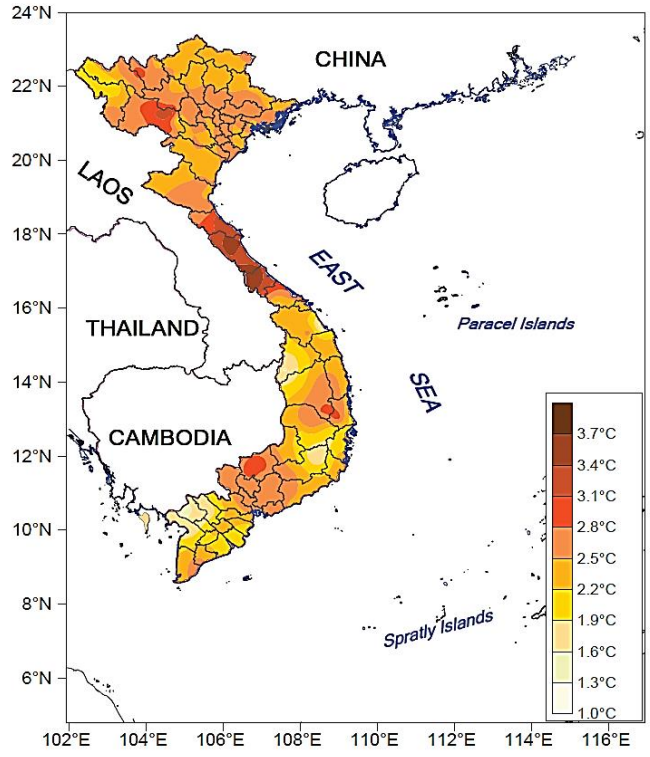

Figure 1-7: Estimation of average tempurature rised up to 2100

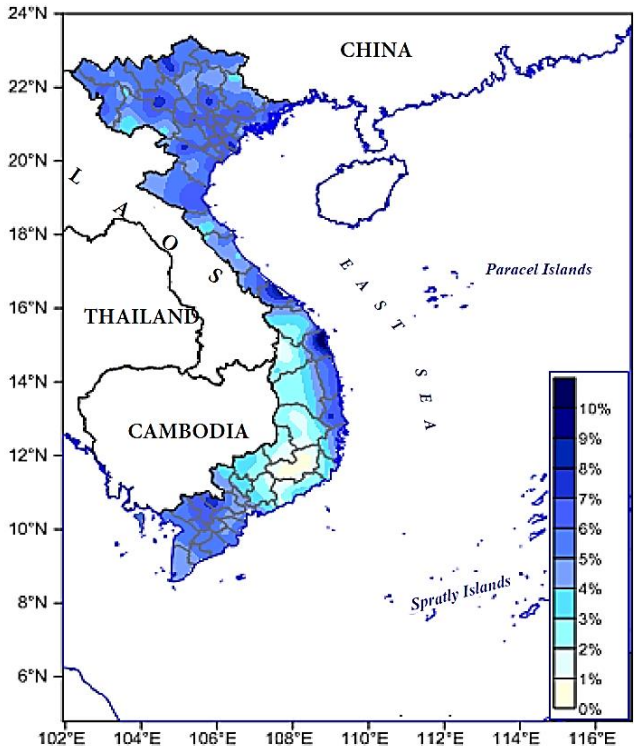

Figure 1-8: Estimation of changes in annual precipitation up to 2100

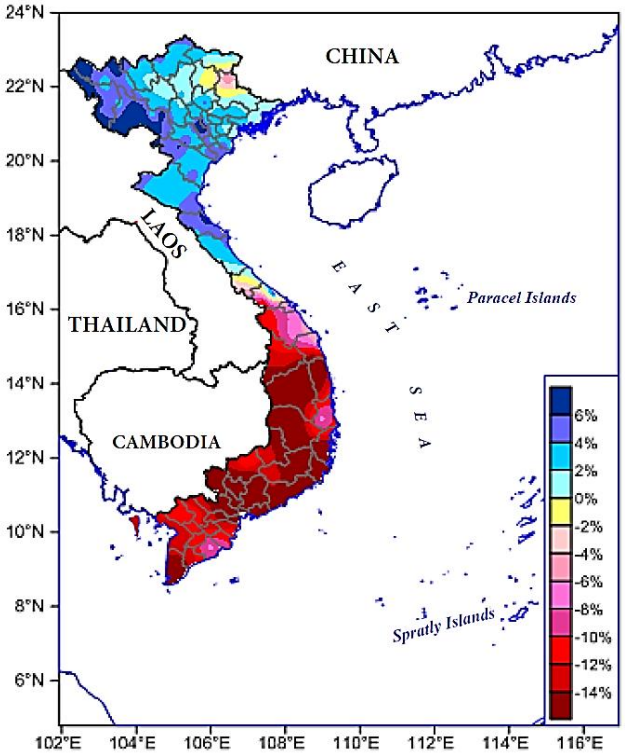

Figure 1-9: Estimtation of changing precipitation in wet season up to 2100

Nowadays, climate change is trusted as remarkable challenges to coastal cites located among of river basins with the influence of sea tide regime, especially in low-lying urban deltas (Arjan *et al.*, 2010). The predicted changes in sea level, river discharge and weather extremes, combined with increasing potential impacts due to population growth and rapid urbanization, enlarge concerns to make cities "climate proof". Negative impacts of climate change are inevitable, but the strategic orientation for adaptation in order to mitigation of fatality, economic and social damages will be much-needed.

1.3. Statement of the problems

The downstream of the Dong Nai - Saigon River Basin spreads over a wide area, including HCMC and six provinces: Binh Duong, Dong Nai, Tay Ninh, Long An, Dong Thap, Tien Giang, with a total area of 10,805 km^2. This area is low-lying land, adjacent to the East Vietnam Sea. Hence, about 15% of this area have been often intertidal areas (1,594 km^2). In general, this low-lying area is strongly influenced by the variation of two factors: river flow and tidal current (Ngoc *et al.*, 2013c).

In recent years, many large reservoirs have been constructed in upstream. These reservoirs reduce the average flood flow and the river flow is weakened. In other hand, failure of equipment causing measurement interruption or effect of natural hazards like hurricanes, landslides, actions of human beings like war, civil unrest, mishandling of observed records, or even loss of data in computer system by accident, could cause a huge disaster to downstream.

Major flood events took in many cities located at the downstream of the Dong Nai – Saigon River Basin as HCMC, Long An, Binh Duong, Dong Nai, Tay Ninh. The short-term impacts included hundreds of casualties, many displaced people and enormous damage to property and infrastructure. In this research, the extreme flood events mentioned typical including the historical

floods in 1952 and 2000. There was not any observed data that monitored, but they said that the ferocious flood of 1952 (estimated frequency of 2%) submerged nearly 70% area of HCMC. It seriously caused fatality and economic and social damages beyond estimated losses. Closely, the typical flood of 2000 (estimated frequency of 5%) is remarked as the flooding events used for assessing inundated areas and damages in many studies. According to the observation and simulated results, the consequences of this flood dealt a big devastating blow to economy, property, as well as infrastructure.

Moreover, the impact of tidal current considerably increases. In addition, salt water intrusion problems and lack of fresh water have been seriously happening on the Saigon River. In the study area, the leveling of low-lying land, flood embankments, tidal flooding prevention constructions, anti-salinity constructions have been continuously built along the river. They prevent the river current and tidal current overflowing, and water level of the high tide is raised, whereas that value of the low tide is declined. Besides, climate change - rising sea level are also an important factor which govern increase of salinity intrusion, flooding, and hamper flood drainage of the Plain of Reeds and HCMC. Extreme rainfall on the Dong Nai - Saigon River Basin in HCMC area, combining the high tides - rising sea levels will progressively put pressure on the drainage system and increased flooding to HCMC in the near future. The measured data of Phuan station, Phuan station (in HCMC) and Vungtau station, indicate that the water level has continuously risen from 2005 to now. To be specified, highest water level recorded in 61 years was 1.68m at Phuan station on October 20th 2013, entailing a natural disaster of serious inundation to HCMC and causing fatality, severe economic and social damages. Furthermore, the feasibility study and the stormwater drainage systems with JICA (Japan International Cooperation Agency) assistance in the execution stage reveals inconsistencies when the rainfall storage areas are lower than tidal water level, hence tidal flooding happens in many parts of HCMC. Actually, the technical design of the project

East-West Highway and Water Environment Improvement - Phase I of JICA based on the highest tide in the Saigon River is 1.32m, have the ability to control flooding rainfall (with maximum 90mm). Nevertheless, the tidal water level currently reaches over 1.60m, and it combines with heavy rain, consequently, the sewer – system cannot respond.

1.4. Objectives of the study

The objectives in this research are to focus on numerical modeling for rainfall runoff process, optimal operation of Dautieng Reservoir, hydraulic model for simulating water level and discharge in river network for the Dong Nai-Saigon River Basin, flood vulnerablility assessment based on GIS modeling for the downstream of HCMC, and 2D-Hydrodynamic model for simulating the erosion and deposition in Tien River Ensturies. Accordingly, key objectives can be listed as bellows:

- To analyze the data collection related to the Dong Nai-Saigon River Basin including hydro-meteorological data, reservoir characteristics, historical operating records, water needs for human activities, etc.
- To select suitable hydrological models among various conceptual numerous models to restore and predict runoff coming into the watershed and estimate the effects and applicable ability of each model on the simulated flow.
- To investigate the design of reservoir operation model based on optimizing the rule curves in attempt to carry out the effective suitable policies in management and operation of water supplies and storages, and to avoid unnecessary disadvantages due to water shortages and flood inundation.
- To simulate hydrodynamic on river system of the Dong Nai-Saigon River Basin and estimate water level and water discharge on rivers.

- To construct a tool of vulnerability assessment based on GIS modeling to estimate flood damage to separate area types that caused by inundation to the downstream of the Dong Nai-Saigon River. The derived outcomes of loss estimation are the concrete basis for finding suitable ways to avoid the mistakes of past and build resilience into urban management, critical infrastructure investments and disaster risk mitigation measures in jurisdiction balance of sectors.
- To apply the MIKE 21/3 Coupled Model FM included seaveral modules such as: the Mike 21 Hydrodynamic Module FM (Mike 21 HD), the Spectral Wave FM Module (Mike 21 SW), and the Mud Transport Module (Mike 21 MT) to study the morphological evolution of the Tien River Estuaries under effects of sea level rise scenarios.

1.5. Scope of study

The scope of study is outlined the following points:

- To apply hydrological models incorporated optimization search method to the Dong Nai-Saigon River Basin and evaluate effectiveness and performance of each model, then simulate and predict the outlet flow at Dautieng Reservoir.
- To investigate optimizing the rule curves through modeling of reservoir operation incorporated a genetic algorithm with a penalty strategy. Next, make plan of reservoir operation based on water demands in context of climate change and water shortage.
- To apply hydrodynamic model for simulating water level and discharge on river in attempt to address water level in downstream, and provide suitable measures for protecting the downstream of the Dong Nai-Saigon River Basin from inundation.
- To design GIS-based modeling of flood vulnerability assessment to assess vulnerability and estimate economic damage of Cities in

downstream. This part is conducted to present a framework of flood risk assessment in attempt to identify and evaluate adaption options in the developing urban context located in downstream of cascade of reservoirs.

- To apply the MIKE 21/3 Coupled Model FM to access the effects of sea level on sedimentation of the Tien River Estuaries under sea level rise scenarios.

CHAPTER II

LITERATURE REVIEW AND APPLIED METHODOLOGY

In this statement, various approaches in which developing and applying models in hydrology prediction, hydrodynamic and water resources management are reviewed. They can be summarized as follows:

2.1. Probable approaches

In order to develop a model which can restore the inflow of watersheds with limited data and rebuild optimal reservoir operating rule curves, the judicious approach should be considered and values of the process parameters should be determined as bellows:

- Select suitable hydrological models for selected watersheds where the characteristics and limited data record are resemble, then apply and develop the models achieving good performance.
- The obtained results of these models are calculated from observed data and available historical records and evaluated by the error indicators and effective performance.
- Based on the watershed's characteristics and particular reservoir operation, the judicious approach method for water resources management is proposed to optimize processes of reservoir operating rule policy.
- Simulate hydrodynamic on rivers based on anticipated senarios to estimate inundation in downstream of Dong Nai-Saigon River Basin.
- Construct a tool of flood risk management based on GIS modeling to economic damage of Cities. The findings of outcomes are the concrete

basis in contribution to propose sustainable measures for improving positive effects and restricting negative impacts on cultivation, guiding Ho Chi Minh City towards aspired benefits.

- Develop and apply the MIKE 21/3 Coupled Model FM for simulating sediment erosion and deposition of Tien River Enstuaries to study the morphological evolution in coatal zone.

On the other hand, applied genetic algorithms for optimizing parameters of those models can be used to calibrate and evaluate effective performances. These attempts are reviewed as follows:

2.2. Reviewed models

2.2.1. Hydrological models

The first approach to a short-term rainfall-runoff model called "Unit Hydrograph Theory" was devised by Sherman (1932). Sherman pointed out that the flood hydrographs from a given basin were noticeably similar in the shape when caused by reduced rainfall of similar durations and that, if the hydrographs were to a unit volume, they tended to be approximately identical. This concept, called the unit hydrograph, was the first expression of the linear system approach in flow simulation. Lately, Clark (1945) demonstrated the equivalence of the linear routing procedure known as the Muskingum method and showed that a unit hydrograph could be constructed by routing of the time-area diagram of the basin converted to flow units. Many other researchers contributed to the general development of the unit hydrograph concept.

Sugawara (1961) proposed a model - the TANK model consisting of a complex cascade of linear storages for simulating the entire runoff process from rainfall to stream flow. This model designs a series of storage-type tanks to account for the non-linear relationship between rainfall and runoff. The series of storage type tanks is based on the hypothesis that runoff and infiltration are the functions of the amount of water stored in the ground. Sugawara did not,

however, relate the various storages to features of the natural process, and hence, his model can be fitted to a real watershed only by a trial-and-error process. The applicability of TANK to various conditions have been studied by many hydrologists (Balasubramaniam and Uddin, 1977).

Nielsen and Hansen (1973) developed the NAM model. It is a relatively simple model for the prediction of runoff from rural catchments. A mathematical hydrological model like NAM is a set of linked mathematical statements describing, in a simplified quantitative form, the behavior of the land phase of the hydrological cycle. The NAM model is a so-called deterministic, conceptual, lumped type of model with moderate input data requirements. NAM model has 'been applied to a number of catchments in different climatic regions of the world.

Intahvong (1983) calculated the long-term average annual runoff for ungauged small rivers in Vientiane, Laos. He presented a simplified technique of estimating runoff using the Pearson type III (P3) distribution. This concept availed of the functional relationship of the skew-ness coefficient with the coefficient of variation of the precipitation data

Tawatchai and Gaum (2000) conducted the research to application of TANK, NAM, ARMA and neural network models to flood forecasting for the Wichianburi basin using developed flood forecasting procedure. The results were found to improve significantly by coupling stochastic and deterministic models (TANK and NAM) for updating forecast output. The neural network (NN) model was compared with the TANK and NAM models. The NN model does not require knowledge of catchment characteristics and internal hydrological processes. The training process or calibration is relatively simple and less time consuming compared with the extensive calibration effort required by the Tank and NAM models. However, the performance of the aforesaid three models was evaluated statistically (Rajurkar *et al*., 2004).

Arcelus (2000) discussed the combination of an event model (HEC-HMS) and a continuous water accounting model (NAM) to obtain discharge series from

ungauged basins Cebollati River Basin (Uruguay). Considering the lack of detailed spatial rainfall information, the applied procedure showed acceptable results. A procedure to obtain discharges from rainfall in ungauged basins was developed based on the characteristics and advantages presented by each hydrological model (HEC-HMS and DHI-NAM). In this manner, it was possible to adjust the overland flow runoff coefficient and the time constant overland flow routing parameter, since both values are difficult to extrapolate to ungauged basins.

The application of artificial neural network (ANN) methodology for modeling daily flows during monsoon flood events for a large size catchment of the Narmada River in Madhya Pradesh (India) was presented (Rajurkar *et al.*, 2004). The spatial variation of rainfall was accounted for by subdividing the catchment and treating the average rainfall of each sub-catchment as a parallel and separated lumped input to the model. A linear multiple-input single-output (MISO) model coupled with the ANN was shown to provide a better representation of the rainfall–runoff relationship in such large size catchments compared with linear and nonlinear MISO models. The present model provided a systematic approach for runoff estimation and represents improvement in prediction accuracy over the other models studied herein.

Lakshmi (2004) studed “Use of Satellite Remote Sensing in Hydrological Predictions in Ungagged Basins” to determine and access vegetation data (by Moderate Resolution Imaging Spectroradiometer), Surface Temperature (Advanced Intra-Red Sounder), Surface Air temperature and Precipitation (from Tropical Rainfall Measuring Mission Microwave Imager) on hydrological models when lacking of both calibration and validation data. The synergistic used of these data sets along with hydrological models would help us to (a) input precipitation and vegetation information into a hydrological model and calculate the soil moisture and surface temperature using the water and energy balance equations and (b) use the measured soil moisture and surface temperature in two

ways (i) to calibrate certain model parameters and (ii) to verify the output of the model through validation. The overland runoff from the hydrological model would be routed in the stream channel network (obtained from the Digital Elevation Data) to obtain the stream flow at the catchments outlet.

Hiramatsu *et al.* (2004) developed a continuous tank model to simulate and analyze the inundation in a flat, low–lying paddy–cultivated area in the Red River delta in Vietnam. In this model, field and regional drainage systems constructed as many interconnected tanks; therefore, the model can generally apply for every field and many kinds of drainage and boundary conditions. Later, the distributed tank model has been developed and applied to Chikugo River Basin successfully by him and his students (Chinh *et al.*, 2006). In addition, the developed Tank model applied to upstream area of Song Hue hydraulic structure scheme, Hanoi –Vietnam with accurate and good performance (Nguyen, 2011).

2.2.2. Models for optimizing reservoir operation

The characteristics of hydrologic parameters in reservoir management models is uncertain. In mathematical programing models, the uncertainties are dealt with either indirectly (sensitivity analysis of a deterministic model) or directly by applying a chance-constrained type of formulation or some of the stochastic programing techniques as stochastic linear programing (LP) and stochastic dynamic programing (DP) based models. In the past twenty years optimization techniques have been applied to planning, design and management of reservoir as an alternative or complement to standard engineering techniques and models. Reznicek and Cheng (1991) have applied and reviewed the stochastic modeling of reservoir operations with constructed various programing models: stochastic linear programing, stochastic linear programing with recourse, chance-constrained linear programing, stochastic dynamic programing, etc.

Karamouz *et al.* (2009) resulted in the probabilistic reservoir operation using Bayesian stochastic model and support vector machine in order to reconcile water quantity and quality objectives for long-tern reservoir operation polices.

The final results showed the iso-probabilistic curves of joint probabilities of standardized on-supplied water demand and total dissolved solid concentration values.

Hashemi *et al.* (2008) developed an optimal reservoir operation model by genetic algorithm (GA) considering inflow probabilities. The model parameters were calibrated by using GA optimization search through a fitness function based on finding minimum deficient of water applies and water needs. The proposed model showed the results of the monthly reservoir storage volume based on inflows with various probabilities.

A conditional genetic algorithm model for searching optimal reservoir rule curves was developed by Hormwichian *et al.* (2009). This model proposed GA to connect with a reservoir operation simulation model based on the concept of HEC-3 (US Army Corps of Engineers, 1974) for searching the optimal rule curves of reservoir. The minimum average water shortage was applied as an objective function of the search process. The simulated results of proposed model achieved the new rule curves with smaller shortage and minimum over-flow via spillway of reservoir.

Chaves and Chang (2008) proposed a novel intelligent reservoir operation system-based on evolving artificial neural networks (ANN). Accordingly, the ANN model was designed for the operational strategies of reservoir operation with the main advantages of the evolving ANN intelligent system (ENNIS) as follows: a small number of parameters to be optimized even for long optimization horizons, easy to handle multiple decision variables, and the straightforward combination of the operation model with other prediction models. This model was constructed and applied for calculating two cases, single objective and multiple objectives of the reservoir as membership functions. The results of ANN-based model showed great potential to incorporate other forecast models, and take simultaneously a great number of decisions without compromising its optimality.

Li *et al.* (2010) designed and developed a reservoir operation model with dynamic control of flood limited water level (FLWL) by considering inflow uncertainly. This model included three modules: a pre-release module, a refill operation module and a risk analysis module. Monte Carlo simulation was used to estimate dynamic control bound of reservoir FLWL. The results showed that the dynamic control of reservoir RLWL could affectively increase hydropower generation and floodwater utilization rate without forecasting flood control risk.

A large scale reservoir operation by constrained particle swarm optimization algorithm (CPSO) was constructed and applied by Afshar (2012). The periods of the operations were treated in a reverse order prior to the CPSO search to define a new set of bounds for each storage volume in attempt to solve two problems of water supply and hydropower operation of reservoir. The results of three simulated cases, short, medium and long term operations illustrated the efficiency and effectiveness of the proposed method for the solution of large scale operation problems. It greatly opens a new approach for applying artificial intelligent techniques with a rational orientation.

A constrained genetic algorithm (CGA) for optimizing multi-use reservoir operation was proposed by Chang (2008) and Chang *et al.* (2010) under considering ecological base flow requirements to optimize reservoir operations for multiple water users. Water limits-based rule curves M-5 and reservoir characteristics were incorporated as constraints integrated into reservoir operational objectives to form the fitness function, and a generalized shortage index (GSI) was used to validate the performance of model (Hsu, 1995). By demonstration of the simulated results, the proposed model applied to the Shih-Men reservoir for last 20 years using penalty-type genetic algorithm can be a powerful tool in searching for optimal strategy for multi-use reservoir operations in water resources management.

2.2.3. Models for flood risk and vulnerability analysis

Flood events have an enormous impact on human wellbeing, social development goals such as addressing poverty, ensuring adequate food, water, and sanitation, and protecting the environment. Accordingly, floods are among the most devastating of all natural disasters. Direct losses from floods include drownings and injuries as well as damage to infrastructure and property, agricultural production, and sites of historical and cultural value. Indirect health problems often arise, such as water-borne infections, exposure to chemical pollutants released into flood waters, and vector-borne diseases (Jason *et al.*, 2005).

Frequent extreme weather events and increased flood risk in coastal cities have become the hot issues for national governments and academia. Under the framework of United Nations' international strategy for disaster reduction (ISDR), a lot of international or regional organizations and governments have focused on flood disasters and carried out a series of research projects to enhance the capacity in disaster prevention of human beings and to reduce disaster risk since the extreme events in 2000. Additionally, the obligatory targets for risk identification, assessment and monitoring of floods and other natural disasters are set in the outline of Vietnam National Plan for Medium- and Long-Term Scientific and Technological Development for Integrated Disaster Reduction (MONRE, 2012).

Choong *et al.* (2010) indicated the estimation of economic loss from flood damage for the Anyang Stream Basin in Korea by GIS-based distributed technique. They considered two aspects of flood damage from an engineering and economic perspective, i.e. flood inundation analysis and multi-dimensional flood damage analysis (MD-FDA).

Honghai *et al.* (2014) applied GIS-Based Spatial Monte Carlo Analysis for Integrated Flood Management with Two Dimensional Flood Simulation. By this technique, they developed a new flood management tool within the

framework of widely used GIS software ArcGIS. This tool has also the ability to interact with and use of classified Remote Sensing (RS) image layers, and other GIS feature layers like census block boundaries for flood damage calculation and loss of life estimation. They has applied this tool for flood management to Oconee River near the City of Milledgeville, Georgia, USA and the test result indicates that this tool provides a very versatile environment for spatial comparison of various flood mitigation alternatives by taking into account various uncertainties, which will greatly enhance the quality of the decision making process.

2.2.4. Models of Estuarine morphodynamics

In the past several decades, morphodynamic models have been rapidly developed with high performance, and a variety of mathematical models has been proposed for sediment transport by addressing different aspect of sediment characteristics. One of the famous models for simulating morphodynamics developed by the Danish Hydraulic Institute is MIKE (DHI, 2007b). The other models developed by Delft Hydraulics (DELFT2D-MOR, DELFT3D) to determine the total potential transport rate. There are some newest morphodynamic models (e.g. SHORECIRC, TELEMAC, MOHID, MORSYS2D, and etc.) were developed. The most popular numerical morphodynamic models above are generally related on engineering methods and techniques for coastal defense.

A number of studies have provided new and interesting results (Wolanski et al., 1998; Nguyen, 1995; Nguyen et al. 2000). It was pointed out that most of the suspended sediment (SS) is fine silt and that sediment transport is influenced by many factors, particularly river currents, sea currents (monsoon currents), tidal currents, and wave-generated currents. Furthermore, the combination of meteorological and oceanic effects produces strong variations in coastal areas, mainly at seawater level and coastal currents. A small number of those studies,

used the numerical models and those studies applied for small areas or the individual estuaries of the Mekong River. Those researches did not show the changing of erosion and deposition of sedimentation in coastal areas between the Mekong River estuaries and sea areas by the sea currents.

In this study, the MIKE 21/3 Coupled Model FM was applied to simulate erosional and depositional processes in the Tien River Estuaries, Mekong River System, including the effects of sea level rise.

2.3. Methodology

According to the aforesaid literature reviews, this study aims at working out the decision framework support for assistance of water storage and release policies to planning and management of reservoir in long-term and short-term. Hence, there are four major parts involving this research: (1) Two hydrological models, the Tank model and the NAM model, were selected to simulate rainfall – runoff process in Dautieng River Watershed; (2) Optimal operation of multi-use Dautieng reservoir using constrained genetic algorithm, hereinafter describes the flow chart of methodology in overview (**Figure 2-1**); (4) design and estimate the flood risk and vulnerability analysis for the downstream of the Dong Nai-Saigon River Basin (**Figure 2-2**); (4) apply the 1/2D-hydrodynamic model – the MIKE 21/3 to study the effects of sea level rise on sedimentation of Mekong River Delta as well as Enstuaries. The detailed approach methods will be mentioned in the next chapters.

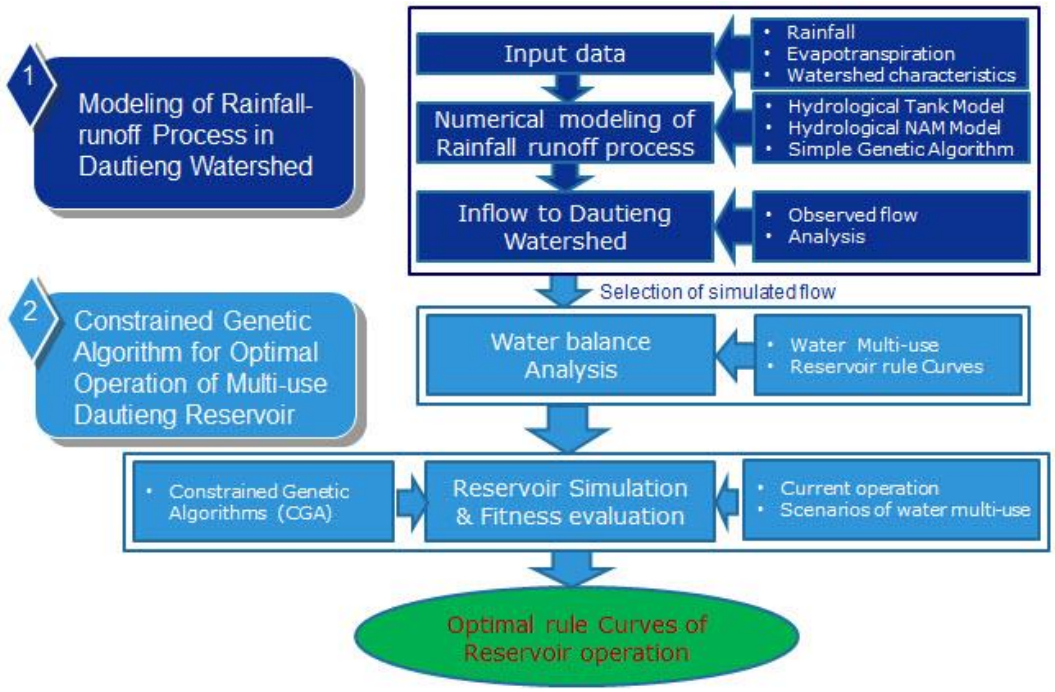

Figure 2-1: Flow chart of methodology for hydrologcal and reservoir operation models

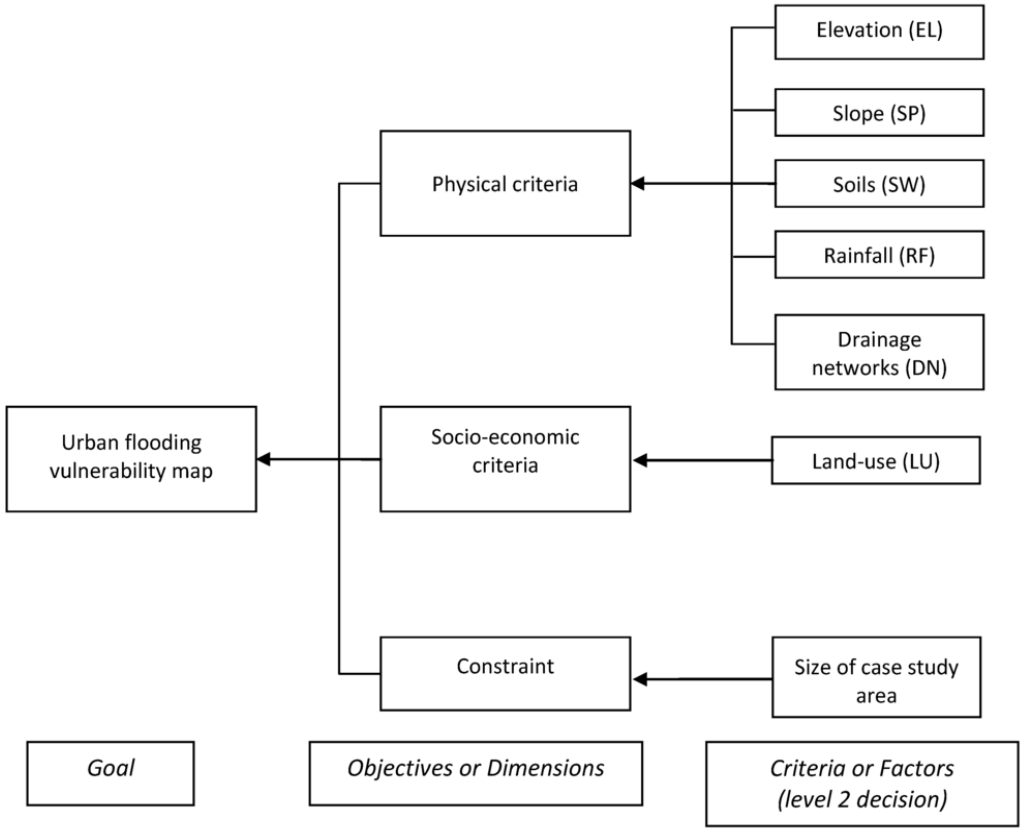

Figure 2-2: Flow chart of hydrodynamic and GIS-based modeling

CHAPTER III

NUMERICAL MODELING FOR RAINFALL RUNOFF PROCESS

3.1. Dautieng Watershed

3.1.1. Background

The Dautieng River Watershed is located at the upper Saigon River in Tay Ninh Province in southeast Vietnam, approximately 90km from HCMC. It is a main reach of the upper Dong Nai - Saigon River system, outside of the estuarine basin as shown in **Figure 3-1**. The upper Saigon reach comes from Cambodian river branches and discharges into the downstream portion of the Dong Nai - Saigon River system. The Saigon River is a large reach of the Dong Nai - Saigon River where flows through HCMC area.

The upstream of the Saigon River is intercepted by the Dautieng reservoir, with the length of the main course about 130 km. Its watershed area is well known as the largest reservoir for irrigation in Vietnam, with a river slope of 0.25% and a total length of 130.5 km. The effective water conversation of Dautieng reservoir is 1.57 billion m^3 and this water storage is utilized not only for irrigating the downstream agricultural area, but also for preventing saltwater intrusion and maintaining freshwater discharge into the river. The Dautieng reservoir has a total watershed of 2,700 km^2, with a water surface area of about 270 km^2, and the elevation of from 24 m to 100 m above mean sea level. It received annual average 1,800 mm of rainfall in last 30 years; however, the rainfalls was uneven with 77% occurred between July and November.

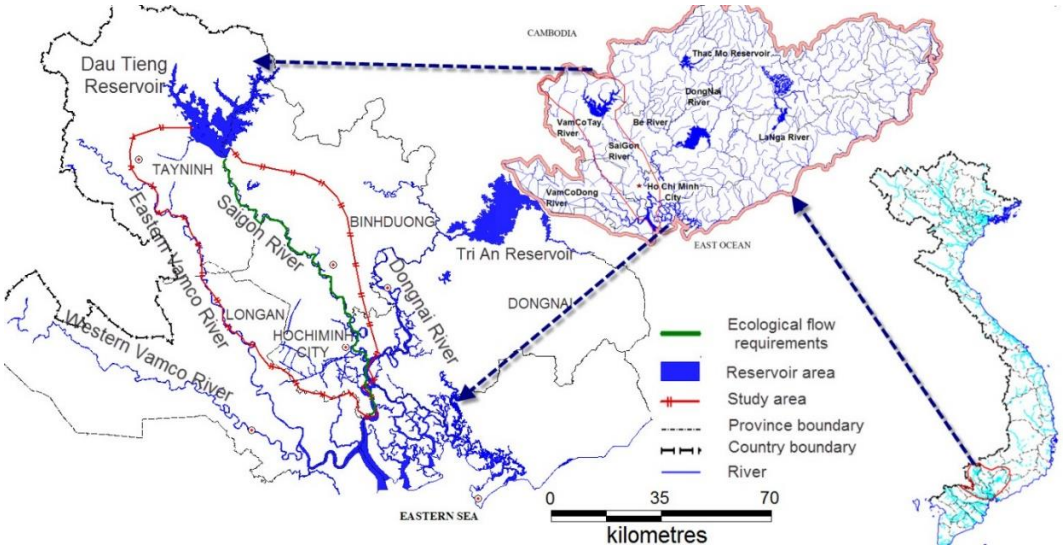

Figure 3-1: Location of Dautieng Watershed

The designed goals of Dautieng reservoir are as: (1) supply water for agricultural and industrial areas, and human activities, (2) control flood and cut peak discharge in wet season, (3) prevent the saltwater intrusion in downstream, and (4) improve environmental quality in downstream area.

3.1.2. Data collection

1) Soil and landuse

Soil in Dautieng River Watershed are clay soil and basalt soil. Of these, clay soil is covered by long-term industrial land accounts for about 90,000ha and basalt soil is covered by upland field and forest accounts for 180,000ha.

The water surface area of Dautieng reservoir accounts for about 10% of total watershed area, and the remaining area is covered by brushwood, grass and poor natural forest. For details, the proportional area rates are follows: long-term industrial land of 10%, short-term industrial land of 13%, fruit tree land of 7%, wasteland and brushwood of 37%, natural forest of 14% and paddy field of below 5%. **Figure 3-2** shows the landuse map in Dautieng River Watershed.

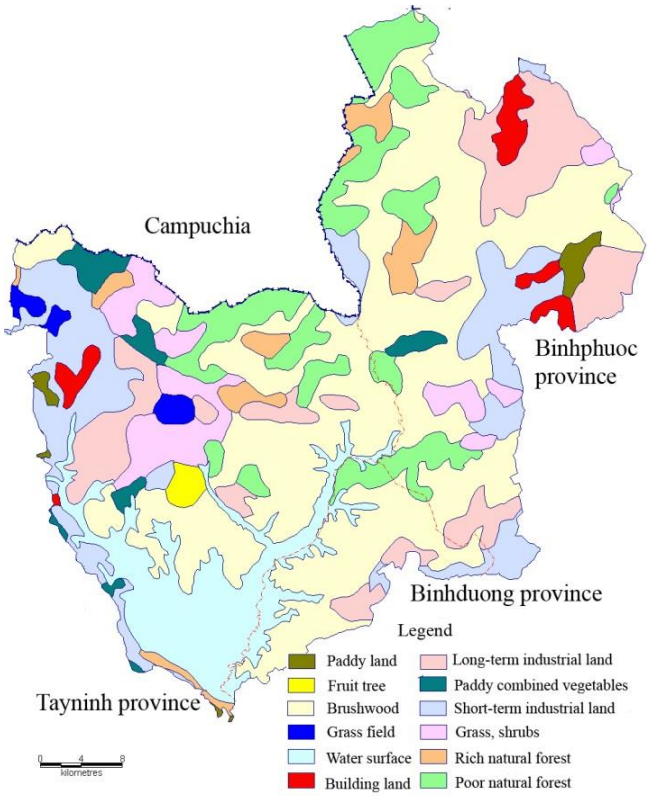

Figure 3-2: Map of land use in Dautieng River Watershed

2) Topography and geology

Topographical map of the study area, including elevation, river network, boundary and landuse were collected for calculating in the model. **Figure 3-3** shows the 90m-DEM map in Dautieng River Watershed.

3) Rainfall data

To evaluate the applicability of the selected two hydrological models incorporated with GA optimization, daily rainfall, evaporation, and river discharge data were recorded at three stations, Chon Thanh (CT), Tay Ninh (TN), and Dautieng (DT). The location and obtained data for each station are shown in **Figure 3-3** and **Table 3-1**. These data were collected by the Dautieng Irrigation Exploitation and Management Company under the Ministry of Agriculture and Rural Development, Vietnam, and provided by the Division of Applied Science and Technology, Thuyloi University–Second Base, Vietnam.

The data used for calibrating hydrological models included rainfall, evaporation, and discharge in 1995 and 2000. The year 1995 represented hydrological years with rainfall less than annual average rainfall, and the year 2000 represented hydrological years with rainfall more than annual average rainfall. The calibrated models were validated in 2 years, 1998 and 2001. Both validation years represented typical hydrological years with high-quality observed data. The data used for estimating hydrological models and restoring outlet runoff at Dautieng Reservoir from 1983 to 2008.

Table 3-1: Rainfall data of each gauge station

Basin	Station	Sub-catchment Area(km^2)	Thiessen Weight	Latitude	Longitude	Data type	Year
Dautieng River Watershed	Tayninh	810	0.3	11 °40'33"	106 ° 13'15"	Rainfall	1978-2008
	Chonthanh	810	0.3	11 °23'54"	106 ° 38'31"	Rainfall	1978-2008
	Dautieng	1080	0.4	11 ° 5'39"	106 °22'32"	Rainfall Evaporation Discharge	1878-2008 1878-2008 1978-2008

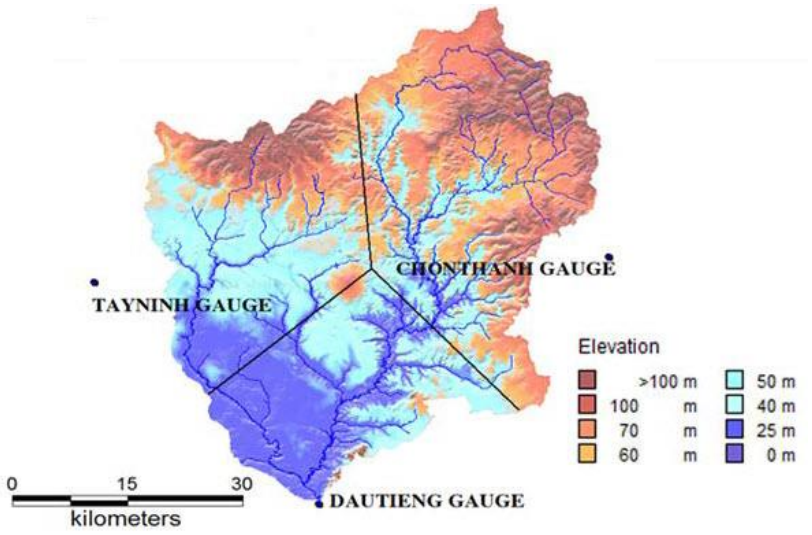

Figure 3-3: 90-m DEM, and Thiessen polygon method for the Dautieng River Watershed

Because the daily rainfall data collected from each station did not reflect uniform rainfall distribution throughout the Dautieng River Watershed, the Thiessen polygon method was used to obtain average watershed rainfalls, as shown in **Figure 3-3**.

4) Potential evapotranspiration data

Evaporation was observed by the instrument – Pichhe tube used since 1978. The data were collected from 1978 to 2008 as shown in Table 3-1.

An empirical relationship between "Piche" evaporation and pan evaporation is formulated the equation of hydrological Department, Vietnam in 1970 as below:

$$E_{pan} = E_{piche} * K \quad (3\text{-}1)$$

Where:

E_{pan}: Pan evaporation (mm/day)

E_{piche}: Piche evaporation (mm/day)

K: empirical coefficient, K depend on the crop seasons

In the winter-spring: K = 1.10 to 1.20

In the summer-autumn: K = 1.20 to 1.30

In this study, the value of K = 1.20 was set in the dry season, and 1.1 in the wet season.

The following equation was used for converting the pan evaporation to potential evapotranspiration:

$$ET_p = K_p * E_{pan} \quad (3\text{-}2)$$

Where:

ET_p: Potential evaporanspiration

K_p: Pan evaporation coefficient.

According to previous studies, the value 0.9 was selected for Kp in the Dong Nai basin (MORE,2009).

5) Characteristics of Reservoirs in Dong Nai-Saigon River Basin

The characteristics of the Dautieng reservoir, consist of relative curves between volume V and elevation Z (V~Z), water surface area F and elevation Z (F~Z), and opening height H of culvert gates and discharge Q (H~Q), were used for calculating optimal operation of reservoir simulation model.

6) Historical operation records

Historical operation records including the data of reservoir water level, and opening height of culvert gates were used for calculating water balance. The series of historical operation records were collected from 1984 to 2008.

3.1.3. Water needs and water balance calculation

Water needs were selected based on undergraduate thesis of Ngoc (2006). **Table 3-2** shows the water needs of various fields including agriculture, industry, economy, domestic human activities and environmental base flow requirements for preventing saltwater intrusion and improving water quality in downstream area of HCMC.

Table 3-2: Total water needs in downstream of Dautieng Reservoir Watershed

Month	Agriculture (10^6 m^3)	Eviromental flow (10^6 m^3)	Agr-product plant (10^6 m^3)	Suggar-product plant (10^6 m^3)	Water Treatment Plant (10^6 m^3)	Human actives (10^6 m^3)	Total (10^6 m^3)
Jan	198.58		0.02	5.36	19.55	0.29	223.80
Feb	250.02	48.38	0.02	4.84	17.66	0.26	321.18
Mar	221.49	53.57	0.01	5.36	20.09	0.29	300.80
Apr	195.62	51.84		2.42	18.92	0.28	269.08
May	97.09			-	19.55	0.29	116.93
Jun	73.61			-	18.92	0.28	92.81
Jul	13.39			-	19.55	0.29	33.23
Aug	36.25			-	-	0.29	36.54
Sep	35.82			-	-	0.28	36.10
Oct	47.03			-	-	0.29	47.32
Nov	158.73		0.01	2.59	-	0.28	161.61
Dec	105.59		0.02	5.36	-	0.29	111.26
Year	***1 ,433.23***	153.79	0.09	25.92	134.25	3.39	***1,750.67***

Figure 3-4: Upstream Dautieng Reservoir

Figure 3-5: Spillway of Dautieng Reservoir

Figure 3-6: East Culvert of Dautieng Reservoir

Figure 3-7: Upstream Dautieng Reservoir in the dry season

3.2. Overview of hydrological model

3.2.1. Hydrological NAM Model

NAM is an abbreviation for "Nedbor-Afstromings Model"," a Danish phrase meaning "precipitation runoff model." The hydrological NAM Model simulates the rainfall runoff process that occurs at the watershed scale. The NAM Model forms part of the rainfall runoff module of the MIKE 11 River Modeling System and was originally developed at the Institute of Hydrodynamic and Hydraulic Engineering at the Technical University of Denmark (Gunawan, 2010; Ngoc *et al.*, 2011a). During the past decade, the NAM Model has been extensively applied and modified in many projects by the Danish Hydraulic Institute.

A lumped conceptual model of the NAM Model treats each subcatchment as a unit. The NAM Model simulates the rainfall runoff process in rural catchments and has 10 parameters (as shown in **Table 3-2**): U_{max}, L_{max}, CQ_{OF}, CQ_{IF}, T_{OF}, T_{IF}, CK_1, CK_2, T_G, and CK_{BF}. Various components of the rainfall runoff process represent average values for the entire subcatchment by continuously accounting for water contents in four different but mutually interrelated forms of storage: snow, surface, lower zone, and groundwater. The routine for overland flow, interflow, and baseflow, shown in **Figure 3-8**, is also based on the linear reservoir. In this study, snow storage was not considered.

Rain intercepted on vegetation as well as water trapped in depressions and in the uppermost, cultivated part of the ground is represented as surface storage. U_{max} denotes the upper limit of surface water storage.

Evapotranspiration demand is initially met at the potential rate from the surface storage. If moisture content, U, in the surface storage is less than this requirement, the remaining fraction is assumed to be withdrawn by root activity from the lower zone storage at an actual rate, E_a. The value E_a is set to be proportional to potential evapotranspiration, E_p, according to:

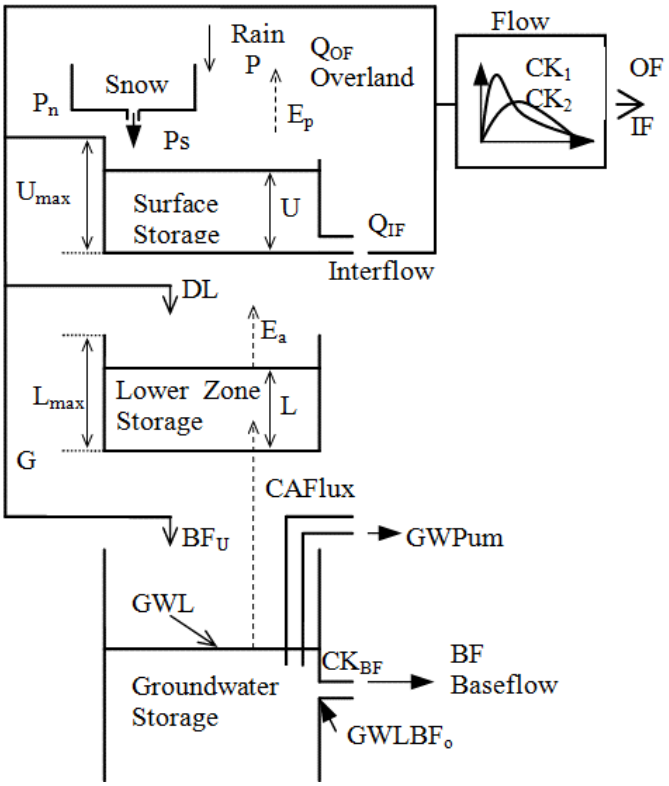

Figure 3-8: Structure of the NAM model

$$E_a = E_p * \frac{L}{L_{max}} \tag{3-3}$$

where L and Lmax are the actual and maximum possible moisture contents, respectively, in the lower zone storage.

When the surface storage spills, $U \geq U_{max}$, the excess maximum water, P_n, induces overland flow as well as infiltration. Q_{OF} denotes the part of P_n that contributes to overland flow. Q_{OF} is assumed to be proportional to P_n and to vary linearly with the relative soil moisture content, L/L_{max}, of the lower zone storage.

Then, overland flow, Q_{OF}, is determined as:

$$\begin{cases} Q_{OF} = CQ_{OF} \dfrac{L_{t-1}/L_{max} - T_{OF}}{1 - T_{OF}} P_n & \text{for } L_{t-1}/L_{max} > T_{OF} \\ Q_{OF} = 0 & \text{for } L_{t-1}/L_{max} \leq T_{OF} \end{cases} \tag{3-4}$$

where L denotes the soil moisture content of the lower zone storage, CQ_{OF} and T_{OF} are the positive constants less than unity and without dimension, and t is time.

Interflow contribution, Q_{IF}, is assumed to be proportional to U and to vary linearly with the relative moisture content, L/L_{max}, of the lower zone storage. Q_{IF} is determined as:

$$\begin{cases} Q_{IF} = CQ_{IF}\dfrac{L_{t-1}/L_{max} - T_{IF}}{1 - T_{IF}} U_t & \text{for} \quad L_{t-1}/L_{max} > T_{IF} \\ Q_{IF} = 0 & \text{for} \quad L_{t-1}/L_{max} \le T_{IF} \end{cases} \tag{3-5}$$

where CQ_{IF} is the time constant for interflow and T_{IF} is the root zone threshold value for interflow.

The proportion of excess rainfall, P_n, that does not run off as overland flow infiltrates into the lower zone storage representing the root zone. A portion DL of the amount of infiltration, $P_n - Q_{OF}$, is assumed to increase soil moisture content, L, in the lower zone. G is assumed to percolate deeper and recharge groundwater storage.

$$\begin{cases} G = (P_N - Q_{OF})\dfrac{L_{t-1}/L_{max} - T_G}{1 - T_G} & \text{for } L_{t-1}/L_{max} > T_G \\ G = 0 & \text{for } L_{t-1}/L_{max} \le T_G \\ DL = (P_N - Q_{OF}) - G & \end{cases} \tag{3-6}$$

where T_G is the root zone threshold value for groundwater recharge.

Percolation, G, is routed through a linear reservoir with the time constant, CK_{BF}, before reaching the groundwater table as recharge, BF_u.

Base flow is determined as:

$$BF_{u(t)} = BF_{u(t-1)} \cdot e^{(-\frac{t}{CK_{BF}})} + G_t(1 - e^{(-\frac{t}{CK_{BF}})}) \tag{3-7}$$

Table 3-3: NAM model parameters used for calibration

Parameter	Description	Lower limit	Upper limit
U_{max}(mm)	The maximum water content in surface storage	5	35
L_{max}(mm)	The maximum water content in root zone storage	50	350
CQ_{OF}(-)	Overland flow runoff coefficient	0	1
CQ_{IF}(h)	Time constant for routing interflow	500	1,000
T_{OF}(-)	Root zone threshold value for overland flow	0	0.9
T_{IF}(-)	Root zone threshold value for interflow	0	0.9
CK_1(h)	The time constant for routing interflow	3	72
CK_2(h)	The time constant for routing overland flow	3	72
T_G(-)	Root zone threshold value for groundwater	0	0.9
CK_{BF}(h)	Time constant for routing base-flow	500	5,000

Based on meteorological data input, the NAM Model produces watershed runoff and other information about the land phase of the hydrological cycle such as temporal variation in evapotranspiration, soil moisture content, groundwater recharge, and groundwater levels. The resulting watershed runoff is conceptually divided into overland flow, interflow, and baseflow components (DHI, 2007a, 2007b).

3.2.2. Hydrological Tank Model

The Tank Model is a synthetic flow model based on rainfall in a watershed. It was first developed and introduced in 1956 by a Japanese hydrologist, Dr. Masami Sugawara. The model has been widely used throughout the world and was evaluated as good by the World Meteorological Organization (Nielsen *et al.*, 1973). The Tank Model can be applied to reproduce streamflow from observed rainfall data for the planning, design, and management of water resources. In Vietnam, the Tank Model has been applied in many studies and is considered moderately suitable for river and stream systems.

The hydrological Tank Model used in this study has a simple structure with four tanks, a surface tank (A), an intermediate tank (B), a sub-base tank (C),

and a base tank (D) (Gunawan, 2010), laid vertically in a series, as shown in **Figure 3-9**. The two assumptions of the Tank Model are that (1) water is able to fill the storage that lies beneath and (2) water flows from a horizontal outlet in each tank and the total amount of water that flows represents runoff. Each tank has a vertical outlet at the bottom (except Tank D) and one horizontal outlet at the side (except Tank A, which typically has two horizontal outlets). Precipitation on the watershed minus evapotranspiration is entered into tank A and then falls partly through the vertical outlet into the tank below. The remainder of the rainwater pours into the horizontal outlets to create flow when the water level in the tank is higher than the height of a horizontal outlet (Ngoc *et al.*, 2011b).

The total outflow, $Q_{(t)}$, at time t from the side outlets of all tanks represents the accumulation of the outflows from the river system in the watershed and can be expressed as follows:

$$Q_{(t)} = \left\{ Q_{a1(t)} + Q_{a2(t)} + Q_{b(t)} + Q_{c(t)} + Q_{d(t)} \right\} \tag{3-8}$$

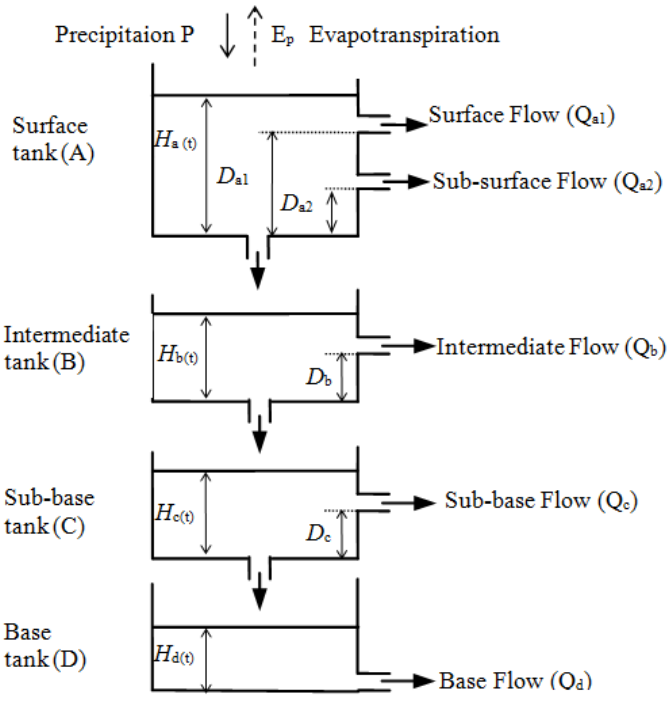

Figure 3-9: Structure of the Tank model

Given the initial conditions of the water levels in storage tanks A, B, C, and D at the initial time step, the storage in each tank is updated as follows:

$$H_{a(t+1)} = H_{a(t)} + P_{(t)} - E_i - Q_{a1(t)} - Q_{b(t)} - I_{a(t)} \quad (3\text{-}9)$$

$$H_{b(t+1)} = H_{b(t)} + I_{a(t)} - Q_{b(t)} - I_{b(t)} \quad (3\text{-}10)$$

$$H_{c(t+1)} = H_{c(t)} + I_{b(t)} - Q_{c(t)} - I_{c(t)} \quad (3\text{-}11)$$

$$H_{d(t+1)} = H_{d(t)} + I_{c(t)} - Q_{d(t)} \quad (3\text{-}12)$$

where H is water storage level (mm), P is precipitation (mm/day), E is evapotranspiration (mm/day), Q is total runoff (mm/day), and t is time step (day). I is infiltration through the vertical outlet into the tank below (mm/day).

Although the Tank Model provides some indication of the lag time between rainfall and runoff, this lag time is often insufficient. In rainfall runoff, when discharge increases quickly, velocity also increases. Therefore, lag time must decrease, which means that lag time is inversely proportional to velocity. In small watersheds, lag time often is short; even if velocity increases because of the change in discharge, and thus we can assume this lag time is constant (Sugawara, 1995). However, in large watersheds with a long lag time, we need to consider an artificial lag time, TL, of watershed discharge, as follows:

$$Q_{E(t)} = (1 - D_{(TL)}) \times Q_{(t+[TL])} + D_{(TL)} \times Q_{(t+[TL]+1)} \quad (3\text{-}13)$$

where $Q_{E(t)}$ is the calculated discharge, TL is lag time, $[TL]$ is the integer part of TL, and $D_{(TL)}$ is the decimal part of TL.

Table 3-4: Tank model parameters used for calibration

Parameter	Functions	Description	Lower limit	Upper limit
C_{A1}(1/h)	$Q_{A1(t)} = C_{A1} \times (H_{A(t)} - D_{A1})$	Surface runoff coefficient	0	1
C_{A2}(1/h)	$Q_{A2(t)} = C_{A2} \times (H_{A(t)} - D_{A2})$	Sub-surface runoff coefficient	0	1
C_{A0}(1/h)	$I_{A(t)} = C_{A0} \times H_{A(t)}$	Infiltration coefficient	0	1
C_{B1}(1/h)	$Q_{B(t)} = C_{B1} \times (H_{B(t)} - D_{B})$	Intermediate runoff coefficient	0	1
C_{B0}(1/h)	$I_{B(t)} = C_{B0} \times H_{B(t)}$	Infiltration coefficient	0	1
C_{C1}(1/h)	$Q_{C(t)} = C_{C1} \times (H_{C(t)} - D_{C})$	Sub-base runoff coefficient	0	1
C_{C0}(1/h)	$I_{C(t)} = C_{C0} \times H_{C(t)}$	Infiltration coefficient	0	1
C_{D1}(1/h)	$Q_{D(t)} = C_{D1} \times H_{D(t)}$	Base runoff coefficient	0	0.1
D_{A1}(mm)		Height of surface outlet	0	500
D_{A2}(mm)		Height of sub-surface outlet	0	500
D_{B}(mm)		Height of intermediate outlet	0	500
D_{C}(mm)		Height of sub-base outlet	0	500
SA(mm)		Initial storage of Tank A	0	500
SB(mm)		Initial storage of Tank B	0	500
SC(mm)		Initial storage of Tank C	0	500
SD(mm)		Initial storage of Tank D	0	1,000
SM(mm)		Limit moisture threshold	0	10
TL(h)		Time lag	0	72

3.3. Genetic algorithm method

The GA was originally developed and introduced in 1975 by John Holland (Chu-Tain *et al.*, 2006; Holland, 1975). It is a population-based optimization method that mimics the process of natural selection and natural evolution. The GA is used to search large, nonlinear spaces where expert knowledge is lacking or is difficult to encode8. The GA optimization search uses the idea of fitness to analyze a variety of solutions and generate a new and better solution.

The GA begins with a randomly generated initial set of solutions called the population. Each individual in the population is called a chromosome, a string of symbols that is encoded into binary code, which represents a solution to a problem. The chromosome develops through consecutive repetitive revolutionary processes, called generations. During each generation, the chromosomes are assessed by fitness function. Then, the chromosome passes through several main processes: selection, crossover, and mutation. To create the new generation, parent chromosomes with higher fitness values have higher probabilities of being selected. Then, crossover and mutation processes are conducted to reproduce new offspring. These processes are repeated and stop only when the condition is satisfied. After several generations, the fitter chromosomes converge to the best chromosome, which represents the optimal solution to the problem (see in **Figure 3-10**).

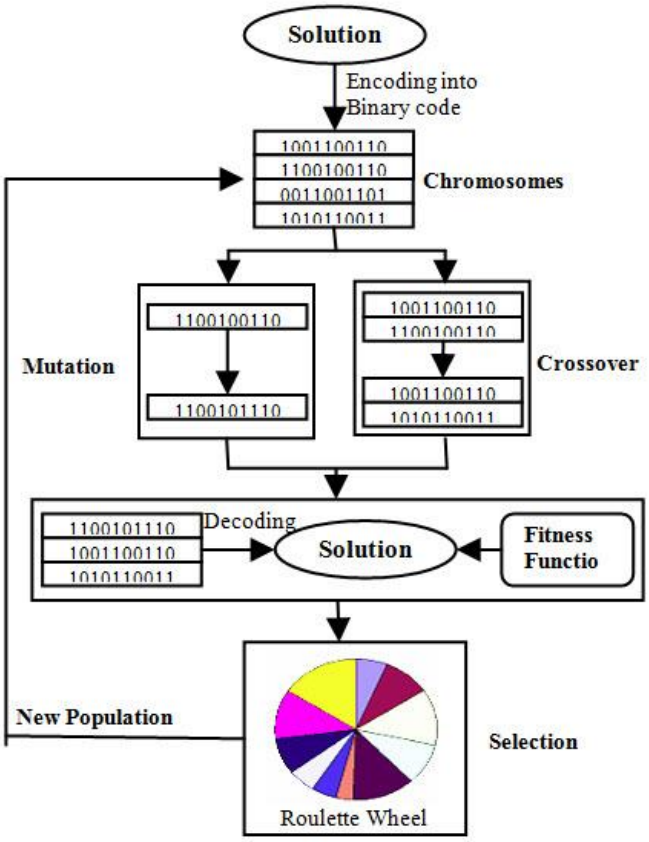

Figure 3-10: The general structure of GA

3.4. Fitness function and error indicators

In this study, fitness function was based on the error indicator mean square error (MSE). Fitness function was used to evaluate GA optimization performance in calibrating model parameters. The equation of fitness function, F_t, is given by equations (**4-14**) and (**4-15**).

$$\text{Maximum of } [F_t] = \text{Maximum of } \left[\frac{1}{MSE}\right] \tag{3-14}$$

$$MSE = \frac{\sum_{i=1}^{N}\left[Q_{\text{obs},\,i} - Q_{\text{sim},\,i}\right]^2}{\sum_{i=1}^{N}\left[Q_{\text{obs},\,i} - \overline{Q_{\text{obs}}}\right]^2} \tag{3-15}$$

where obs, i is the observed discharge at the i^{th} time step, sim, i is the simulated discharge at the i^{th} time step, $\overline{Q_{\text{obs}}}$ is the average of observed discharge, i is the time step (day), and N is the total number of time steps.

According to national forecasting criteria in Vietnam, the percentage error of peak discharge, peak time, and total runoff volume are important indicators that evaluate the accuracy of simulated discharge. In this study, a comparison of simulated discharge accuracy with observed discharge was expressed by the error indicators coefficient of correlation (R^2), Nash-Sutcliffe coefficient (E_2), mean absolute error (*MAE*), root mean square error (*RMSE*), and relative error (*RE*).

$$R^2 = \frac{\sum_{i=1}^{N}\left[\left(Q_{\text{obs},i} - \overline{Q_{\text{obs}}}\right)\left(Q_{\text{sim},i} - \overline{Q_{\text{sim}}}\right)\right]}{\sqrt{\sum_{i=1}^{N}\left[Q_{\text{obs},i} - \overline{Q_{\text{obs}}}\right]^2}\sqrt{\sum_{i=1}^{N}\left[Q_{\text{sim},i} - \overline{Q_{\text{sim}}}\right]^2}} \tag{3-16}$$

$$E_2 = 1 - \frac{\sum_{i=1}^{N}\left[Q_{\text{obs},i} - Q_{\text{sim},i}\right]^2}{\sum_{i=1}^{N}\left[Q_{\text{obs},i} - \overline{Q_{\text{obs}}}\right]^2} \tag{3-17}$$

$$MAE = \frac{1}{N}\sum_{i=1}^{N}\left|Q_{\text{obs},i} - Q_{\text{sim},i}\right| \tag{3-18}$$

$$RMSE = \sqrt{\frac{1}{N}\sum_{i=1}^{N}\left[Q_{\mathrm{obs},i} - Q_{\mathrm{sim},i}\right]^2} \tag{3-19}$$

$$RE_i = \left|\frac{Q_{\mathrm{obs},i} - Q_{\mathrm{sim},i}}{Q_{\mathrm{obs},i}}\right| \times 100\% \tag{3-20}$$

$$VE_i = \frac{\left[\sum_{i}^{N}(Q_{\mathrm{Sim},i} \times 86400) - \sum_{i}^{N}(Q_{\mathrm{Obs},i} \times 86400)\right]}{\sum_{i}^{N}(Q_{\mathrm{Obs},i} \times 86400)} \times 100\% \tag{3-21}$$

3.5. Results

The GA optimization search was combined into the parameter calibration of two hydrological models (GA–NAM and GA–Tank). Unlike other search techniques, GA optimization generally is conducted among a population using a coded parameter set and the probabilistic rules of roulette wheel selection. A GA optimization set consists of four parameters: crossover probability, mutation probability, population size, and maximum number of generations.

The crossover probability parameter controls the frequency of the crossover operation. If the crossover probability value is too large, the structure of a high-quality solution could be damaged quickly; if the crossover probability value is too small, search efficiency may be low. Generally, the crossover probability parameter is between 0.5 and 0.8. The mutation probability parameter is a critical factor that can lead to a new search direction in the solution space and extension of population diversity. If this parameter is too small, new gene segments may not be inducted; if this parameter is too large, genetic evolution degenerates into a random local search. Generally, the mutation probability parameter is between 0.001 and 0.1. The population size parameter significantly affects solution quality and GA efficiency. If this parameter is too large, computation time exceeds a tolerable limit and convergence time is prolonged.

Generally, the population size parameter is between 150 and 300 (Chu-Tian *et al.*, 2006).

Table 3-5: Parameters used for genetic operations

Bit-length for one parameter	16
Population size	150
Generation	2,000
Crossover rate	0.7
Selection method	Roulette Wheel
Mutation rate	0.01

Table 3-6: Calibrated NAM model parameters

Parameter	Year 1995	Year 2000
U_{max}(mm)	31.05	22.99
L_{max}(mm)	233.94	345.90
CQ_{OF}(-)	0.23	0.75
CQ_{IF}(h)	329.78	200.00
T_{OF}(-)	0.22	0.57
T_{IF}(-)	0.35	0.07
CK_1(h)	27.01	17.30
CK_2(h)	64.01	40.90
T_G(-)	0.44	0.001
CK_{BF}(h)	4,875.10	4,069.52

To select a set of GA parameters, correlations among them were considered, as mentioned above, and test runs for calibration data were conducted, as shown in **Table 3-5** (Ngoc *et al.*, 2011b). The lower and upper limits of each parameter for two hydrological models that define the GA search domain are also shown in **Table 3-4**.

For model calibration, the boundaries for GA operations shown in **Table 3-3** and **3-4** were applied to the optimization search for two typical years, 1995 and 2000. NAM Model and Tank Model parameters calibrated by GA optimization are shown in **Table 3-6** and **Table 3-7**, respectively, and the results of error indicators by the GA optimization search are compared for the NAM and the Tank Models in **Table 3-8**.

Table 3-7: Calibrated Tank model parameters

Parameter	Year 1995	Year 2000
C_{A1}(1/h)	0.38	0.17
C_{A2}(1/h)	0.52	0.79
C_{A0}(1/h)	0.88	0.59
C_{B1}(1/h)	0.65	0.51
C_{B0}(1/h)	0.60	0.09
C_{C1}(1/h)	0.47	0.14
C_{C0}(1/h)	0.48	0.07
C_{D1}(1/h)	0.0018	0.0014
D_{A1}(mm)	269.60	242.80
D_{A2}(mm)	203.46	130.49
D_{B}(mm)	346.70	427.83
D_{C}(mm)	418.52	264.15
SA(mm)	87.36	139.68
SB(mm)	126.29	36.34
SC(mm)	252.60	12.55
SD(mm)	435.24	553.7
SM(mm)	3.00	1.62
TL(h)	8.15	3.17

Table 3-8: Results of error indicators for the GA–NAM and GA–Tank models

Error indicators	GA- NAM				GA-Tank			
	Calibration		Validation		Calibration		Validation	
	1995	2000	1998	2001	1995	2000	1998	2001
R	0.86	0.93	0.91	0.91	0.90	0.93	0.88	0.92
E_2	0.72	0.86	0.82	0.82	0.80	0.86	0.77	0.83
MSE	0.28	0.14	0.18	0.18	0.20	0.14	0.23	0.17
RMSE	1.66	2.27	1.68	0.18	1.39	2.29	1.88	1.67
Max.*RE* (%)	34.80	19.07	31.71	41.59	28.22	30.44	29.73	28.87
MAE	3.13	6.90	3.23	1.20	1.70	0.47	1.71	7.05
Observed peak flow (m^3/s)	464.37	1,078.40	579.12	409.34	464.37	1,078.40	579.12	409.34
Observed peak time	9/22	10/10	9/30	10/30	9/22	10/10	9/30	10/30
Simulated peak flow (m^3/s)	421.00	981.73	459.33	348.60	429.89	965.63	529.10	381.95
Simulated peak time	9/22	10/10	9/30	10/30	9/22	10/10	9/30	10/30
Peak flow error (m^3/s)	43.37	96.67	119.80	60.74	34.47	112.77	50.02	27.39
RE of peak flow (%)	9.34	8.96	20.69	14.84	7.42	10.46	8.64	6.69
Observed volume (10^9 m^3)	1.49	2.52	1.88	2.88	1.49	2.52	1.88	2.88
Simulated volume (10^9 m^3)	1.40	2.30	1.78	2.84	1.55	2.50	1.94	3.10
Volume error (%)	-6.61	-8.64	-5.41	-1.32	3.58	-0.59	2.85	7.73

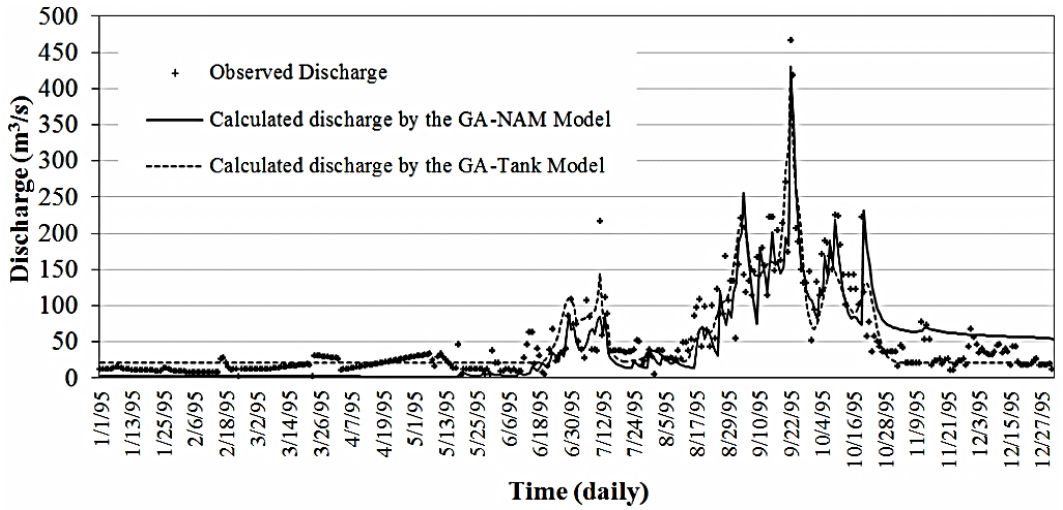

Figure 3-11: Model calibration of daily discharges in 1995

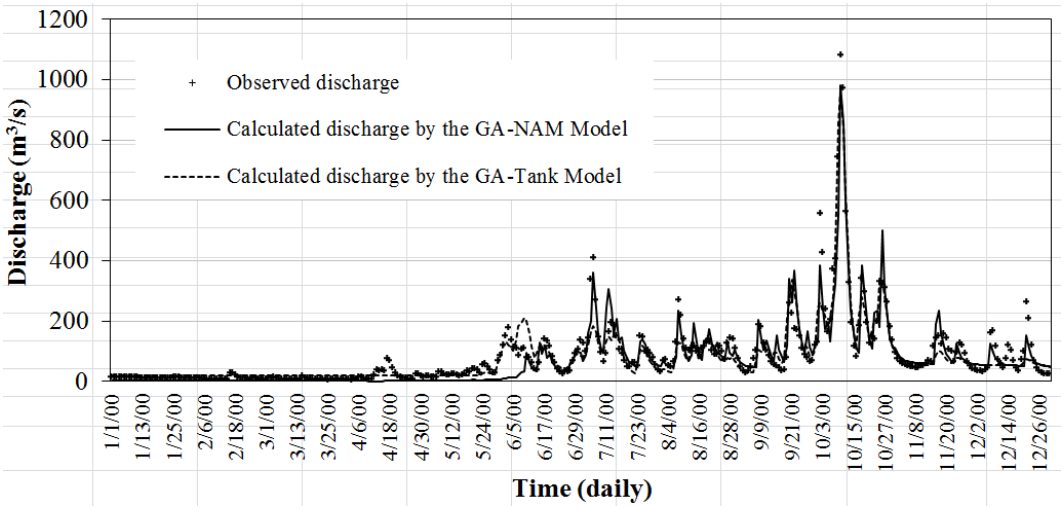

Figure 3-12: Model calibration of daily discharges in 2000

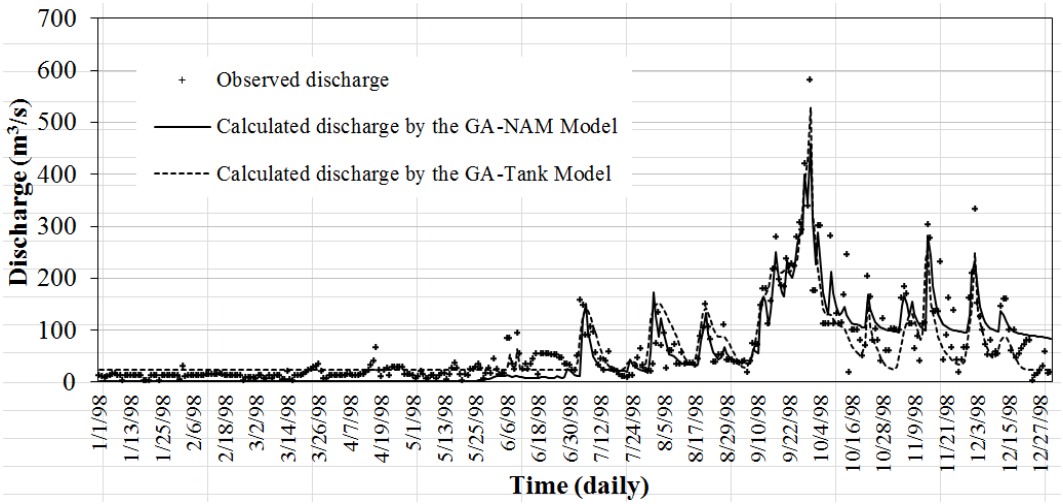

Figure 3-13: Model validation of daily discharges in 1998 using calibrated parameters in 2000

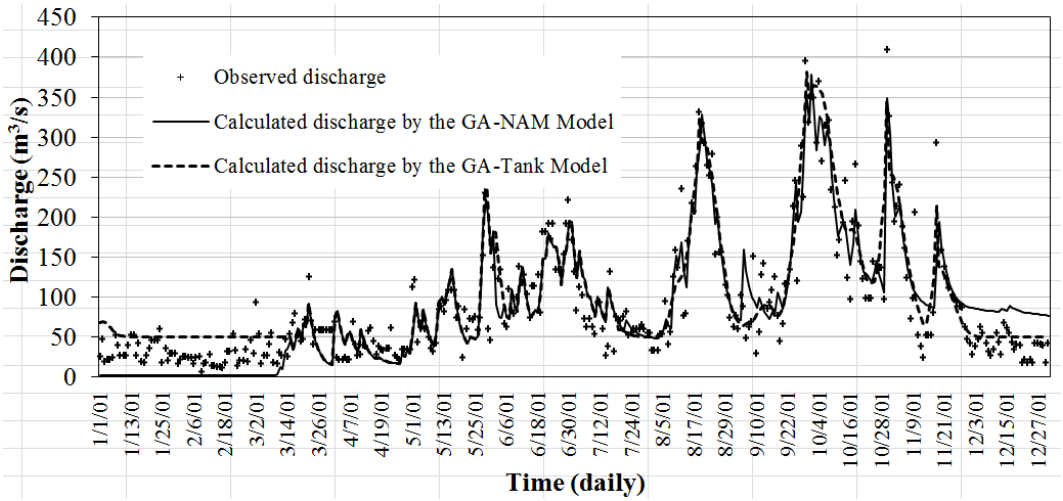

Figure 3-14: Model validation of daily discharges in 2001 using calibrated parameters in 2000

Table 3-9: Average efficiency coefficients of the GA–Tank and GA–NAM models

Coefficiency	GA-NAM	GA-Tank
R	0.90	0.90
E_2	0.80	0.82

3.5.1. Results of GA-NAM Model

Table 3-8 and **Figure 3-11** and **Figure 3-12** indicate that the results of two calibrated years showed similar performance with acceptable accuracy in simulated flow hydrographs. However, the calibrated parameters of the GA–NAM Model were different between 1995 and 2000 (see Table 3-8); for example, the parameters U_{max}, L_{max}, CQ_{OF}, T_{OF}, T_{IF}, and T_G were 31.05, 233.94, 0.23, 0.22, 0.35, and 0.44, respectively, for 1995 and 22.99, 345.90, 0.75, 0.57, 0.07, and 0.001, respectively, for 2000. In addition, U_{max} was higher in 1995 than in 2000, indicating that surface-water storage capacity was larger in 1995 than in 2000. Meanwhile, CQ_{OF} and T_{OF} were lower in 1995 than in 2000, showing that the rate of contributed overland flow was lower in 1995 than in 2000. Because 1995 represented dry hydrological years with rainfall less than the annual average, the amount of potential water in surface storage increased, contributed overland flow decreased, and root threshold capacity for groundwater recharge was high. Conversely, 2000 represented hydrological years with rainfall slightly higher than annual average rainfall; therefore, the rate of contributed overland flow was higher (U_{max} was lower, CQ_{OF} and T_{OF} were higher) and the amount of potential water in surface storage (L_{max} was higher) was lower in 2000 than in 1995.

According to calibration results of the GA–NAM Model presented in **Table 3-8**, the error indicators R, E_2, and MSE were 0.86, 0.72, and 0.28, respectively, in 1995 and 0.93, 0.86, and 0.14, respectively, in 2000, showing that all error indicators were lower in 2000 than in 1995. In particular, max.RE and RE of peak flow values were 19.07% and 8.96%, respectively, in 2000 and were lower than 1995 values (34.80% and 9.34%, respectively). These results demonstrate that the simulated discharge of the GA–NAM model was more robust and accurate in 2000 than in 1995. Thus, the calibrated parameters produced in 2000 were selected for validation.

The GA–NAM Model validation results are shown in **Figure 3-13** and **3-14** and in **Table 3-8**. The GA–NAM Model achieved good agreement between

observed and simulated flow hydrographs in the validation as well as in the calibration. In the validation, the error indicators R = 0.91, E_2 = 0.82, and MSE = 0.18 were obtained in 1998 and 2001, showing that the calibrated parameters in 2000 (R = 0.93, E_2 = 0.86, and MSE = 0.14) provided a versatile model, although accuracy was slightly lower. The volume errors in the two validated years, 1998 and 2001, were −5.41% and −1.32%, respectively, and were less than the volume error in 2000 (−8.64%). We concluded that the calibrated parameters obtained in 2000 provided stabilizing and versatile forecasts for the NAM model.

3.5.2. Results of GA-Tank Model

Table 3-7 shows the calibrated parameters of the GA–Tank Model, and **Table 3-8**, **Figure 3-11** and **Figure 3-12** show the comparisons between simulated and observed flow hydrographs in the calibration. The calibrated parameters in 2000 resulted in the error indicators R = 0.93, E_2 = 0.86, MSE = 0.14, $RMSE$ = 2.29, and RE = 30.44, as shown in **Table 3-8**, indicating that simulation results were more accurate in 2000 than in 1995. The calibrated parameters in 1995 also gave good agreement in a comparison between observed and simulated discharges. However, the parameters obtained in the two calibrated years were different, especially for C_{A1}, C_{A2}, C_{A0}, C_{B1}, C_{B0}, C_{C1}, C_{C0}, D_{A1}, D_{A2}, D_B, and D_C. The values for parameters C_{A0}, D_{A1}, and D_{A2} were 0.88, 269.60, and 203.46, respectively, in 1995 and were higher than the values obtained in 2000 (0.59, 242.80, and 130.49, respectively) because the potential amount of water in the surface Tank was relatively higher in 1995 than in 2000. C_{A2} was 0.58 in 1995 and 0.79 in 2000, which means that subsurface flow from the Tank Model was larger in 2000 than in 1995 for reasons similar to those for the GA–NAM Model. In 1995, which represented dry hydrological years, the ratios of intermediate flow and sub-base flow to total outflow increased and the ratio of surface flow decreased compared to ratios in 2000. This result was reflected in the calibrated parameters C_{A0} = 0.88, C_{B1} = 0.65, C_{B0} = 0.60, C_{C1} = 0.47, C_{C0} = 0.48, D_B = 346.70, and D_C = 418.52 in 1995 and C_{A0} = 0.59, C_{B1} =

0.51, C_{C1} = 0.09, C_{C0} = 0.14, D_B = 0.07, and D_C = 264.15 in 2000. Based on the calibration results of the GA–Tank Model in 1995 and 2000, shown in **Table 3-7**, the calibrated parameters in 2000, shown in **Table 3-8**, were selected to validate the model in 2 years, 1998 and 2001. Comparisons between simulated and observed flow hydrographs for 1998 and 2001 are shown in **Figure 3-13** and **Figure 3-14** as the validation results. The simulated flow hydrographs using the parameters obtained in calibration year 2000 had good agreement with observed hydrographs. The error indicators in validation years 1998 and 2001 showed almost the same accuracy as those in calibration year 2000. We concluded that the calibrated parameters in 2000 provided stabilizing and versatile forecasts for the Tank Model.

3.5.3. Comparison of GA–Tank and GA–NAM Models

The GA–NAM and GA–Tank Models have similar internal structures. In the GA–NAM Model, overland flow is the flow produced by the excess capacity of the upper storage representing initial abstraction and interception loss. In the GA–Tank Model, surface flow is the outflow from the side outlets of the surface tank. The parameter SM in the GA–Tank Model has some similarity with the parameter U_{max} in the GA–NAM Model. These parameters are filled before infiltration is initiated.

The intermediate flow in the GA–Tank Model is the outlet of the intermediate tank. It is also similar to the interflow in the GA–NAM Model, which is proportional to the amount of water in surface storage and varies linearly with the relative soil moisture content of the lower zone storage. In this flow, the parameters C_{B1} in the GA–Tank Model and T_{IF} in the GA–NAM Model represent the same types of interflow thresholds.

In the routing of flow components, total outflow in the GA–Tank Model is the summation of outflows from the side outlets of all tanks. In the GA–NAM Model, overland flow and interflow are routed through 2 linear reservoirs, and groundwater flow is routed through a single linear reservoir. These flow

components are represented by adding up and routing through a final single linear reservoir to produce a total runoff at the outlet point of the watershed.

Based on these similarities in structure, the GA–NAM Model and the GA–Tank Model produced similar calibrated parameters. In 1995, calibrated parameter values were U_{max} = 31.05 and T_{IF} = 0.35 in the GA–NAM Model and SM = 3.0 and C_{B1} = 0.65 in the GA–Tank Model and were higher than calibrated parameter values in 2000 (U_{max} = 22.99 and T_{IF} = 0.07 in the GA–NAM Model and SM = 1.62 and C_{B1} = 0.51 in the GA–Tank Model).

The values of R and E_2 are essential coefficients to estimate model performance, and **Table 3-9** shows the average values of R and E_2 over the calibration and validation processes. In the GA–Tank Model, the mean values of R and E_2 were 0.90 and 0.82, respectively, and were slightly higher than the mean values of 0.90 and 0.80, respectively, in the GA–NAM Model.

The indicators peak flow, peak time, and volume error also are important for evaluation of model performance. As shown in **Table 3-8**, the peak flow errors of simulated flow were higher in the GA–NAM Model (119.80 in 1998, 60.74 in 2001) than in the GA–Tank Model (50.02 in 1998, 27.39 in 2001). These results indicate that the Tank Model with the GA optimization search was a better model than the GA–NAM Model for simulating daily runoff in the Dautieng River Watershed.

3.6. Restoration of inflow to Dautieng Reservoir Watershed

As above-concluded results, the calibrated parameters of two hydrological models, the Tank and the NAM Models in 2000, were used for simulation with a 25-years period (1983-2008). As shown in **Figure 3-15** and **Figure 3-16**, the simulated peak flow of the NAM Model was delayed in comparison with the observed peak flow. However, the Tank Model led to good agreement between the hydrograph of the simulated flow and that of the observed flow, with the same peak time and similar peak values.

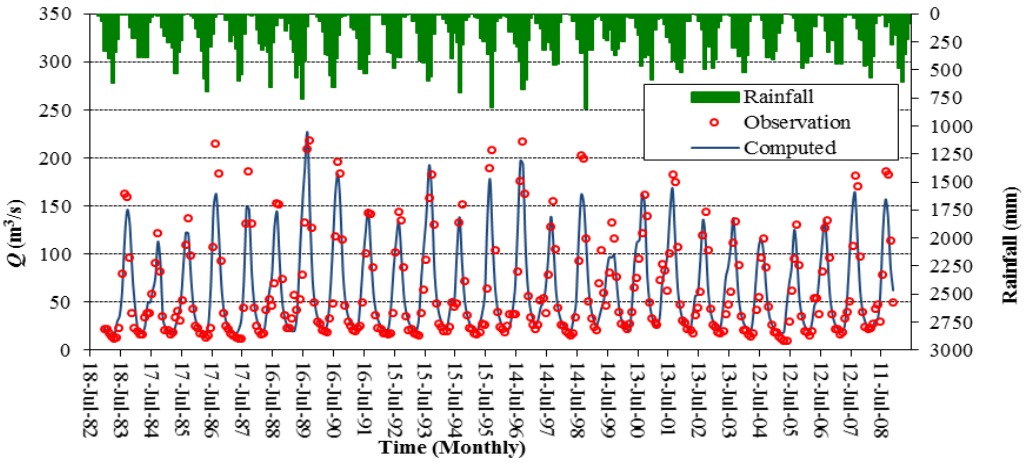

Figure 3-15: Comparison between observed and simulated flows in 1983–2008 with the NAM model

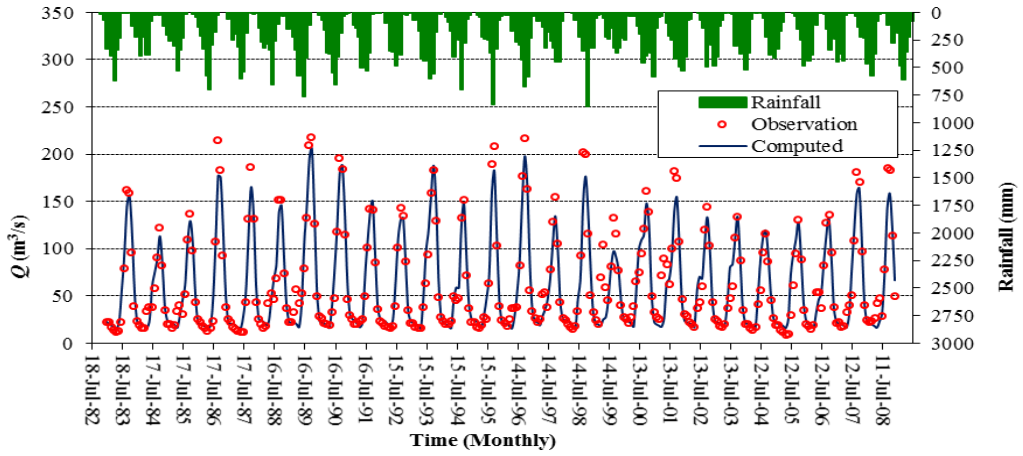

Figure 3-16: Comparison between observed and simulated flows in 1983–2008 with the Tank model

3.7. Conclusions

In this chapter, GA, a powerful optimization technique, was integrated to the NAM and Tank Models and applied to discharge simulations during discharge periods in the Dautieng River Watershed. Thus, GA was enhanced to perform a search of optimal parameters for two hydrological models by comparing hydrograph shapes of simulated flow, observed flow, and error indicators.

Although the GA–NAM and GA–Tank Models have some basic structural differences, they are similar in terms of basic conceptualization (Tawatchi *et al.*, 2000). The GA–NAM Model has fewer model parameters than the GA–Tank Model, but the calibration process by the GA optimization search was conducted with multiple generations (2000 generations in this study). The GA–Tank Model has not many parameters (18); thus, applying the limit of the GA optimization search was not important.

In a comparison of the two hydrological models, calibration and validation results were similar, although error indicators showed that performance was slightly higher in the GA–Tank Model than in the GA–NAM Model. Most errors caused a high Max.*RE* value because flow peaks and volume error were not captured.

The results of this study showed the ability to simulate the models under each condition. However, GA–Tank and GA–NAM models performance is highly dependent on input data quality and specific characteristics of the rainfall periods, and model results control simulated output accuracy in terms of timeliness and magnitude.

CHAPTER IV

OPTIMIZING MULTI-USE DAUTIENG RESERVOIR OPERATION AND PROPOSING A FRAMEWORK OF OPERATING RULE CURVES

4.1. Background

Reservoir is one of the most efficient measures to develop and manage integrated water resources and has become the most important facility to increase the reliability for water supplies to various purposes such as, agriculture, industry, human activities, and environmental base flow requirements, and reduce the vulnerability to water users in droughts (Guo *et al.*, 2004; Wei and Hsu, 2005; Wei and Hsu, 2007). In past decades, water has become a scarce resource as result of the growing demand for various purposes (Li *et al.*, 2010), and water shortages have been occurring more serious due to restriction of effective water use. To overcome the problem of water shortage during period of dry season, researchers have been focused attention on improving water resources management, especially in optimization of reservoir operations (Chang *et al*., 2005; Chen *et al*., 2007), and thus the rule curves of reservoir operation are very important way to support operators in making decisions of operating policies effectively.

The aim of this study was to design a reservoir operation model and optimize reservoir operation rule curves by using a genetic algorithm with a penalty strategy for multi-use water resources management including environmental base flow requirements and flood control storage. The methodology of the proposed model was incorporated constrained genetic algorithm (CGA) where water demands where were assumed as constraints to

water storage discharge of reservoir operation. The penalty functions designed for various constraints were integrated into the objectives of operation process to form the fitness function. The model performance was evaluated through a generalized shortage index (GSI) to water demands.

4.2. Model structure combined CGA search

The genetic algorithm is originally developed and introduced in 1975 by John Holland (Holland, 1975). It is a population-based optimization method that mimics the process of natural selection and natural evolution. The GA is used to search large, nonlinear spaces where expert knowledge is lacking or is difficult to encode (Chu-Tian *et al.*, 2006). The GA optimization search uses the idea of fitness to analyze a variety of solutions and generate a new and better solution. The GA begins with a randomly generated initial set of solutions called the population and progresses to enhance the fitness of solutions through interaction by conducting operators including selection, crossover and mutation operators. However, the restrictions of unfeasible search space by constrained conditions were encountered difficult problems in GA optimization, which would usually engender early convergences or ineffective searches.

During the past few years, several methods such as rejection, repair, and penalization strategies, have been presented for handling constraints when using GA to solve constrained optimization problems (Deep and Dipti, 2008). The advantage of the rejection and repair approaches was that only feasible solutions were generated. Thus, most popular approaches to handling constraints in the GA community were to use penalty functions (Chang, 2008). The strategy by means of penalty functions was set to penalize infeasible solutions in attempt to reduce their fitness values in proportion when constraint violations were found. Following this way, they lead the search direction towards promising solutions. Unfortunately, the constraints that were interior penalty functions played as barriers to impeding the capability of GA search within the feasible domain

(Abedian *et al*., 2006). This was the reason why it was unable to be incorporated into GA. When constraints were exterior penalty functions, a penalty values were designed to add to violated solutions by taking the number of violated constraints and their distance to the feasible domain into account (Chang *et al.*, 2008). The most common methods for using GA with penalty strategy were written in nonlinear programing as follows:

$$F(\vec{\mathrm{x}}) = \begin{cases} f(\vec{\mathrm{x}}) & \vec{\mathrm{x}} \in \text{feasible region} \\ f(\vec{\mathrm{x}}) + p(\vec{\mathrm{x}}) & \vec{\mathrm{x}} \notin \text{feasible region} \end{cases} \tag{4-1}$$

where $f(\vec{x})$ is the objective function and $p(\vec{\mathrm{x}})$ is the penalty function. Nevertheless, there is no common guideline indicated how to find a suitable and effective penalty function. Generally, the equation of the penalty function was designed as follows:

$$p(w) = \sum_{i=1}^{N} \sum_{j=1}^{M} p_{ji}(\mathrm{w}_i) = (W_i^z - W_i) \times K^z \tag{4-2}$$

where z is the object is constrained as water level limits. *M* is a total number of sub penalty functions constructed to model. *K* is a penalty weight of equality constraints. $p_{ji}(w_i)$ is the sub penalty function. W_i is water storage (m^3). *N* is the total years using for simulation. W_i^z is water storage corresponding to water limit based on the rule curves of Dautieng Reservoir.

The flow chart of structure of the proposed model combined CGA search is shown in **Figure 4-1**.

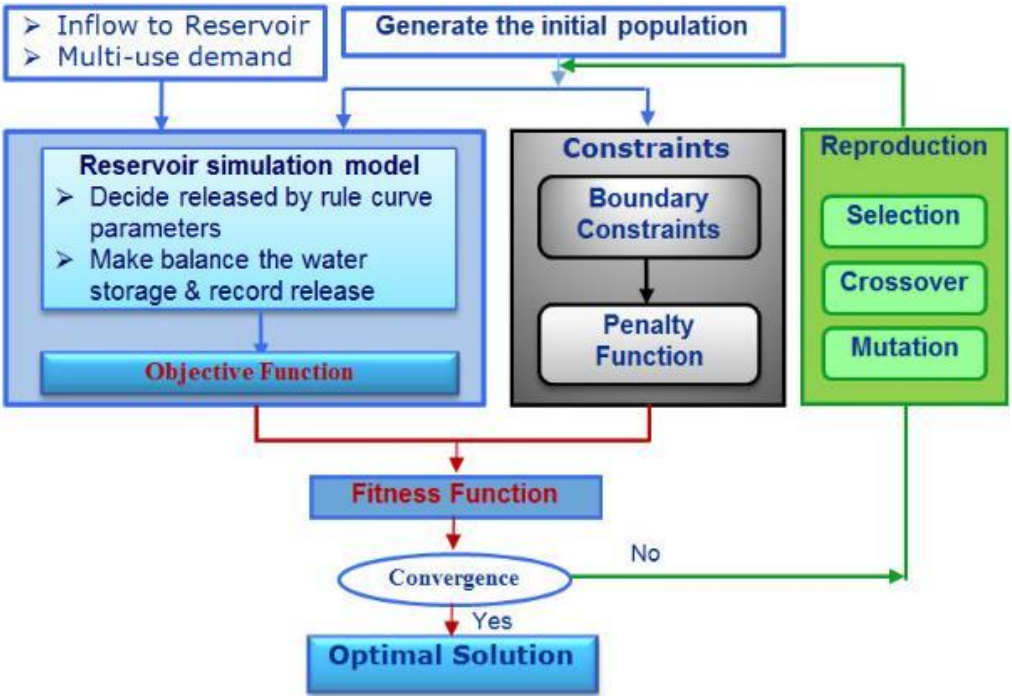

Figure 4-1: Structure of the proposed model combined CGA search

4.3. The reservoir operation formulation and constraints

4.3.1. Water reservoir storages and water supplies

Dautieng Reservoir, which was constructed from 1981 and completed in 1985 by credit fund of World Bank (WB), is one of the biggest reservoir in Vietnam, especially in south of Vietnam. The Dau Dieng Reservoir has a total storage capacity of $2.2\times10^9 m^3$ and an effective storage capacity of 1.57×10^9 m^3. There are four provinces in the downstream area: Tay Ninh, Binh Duong, Long An and Ho Chi Minh City, with a total direct irrigation area of about $640km^2$ and several human water demand facilities in the benefited downstream area. The reservoir was designed to gain the goals where its priorities are in descending order as follows: (1) flood control; (2) human demands including domestic and industrial demands; (2) pushing salt water intrusion in downstream area of Ho Chi Minh City; (4) agriculture irrigation. In these sense, this reservoir operation

have been operated obeying the Dautieng Reservoir operating rule curve (DTOR) (MARD, 1995).

The minimum flow requirements are generally comprehended as a minimum water flow that significantly prevents an injury to the regional ecosystem. Basically, the determination of the minimum base flow requirement should be based on a wide variety of existing information, including biological and topographical information, scientific literature, and water flow data to estimate overall impacts of flow amount on aquatic communities and regional environment (Chang *et al*., 2010). The minimum base flow requirement used in this study was proposed for the water resources management by MARD and the Ministy of Natural Resources and Environment of Vietnam (MONRE) that mainly serves for pushing salt water intrusion in the downstream of Dautieng Reservoir area. The above minimum base flow requirement is also understood as environmental flow requirements that follows to the guideline of MONRE, Vietnam. **Table 4-1** shows the expected cases of minimum ecological flow requirements in dry season during the period of January – May.

Table 4-1: The expected minimum environmental base flow requirements for the Saigon River

Case	Environmental base flow requirement	Methods	References
1	$30m^3/s$ in dry season	Historical flows during period of 1989-2008	Rule regulations of handbook (MARD, 1995)
2	$50m^3/s$ in dry season	Considering the needs for preventing salt water intrusion in the downstream Ho Chi Minh City area	EIA on Water quality of the Saigon River 2006-2008 (MONRE, 2009)
3	$35m^3/s$ in dry season $15m^3/s$ in wet season	Considering the needs for preventing salt water intrusion and improving water quality in the Saigon River	In this study

The existing DTOR approved by MARD consists of four curves: the retarding water level (RWL), the upper water level (UWL), the lower water level (LWL), and the critical water level (CWL) (**Figure 4-2**). Based on the DTOR, the operating regulation can be summarized as follows:

- When the water level in the reservoir reaches at the retarding water level, the spillway is immediately opened in attempt to rapidly reduce the water level to the upper water level.
- When the water level in the reservoir exceeds the upper water level, the water release should be kept the high priority in attempt to maintain the water level at the upper water level.
- When the water level in the reservoir is between the lower water and the critical water levels, the water release is restricted. In this case, the water supply should be satisfied for human demand and cut down for agriculture demand.
- When the water level in the reservoir is below the critical water level, agricultural water demand must be critically cut down in attempt to maintain the water level above the dead water level, but the water supply remains for satisfiable human demands.

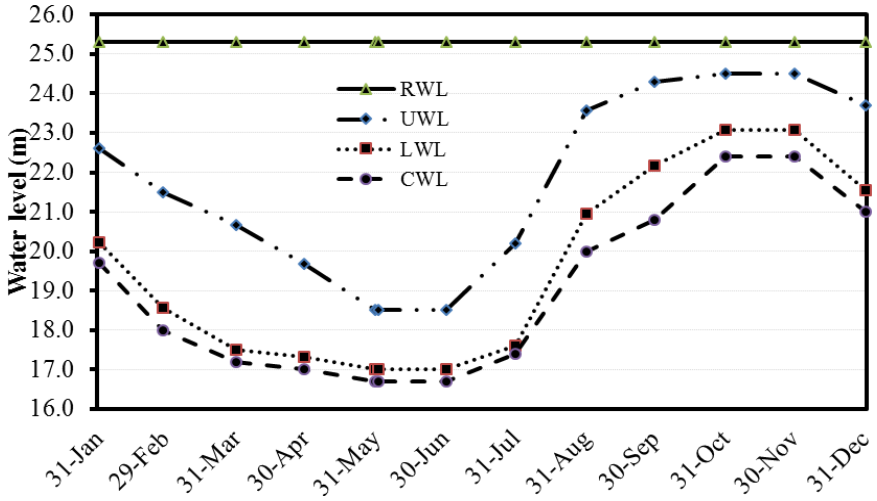

Figure 4-2: The rule curves of Dautieng reservoir operation (DTOR)

4.3.2. The reservoir operation model

The reservoir operation simulation modeling was developed to describe the reservoir behaviors. This model was designed on the basic concept of water balance equation and is written as follows:

$$W_i = W_{(i-1)} + W_i^{\text{Inflow}} - E_i - R_i \tag{4-3}$$

where: W_i is the water storage at i^{th} period; W_{i-1} is the water storage in $(i\text{-}1)^{\text{th}}$ period; W_i^{Inflow} is the water volume by rainfall runoff at i^{th} period; E_i is the evapostranpitation at i^{th} period; and R_i is the water release at i^{th} period as expressed as below:

$$R_i \begin{cases} R_i^{\text{Agr}} + R_i^{\text{Ind}} + R_i^{\text{Dom}} + R_i^{\text{Env}} & W_{i-1} \le W_i^{\text{Upper}} \\ R_i^{\text{Agr}} + R_i^{\text{Ind}} + R_i^{\text{Dom}} + R_i^{\text{Env}} + R_i^{\text{Spil}} & W_{i-1} > W_i^{\text{Upper}} \end{cases} \tag{4-4}$$

where: R_i^{Agr} , R_i^{Ind} , R_i^{Dom} , R_i^{Env} , R_i^{Spil} are the water release that supply corresponding to agricultural, industrial, domestic, environmental demands, and the released water from spillway gate to avoid breakdown of reservoir, and W_i^{Upper} is the upper limit at i^{th} period corresponding to the upper water level in the rule curves of reservoir operation. Supply priorities of water users were set in the descending order: domestic, ecological, industrial and agricultural supply. It means that, the water demand with low priority was only supplied until the water demand with high priority have been received plentifully.

4.3.3. Constraints

The reservoir were operated following the regulations of reservoir operation curves promulgated by MARD and complying with physical characteristic limitations such as water balance and permissible terms of water storages and releases.

$$W^{\text{Dead}} \le W_i \le W^{\text{Max}} \tag{4-5}$$

$$W_i \le W^{\text{Upper}} \quad (\text{wet season}) \tag{4-6}$$

$$W_i \geq W^{\text{Lower}} \quad \text{(dry season)} \tag{4-7}$$

$$W_i^{\text{wet}} \geq 0.9\text{W}_0^{\text{wet}} \quad \text{at the last period in each wet season} \tag{4-8}$$

$$\text{W}_i^{\text{dry}} \leq \text{W}_0^{\text{dry}} \quad \text{at the last period in each dry season} \tag{4-9}$$

where W_0^{wet}, is the water storage limit that must be maintained at the last each wet season in attempt to avoid long term water shortage in next dry season, and W_0^{dry} , is the water storage limit that must be kept water to serve for retarding flood flow in each wet season.

4.3.4. Objective function

The objective function was designed by considering different water demands in order to avoid long term water insufficiency and highly attach special importance to short term water insufficiency. It consisted of total water demands of different users in the downstream of the Dautieng Reservoir area including environmental base flow requirement. Hence, the objective function should be considered as core to meet total water demands of different users and anticipate serious water shortages, while each different water demand and the enforced terms based on the rule curves were considered as constraints when optimizing the reservoir operation. Moreover, the water shortage occurring for a long time might cause inconvenience for users, and the result eventually damages agriculture crops, ecosystem and industrial manufacturing, etc. Therefore, the objective function was defined as the deficit in each period to the power of the number of continuous water insufficiency period, and formulated as follows:

$$f_{\text{ob}}(\text{w}) = \min\left[f_{\text{Env}}(\text{w}) + f_{\text{agr}}(\text{w}) \right] \tag{4-10}$$

The purpose is to maintain the ecological base flow requirements, when the water release is less than the ecological base flow requirement (for pushing salt water intrusion in downstream), $W_i < W_i^{Env}$, the sub-objective function was set as follows:

$$f_{\mathrm{Env}}(\mathrm{w}) = \sum_{j=1}^{20} \max \left\{ \sum_{i=1}^{12} \left[\left(W_{ji}^{\mathrm{Env}} - W_{ji}^{\mathrm{Release}} \right) \right]^{\mathrm{n}_{ji}} \times K^{\mathrm{Env}} \right\} \quad (4\text{-}11)$$

The purpose is to supply water for agricultural demand, when $W_i < W_i^{\mathrm{Agr}}$, the sub-objective function was set as follows:

$$f_{\mathrm{Agr}}(\mathrm{w}) = \sum_{j=1}^{20} \max \left\{ \sum_{i=1}^{12} \left[\left(W_{ji}^{\mathrm{Agr}} - W_{ji}^{\mathrm{Release}} \right) \right]^{\mathrm{n}_{ji}} \times K^{\mathrm{Agr}} \right\} \quad (4\text{-}12)$$

where: W_i^{Release}, W_i^{Env}, W_i^{Agr}, n_i are corresponding to water release of reservoir, ecological flow requirement, agricultural demand and the number of continuous deficit period, respectively. K^{Env}, K^{Agr} are weighed factors corresponding to ecological and agricultural factor, respectively. In this study, the model was simulated for 20 years with the monthly step (12 month in a year).

4.4. Penalty and fitness function

The constraints were divided and placed into the penalty functions. The constraints corresponding to **Eq.4-5** interne the search space to the designed ranges. The constraints corresponding to **Eqs.4-6,7,8,9** are allowed to punish by penalty functions when the obtained variants in the model violate terms of designed penalty mechanism throughout decreasing the fitness values. By this way, the constraints will lead the CGA towards a feasible solution space in the search process. Furthermore, in the computation process, when various genes reach the limits of conditions, the respective penalties are strictly put into the fitness function to promptly reduce the fitness value. Following this way, the penalty function (Eq. 4-15) was combined to the fitness function as defined as bellow:

$$F(\vec{w}) = f_{\mathrm{ob}}(\vec{w}) P(\vec{w}) \quad (4\text{-}13)$$

$$P(\vec{w}) = 1 + \sum_{i=1}^{N} \sum_{j=1}^{M} p_{ji}(\vec{w}) \quad (4\text{-}14)$$

$$p_{ji}(\vec{x}) = \begin{cases} 0 & \text{x} \in \text{feasible region} \\ p_{ji}(\vec{x}) & \text{x} \notin \text{feasible region} \end{cases} \quad (4\text{-}15)$$

The sub penalty functions (**Eqs. 4-16** to **4-22**) were designed as follows:

In wet seasons, the purpose was to keep up the water at a certain level to serve flood control in wet season period, when $W_i > W_i^{\text{Upper}}$ then the penalty function was set as:

$$p_{2i}(w) = \left(W_i - W_i^{\text{retard}}\right) \times K^{\text{retard}} \quad (4\text{-}16)$$

However, the purpose was to always keep the water level below the retarding water level to avoid reservoir breakdown, when $W_i > W_i^{\text{retard}}$, then the penalty function was set as:

$$p_{2i}(w) = \left(W_i - W_i^{\text{retard}}\right) \times K^{\text{retard}} \quad (4\text{-}17)$$

In dry seasons, the purpose was to hoard up the water at a certain level to prevent water shortage, when $W_i < W_i^{\text{Lower}}$ then, the penalty function was:

$$p_{3i}(w) = \left(W_i^{\text{Lower}} - W_i\right) \times K^{\text{Lower}} \quad (4\text{-}18)$$

The purpose was to avoid water shortage in long term; the water storage should be hoarded up at a certain level all the time. When $W_i < W_i^{\text{Critical}}$, then the penalty function was set as:

$$p_{4i}(w) = \left(W_i^{\text{Critical}} - W_i\right) \times K^{\text{Critial}} \quad (4\text{-}19)$$

This reservoir was operated for regulation in several years, hence, to avoid water shortage in long term. When $W_i^{\text{Wet}} < W_0^{\text{Wet}}$, then penalty function was set as:

$$p_{5i}(w) = \left(0.9W_0^{\text{Wet}} - W_i^{\text{Wet}}\right) \times K^{\text{Wet}} \quad (4\text{-}20)$$

And to maintain water storage space in wet season in attempt to retarding flood flow. When $W_i^{\text{Dry}} < W_0^{\text{Dry}}$, then penalty function was set as:

$$p_{6i}(w) = \left(W_i^{\text{Dry}} - W_0^{\text{Dry}}\right) \times K^{\text{Dry}} \quad (4\text{-}21)$$

To avoid exceeding the limitation of physical reservoir characteristic; when $W_i < W^{\text{Dead}}$, then the penalty function was set as:

$$p_{7i}(w) = \left(W^{\text{Dead}} - W_i\right) \times K^{\text{Dead}} \tag{4-22}$$

where W^{Dead} is the inactive volume of reservoir corresponding to the dead water level.

4.5. Evaluation indicator

To evaluate the performance of the CGA search results in comparison with the current operations, i.e., the generalized shortage index (GSI) proposed by Hsu (1995) were used to express the status of frequency and intensity of water shortage. Its formula is given as follows:

$$DPD = \sum\left(DDP(\%) \times NDC\right) \tag{4-23}$$

$$GSI = \frac{100}{N}\sum_{i=1}^{N}\left(\frac{DPD_i}{100 \times DY_i}\right)^{kcs} \tag{4-24}$$

where *DDR* is 1-month deficit rate, i.e., total deficit in a period/water demand in the period ×100%; *NDC* is the number of 1-month in a continuous deficit, *DYi* is the number of 1-month periods in a year (=12), *N* is the number of sample years; and *kcs* is a constant, usually set as 2 (Chang *et al*., 2010).

4.6. Results

Based on the experience in simulation model and the tested trial-and-errors processing, the *K* factors were determined as shown in **Table 4-2**.

To estimate the performance of the proposed model for optimizing Dautieng reservoir operation rule curves, this study designed three cases of environmental base flow requirements as mentioned above. The obtained results of current operations and CGA operations are shown in **Table 4-3** and **Table 4-4** and **Figure 4-3**.

Table 4-2: The Values of K weighed factors

Factor	Value	Factor	Value
K_{Env}	75	K_{lower}	2
K_{agr}	25	$K_{critical}$	4
K_{upper}	5	K_{wet}	10
K_{retard}	100	K_{dry}	10
		K_{dead}	1000

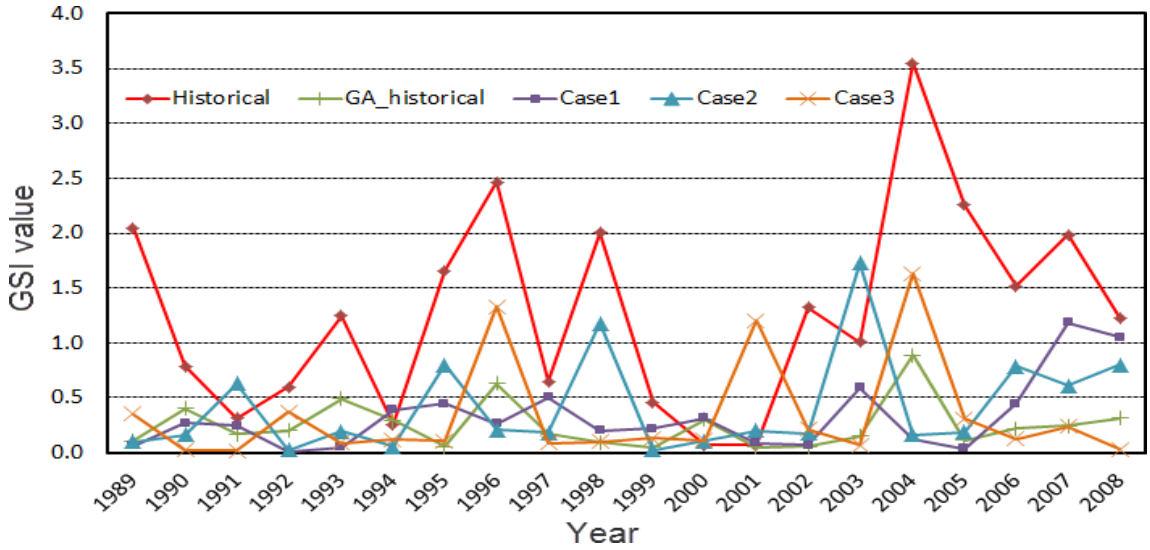

Figure 4-3: The achieved GSI values between current operations and CGA results during 1989-2008

Figure 4-3 represents the achieved annual GSI values of CGA results compared with current operations. It evidenced that most obtained GSI values from CGA research for all cases were much smaller than those of current operations, except the GSI values of case 2 in 1991 and 2003. Most of obtained GSI values for four cases simulated using CGA method were lower than 1 and only six GSI values that achieved larger than 1 were occurred in 2007 of case 1, in 1998, 2003 of case 2; 1996, 2001, 2004 of case 3. In comparison between three cases of base flow requirements, the corresponding GSI values slightly increased in order of case 1 ($30m^3/s$), case 2 ($50m^3/s$) and case 3 ($35m^3/s$ in dry season and 15 m^3/s in wet season).

Table 4-3: Annual water shortages (m3/s) and water usage with current operation and CGA cases

Case		Current operation		CGA_ Current		CGA_Case1		CGA_Case2		CGA_Case3	
Type	Year	Water usage (%)	Deficit	Water usage (%)	Deficit	Water usage (%)	Deficit	Water usage (%)	Deficit	Water usage (%)	Deficit
Drought	1992	62.9	21.2	62.4	13.5	74.4	1.5	70.1	9.8	56.2	20.3
	1995	67.4	25.6	74.6	9.7	66.6	16.8	68.2	19.4	76.8	8.2
	2003	74.0	27.1	84.2	8.0	81.1	10.6	65.2	27.4	84.5	8.4
	2004	80.2	38.1	86.7	17.0	94.1	12.0	92.9	16.8	79.3	22.6
	2005	60.2	32.9	71.0	9.4	73.9	6.7	65.5	18.6	66.4	14.4
	2006	56.3	35.1	63.1	14.4	62.2	15.4	56.2	25.2	65.5	12.8
	2007	55.2	31.5	60.3	13.8	52.2	22.2	56.3	22.0	59.6	15.2
Normal	1989	51.1	31.6	60.1	9.9	60.9	9.2	59.9	14.2	58.2	12.7
	1993	54.1	24.8	56.8	13.2	60.9	8.6	59.2	14.5	57.0	13.5
	1994	68.7	13.9	62.6	15.2	58.3	19.4	67.5	14.5	65.7	12.8
	1996	51.4	25.6	57.3	15.8	58.5	14.5	57.2	19.9	57.7	16.0
	1998	56.4	26.9	63.4	9.6	63.4	9.6	53.7	23.7	60.2	13.6
	2000	49.0	13.9	46.9	12.8	43.6	17.3	46.8	16.9	45.7	15.0
	2002	59.4	21.6	66.3	6.9	66.0	7.2	60.9	16.5	60.6	13.4
	2008	57.9	21.2	57.7	14.0	53.7	18.3	56.0	19.8	63.3	8.5
Wet	1990	56.5	21.5	55.3	14.9	54.9	15.3	56.7	17.3	65.6	4.1
	1991	59.5	12.0	56.3	11.9	58.0	9.9	48.4	24.8	62.4	5.5
	1997	75.6	18.8	77.3	10.6	72.2	15.0	73.9	17.5	74.6	13.5
	1999	59.7	23.2	68.1	6.5	64.4	10.3	69.6	8.9	65.2	10.0
	2001	57.9	10.0	57.6	8.0	55.0	11.0	52.6	17.9	47.7	20.3
Average		60.7	23.8	64.4	11.8	63.7	12.5	61.8	18.3	63.6	13.0

Table 4-3 indicates annual average water shortage and water usage of all cases compared with current operations during 20 years. The average water shortages were obtained by a long term reservoir operation complying DTOR curves and CGA method. According to the obtained results, it is without difficult to remark that water usage (%) of all cases simulated by CGA method attained higher values than those of current operations as a demonstrating of much better

performance (60.7%, 64.4%, 63.7%, 61.8% and 63.6% in current operations, CGA-Current, case 1, case 2 and case 3, respectively). However, we could find some value of annual water shortages in current operation was lower than those of all cases simulated by CGA method, and the value of water usage in current operations also achieved higher in a few years. As shown in **Figure 4-3** and **Table 4-3**, undoubtedly, the obtained results simulated by CGA method had better performance than those operated by current operations using DTOR curves.

Table 4-4: Annual water shortage ($10^6 m^3$) of current operations and CGA results base on associating various environmental base flow requirements

		Current Operations				CGA results			
Type	Year	Current	Case1	Case2	Case 3	Current	Case1	Case2	Case 3
Drought	1992	27.3	30.9	110.9	42.9	0.0	0.0	0.0	10.5
	1995*	7.4	11.4	58.3	17.4	17.2	0.0	19.1	19.7
	2003	23.7	30.7	110.7	42.7	0.0	2.9	33.9	0.0
	2004	37.1	56.2	142.3	80.6	0.0	0.0	0.0	0.0
	2005	31.6	38.6	149.3	55.1	0.0	0.0	19.2	0.7
	2006	26.5	35.6	120.2	47.6	0.0	10.9	44.2	0.0
	2007*	23.6	30.9	150.9	48.9	0.0	33.7	32.8	16.4
Normal	1989	4.2	8.2	106.9	14.4	0.0	0.0	0.0	0.0
	1993	0.0	0.0	55.5	0.0	0.0	0.0	0.0	0.0
	1994	8.5	11.5	51.5	17.5	0.0	3.2	41.3	1.3
	1995	27.8	46.9	126.9	58.9	0.0	0.0	15.5	14.1
	1998	9.5	13.5	76.3	19.5	0.0	0.0	17.0	0.0
	2000*	5.7	8.7	48.7	14.7	0.0	3.3	0.0	0.0
	2002	1.1	4.1	47.7	10.1	0.0	0.0	7.9	2.9
	2008*	8.1	12.1	83.8	18.1	0.0	12.0	7.9	0.0
Wet	1990*	18.8	22.5	102.5	34.5	0.0	25.7	55.1	0.0
	1991	14.5	18.5	58.5	29.3	0.0	0.0	61.6	0.0
	1997	5.1	9.1	51.7	15.1	0.0	0.0	8.2	0.0
	1999*	0.0	0.0	36.7	2.7	0.0	0.0	0.0	0.8
	2001*	0.0	0.0	12.1	0.0	30.5	0.0	0.0	6.0
Averge		14.0	19.5	85.1	28.5	2.4	4.6	18.2	3.6

Table 4-5: Summarized table of the CGA results

Type	GSI			Agricultural unmet water (m3/s)			Environmental unmet water (m3/s)		
	Case 1	Case 2	Case 3	Case 1	Case2	Case 3	Case 1	Case 2	Case 3
Drought	0.40	0.61	0.41	12.0	19.2	14.3	0.2	0.7	0.2
Normal	0.30	0.35	0.29	12.9	17.2	13.1	0.1	0.4	0.1
Wet	0.26	0.24	0.29	12.1	16.5	10.6	0.2	0.8	0.0
20 years	0.33	0.41	0.33	12.39	17.71	12.93	0.15	0.58	0.11

The water shortages of current operations and CGA results based on associating various ecological base flow requirements were shown in **Table 4-4**. In all cases associated by current operations curves, the average water shortages of ecological flow requirements increased in ascending order of 14.0, 19.5, 28.5 and 85.1 for case of current, 1, 2, and 3, respectively. In cases of CGA results, it also gained most ascending tendency like current operations cases. Nevertheless, the obtained values, 2.4, 3.6, 4.6 and 18.2 in cases of CGA-Current, 1, 3 and 2, respectively, were much smaller than those of current operations cases. Especially, the CGA results in case 3 with the average water shortages of ecological flow requirements was 3.6, lower than case 1 of the CGA results, 4.6, although its base flow requirements was set, 30 m^3/s in dry season, lower than those of case 3 (35 m^3/s in dry and 15 m^3/s in wet season) .

Table 4-5, summarized the CGA results show some phenomenon: (1) the water shortages of CGA results of current operation and case 3 occurred higher than those of DTOR of current and case 3 in 1995 of drought years; (2) the water shortages of all cases simulated by CGA method decreased dramatically as compared with all cases of DTOR operation in normal years, remarkably in 2000 and 2008; (3) there are different fluctuation between the water shortages of CGA results and current operations associating various environmental base flow requirements in wet years as indicated in 1990, 1999 and 2001; (4) all water

shortages of environmental requirements from CGA cases decreased remarkably as compared to all cases of current operation. Those aforesaid statements are presented in some years of **Table 4-4** marked the underline. It appears that: (1) in drought years of 1995, although the environmental flow requirements in case 3 was set higher than case 1, those years occurred the average inflows in dry season were not smaller than in normal; (2) in normal years, most of the obtained GSI values from CGA method were very small and especially in case 3 with larger environmental requirements of 50 m^3/s reached to zero in 2000 and 2008. It might explain that the inflows in dry season occurred higher than those of dry season in normal; (3) in wet years: 1990, 1999 and 2001, the inflows in wet season occurred exceeding the effective capability of water reservoir storage. However, the obtained GSI values of all cases from CGA method achieved smaller than those of in current operations and only larger GSI value of CGA-Case 2 in 1991 slightly increased (larger than in current operation case); (4) the Dautieng reservoir was designed for operating several years, mean that it needs to hoard up water year by year to attain full effective volume.

According to analysis as mentioned above, the obtained CGA results of case 3 ($35m^3/s$ in dry and $15m^3/s$ in wet season) achieved much better performance following the requirement for environmental base flow to push salt water intrusion and improve the water quality in downstream of Dautieng Reservoir Watershed for two season, dry and wet. In addition, **Table 4-4** gives the mean values of the CGA results in comparison of difference between cases associated with environmental base flow requirements. Those values in CGA-case 3 demonstrated it handled good performance and efficiency.

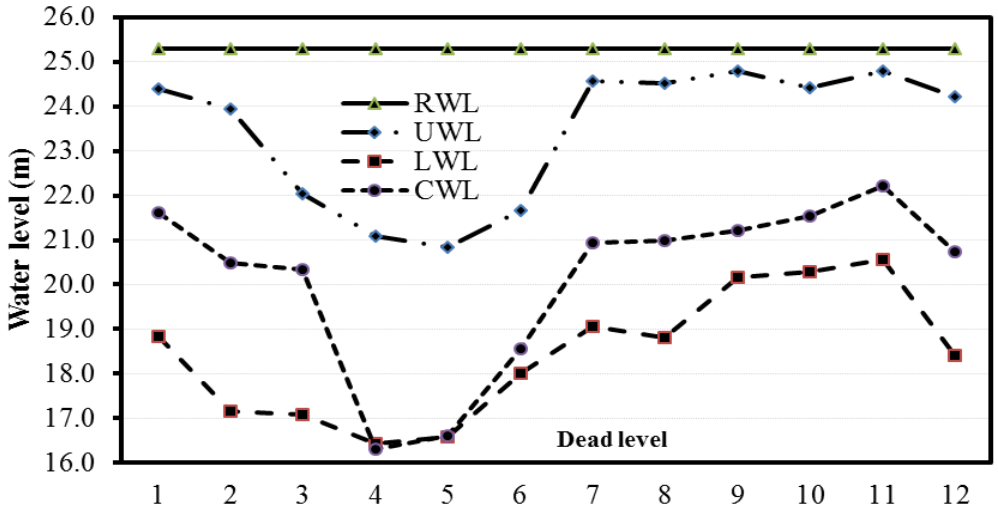

Figure 4-4: Optimized CGA curves for Case 3

Consequently, **Figure 4-4** represents the best set of operating rule curves achieved from CGA-Case 3. The simulated water level of 20 years was been statistical count and drawn as the GA curves. The results also demonstrate that the CGA curves have higher UWL in dry season, and also larger feasible space operating. However, in the ending of dry season, (April and May), the LWL of CGA curve has lower than those of current operations. Besides that, the operating space between the LWL and CWL is larger. It indicates that, as the obtained CGA curves, simulated reservoir operating led to extend the space working to enhance the effective performance of reservoir operation in year by year. The summarized evaluation, the results are presented in tables and figures as above. The obtained CGA curves have better performance than DTOR curves.

4.7. Conclusions

With rapid development computation techniques in current decades, it prompted a great potential in optimizing numerical complex model. This study constructed the model of reservoir operation based on the guiding rational reservoir operation using penalty-type genetic algorithm (Chang, 2008) for multi-use reservoir management. The proposed model with constraints integrated into

objective function configured with a penalty strategy to form fitness function. The designed constraints allow punishing to fitness values once it reaches to infeasible space in attempt to guide the GA towards a promising solution space during search processing. The CGA search is very efficient by using penalty mechanism which is able to avoid the probability of choosing worse solutions as above demonstrated results.

According to previous studies, the designed cases of environmental base flow requirements were set to the proposed model: case 1 – 30 m^3/s in dry, case 2 – 50 m^3/s in dry and case 3- 35 m^3/s in dry and 15 m^3/s in wet season. The reservoir operation model integrated CGA method simulated and carried out the effective performance. It was demonstrated by dramatic decrease of the GSI values in all CGA-case associated different environmental base flow requirements in comparison with the current operations. On the other hand, the results also indicated that water deficits of designed three cases reduced significantly and the water releases were supplied reasonably. To be more specific, the simulated results of the CGA- case 3 showed the better performance where most values of GSI and water deficit decreased remarkably.

Comparing simulated results from all cases shows that, the CGA curves were more efficient than current operations, in there, the CGA results in case 3 were slightly more effective operating than others. In these sense, we trust the obtained CGA curves determined form case 3 were the best performance. However, it will take long time for computing or be ineffective when a large number of variables are set. In this sense, our simulation with 240 variables might be considered.

CHAPTER V

ASSESSING FLOOD RISKS AND ESTIMATING DAMAGED LOSSES FOR THE DOWNSTREAM OF THE DONG NAI-SAIGON BASIN

5.1. Uncertain factors to inundation of Ho Chi Minh City

Flooding in HCMC has emerged as one of the most concerned issues which have arisen in recent years, accompanying the city's rapid growth (**Figure 5-1**). The numbers of flooded locations, flooding frequency and duration have increased steadily, resulting in substantial economic and social losses. These phenomena are an integrated consequence of both climate and non-climate related factors. Uncertain factors causing floods in HCMC may be combinations of: i) high tides, ii) high intense rainfall on the city, iii) high river discharge due to spilling from the reservoirs, iv) diverted flood waters from the Mekong river, v) land subsidence, or vi) policies (**Figure 5-2**).

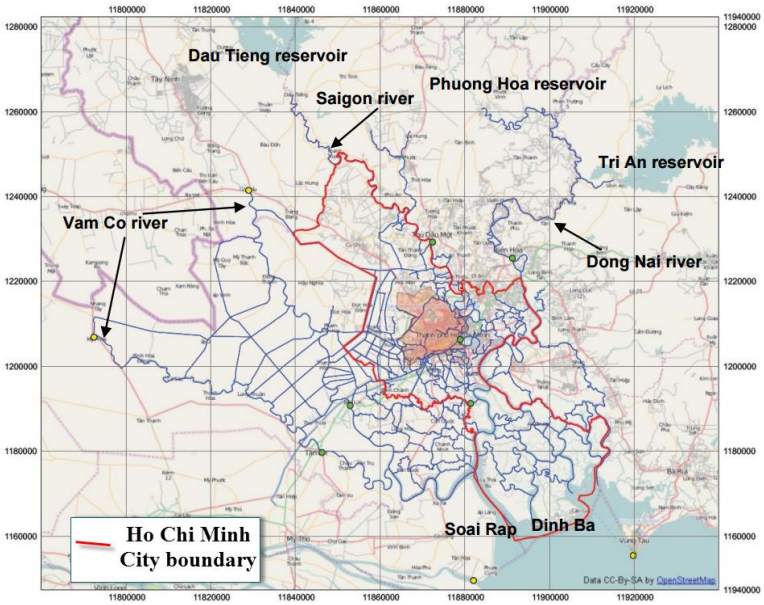

Figure 5-1: Location of Ho Chi Minh City

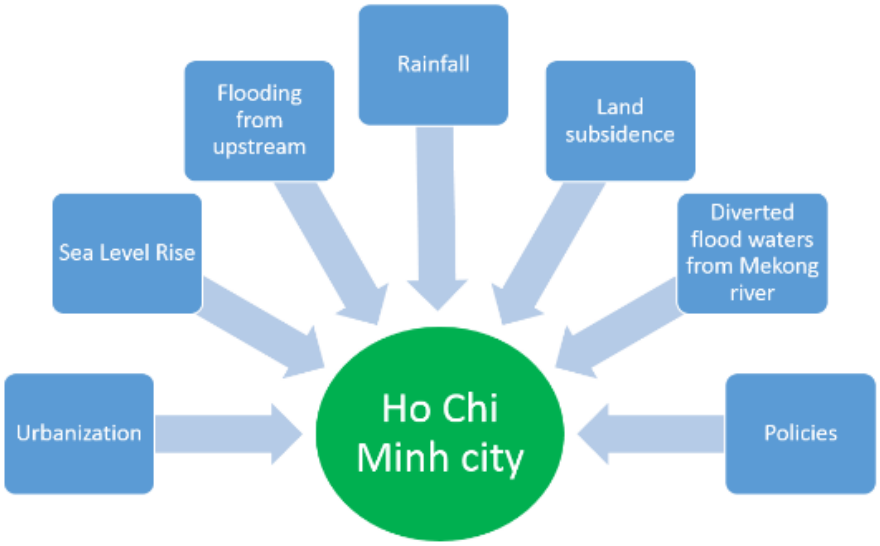

Figure 5-2: Causes of increasing inundation to Ho Chi Minh City

5.1.1. Urbanization

Ho Chi Minh City (HCMC) is the economic center of Vietnam and accounts for a large proportion of the economy of Vietnam. Because the strength of economic growth, HCMC has attracted an increase in the number of migrants from rural areas (Ngoc *et al*., 2014c). After reunification in 1975, the demography and the population pattern of HCMC have dramatically changed. Its population has doubled over the last 25 years from 2.5 million in 1975 to 5.17 million people in 2000. By 2004, the population figure has accelerated to 6.1 million people, accounting for 7% of the country's population in which 5.2 million inhabitants live in urban Districts and 0.9 million people in outlying, up to now, population reaches 8 million people ith a rate of urban growth of 2%. By the growth of economic and increase of population, the need of expanding area for living and infrastructure was essentials, thus urbanization has been raqidly (**Figure 5-3**). HCMC has faced water challenges to sustainable urban development, including groundwater depletion, surface water pollution and inadequate clean water provision for urban dwellers, especially increasing rapidly inundation.

Figure 5-3: Urbanization at Nhabe and District 1, HCMC

5.1.2. Sea level rise

In the period 1980 – 2007, data at Vung Tau station shows that the highest, average and the lowest sea level increases are 14 cm, 13 cm and 12 cm respectively (**Figure 5-4**). Stations on the river belonging to Dong Nai-Saigon River system and stations at estuaries in Cuu Long River system also have recorded mean sea level rise of 9 – 13 cm during this period.

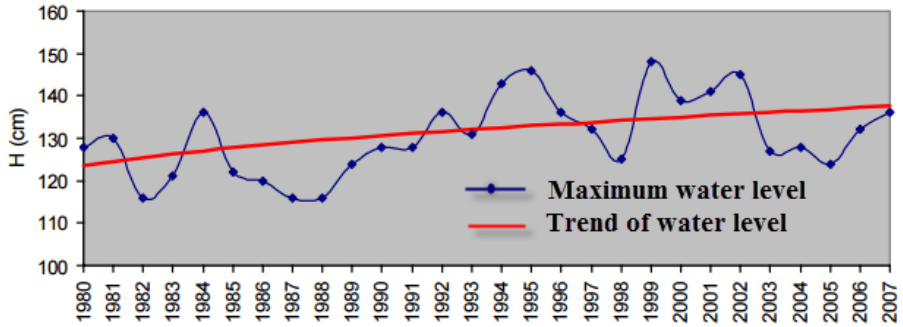

Figure 5-4: Trend of highest water level in the period 1980-2007 at Vungtau station

The impacts of sea level rise on inundation and drainage of downstream of Dong Nai-Saigon area, especially HCMC low lands are becoming clearer (Ngoc *et al*., 2013c). In recent years, due to impact of sea level rise combined with high tide, center of HCMC, coastal area among Saigon River mouth have been heavily inundated. Even high lands such as urban, residential areas and roads in some places have been also inundated.

5.1.3. Flood discharge from the upstream of the Dong Nai-Saigon River

Urban flooding has become a wide-spread phenomenon and a major concern in Ho Chi Minh City in recent years that has been accompanying the city's rapid growth. Especially since the middle of the 1990s, the amount of flooded locations, flood frequencies and flood duration has steadily increased and has caused substantial economic and social losses, such as damage to infrastructure and assets, water pollution as well as traffic jams. Increasing of discharge flows from upstream reservoirs at Dong Nai-Saigon River (see **Figure 5-5**) is one of factors causing to further increase of inundation, putting a major pressure on the city's development (Ngoc *et al*., 2013c).

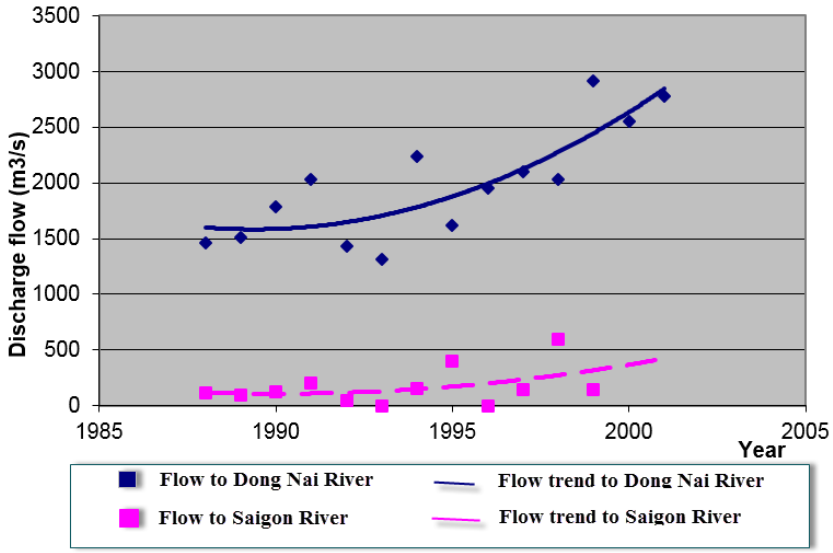

Figure 5-5: Increasing of flood discharge from upstream of Daongnai-Saigon River

5.1.4. Increase in precipitation

Following are some characteristics of heavy rainfall events analyzed from 50-years of data observed and recorded at Tan Son Nhat Station. Statistical data show that heavy rainfall events can occur annually from June to October, with yearly "maximum events" occurring most frequently in June, September and October. As mentioned earlier, heavy rainfall events are usually concurrent with periods when the water level is at its annual high. This fact causes an even more severe problem for urban drainage in Ho Chi Minh City. The overall increasing trend of about 0.8mm per year can be explained as being a result of urbanization, which creates favorable conditions for precipitation caused by the Heat Island Effect (HIE). Heavy rainfall is generally believed to be linked to localised urban warming, which is an unpreventable consequence of urbanization. The compelling evidence for urban-industrial precipitation enhancement was reported by Ngoc (2014b) and Kim (2014). The increasing rate is about 2.45 mm/year (**Figure 5-6**), coincident with the rapid change in urbanization and industrialization occurring in Ho Chi Minh City.

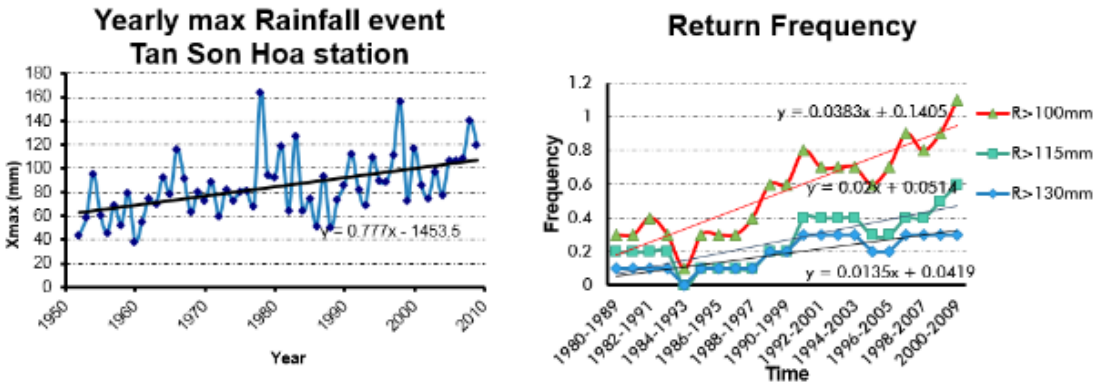

Figure 5-6: Statistics of precipitation at Tansonhoa station

Table 5-1: Numbers of precipitation >100mm in period 1952-2010

Period	1952-1961	1962-1971	1972-1981	1982-1991	1992-2002	2003-2010*
Times	0	1	2	2	4	9

The evidence in **Table 5-1** supports the hypothesis of an increasing trend in the occurrence of heavy rainfall events during recent years. The non-stationary time series of the events may make conventional statistical analysis invalid as statistical parameters are changed with time. The fact should be considered in detailed investigations.

5.1.5. Land subsidence

Land subsidence (LS) has been occurring at a significant rate as observed at some locations in the city. This effect may enhance the flooding situation when combined with rising water levels and more intense rainfall. Similar phenomena were found in Bangkok, Shanghai, Jakarta… and blamed for over-exploitation of groundwater and high-rise buildings. Many elevation landmarks should be checked and replaced to serve infrastructure construction such as roads and storm water sewers. Some typical subsidence sites are reported in **Figure 5-7**. Land subsidence is creating a similar effect as SLR.

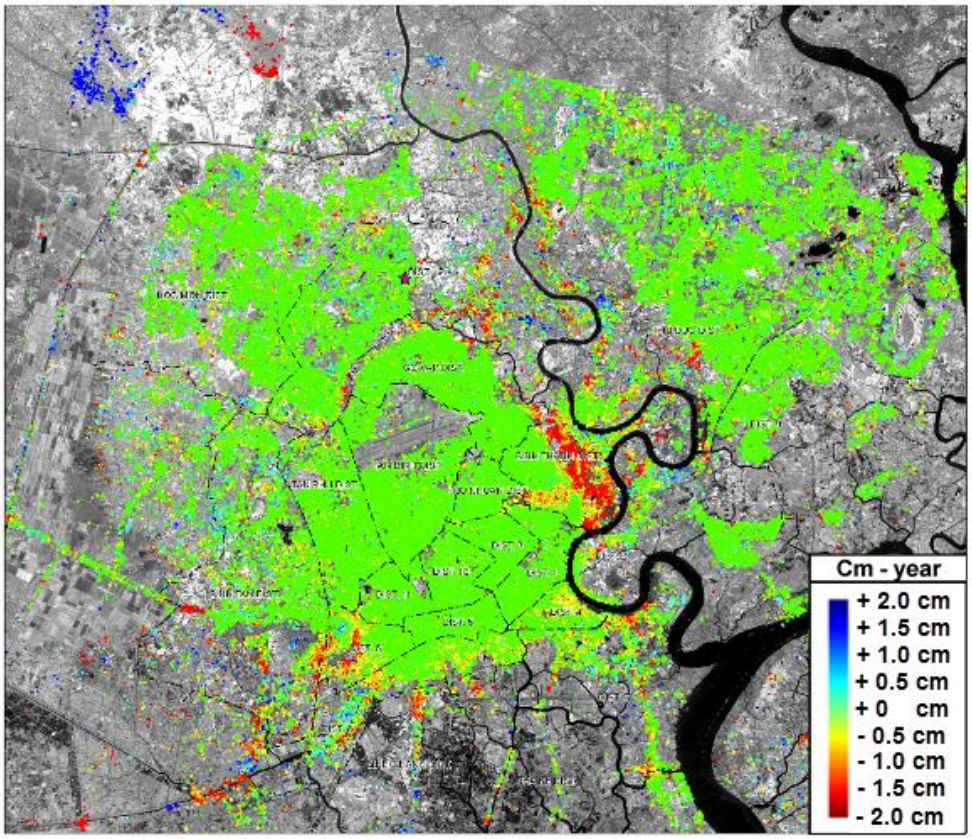

Figure 5-7: Historical mapping of terrain deformations in HCMC (1996-2010) (WB, 2010)

5.2. Project development of flood control structures

Due to a rapidly increase of flood inundation in HCMC, the local government has been attempted to face with urban flooding. There were many projects proposed and completed (see in **Figure 5-8**) in attempt to protect HCMC from heavy rainfall, upstream flooding, tidal regime, etc… from 2000 up to now. The big major projects of flood control strutures for HCMC include as below:

JICA Project: In 2001, the upgrade project of Nhieu Loc-Thi Nghe drainage system (funded by JICA in 2001) was proposed with the purpose for storm water drainage for center of HCMC, and this structure was completed in 2003. However, inundated areas have not only none-declining, but increasing number of inundated sites.

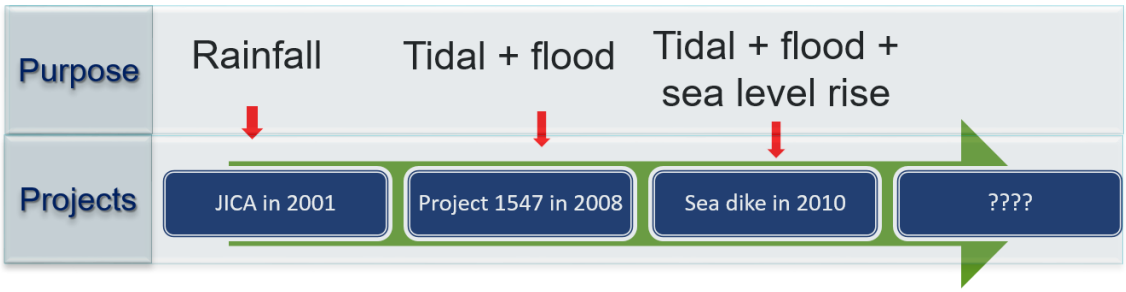

Figure 5-8: Project development for flood control in HCMC

Project 1547/QĐ-TTg: proposed by HCMC Government in 2008. This project aims to protect centre urban areas of HCMC from tide and flood impact. However, there was much attention to this project due to discredit about real protection capability of this project. Anyhow, this project has been starting to be on construction since 2015 and will be finished on 2020. The local government believed that it is no longer to re-think or re-review all aspects due to clearer and stronger occurrence of sea level rise and increase of inundated areas in HCMC.

Project of super sea dike: this project had idea to construct the super sea dike connecting Gocong to Vungtau since 2010. This project aims to flood and inundation control for whole HCMC area in short-term and long-term. The proposed project is goals for enhancing drainage system, anti-salinization for HCMC in context of climate change and sea level rise. But until now there are many arguments to debate negative and positive impacts to environmental water in river as well as in Can Gio Mangrove forest. Somehow, this project also received much attention from researchers. But to be constructed this sea dike, it is a necessary to extend time to pay more attention in later deeply researches.

5.3. Extreme flood events and anticipated scenarios

In response to the increased risk of flooding, there is an urgent need to answer a number of frequently questions is how to best address the increased flood risk driven by abnormal conditions of climate scenarios and quantify the benefits of adapting to such changes (Matttias *et al.*, 2012, Nguyen, 2010). Many

researches have widely determined that the most complete approach is a risk based analysis (Dawson *et al*., 2008; Morita, 2008). Many adaptation actions have been initiated in attempts to mitigate fluvial and tidal floods at large scales (Floodsite, 2009). Many cities are highly vulnerable to flood hazards due to their concentrated population and assets. Furthermore, the technical life times of urban drainage systems and city infrastructures are long, in the order of 50–100 years or more, and it therefore makes sense to include climate predictions in assessments of these options.

This part is to address flood risk management in a view point of climate change based on the losses of extreme flood events and find the sustainable measures to build resilience into urban management, critical infrastructure investments and disaster risk mitigation in jurisdiction balance of sectors (Pahl-Wostl, 2006; Parkison *et al*., 2005; Rose, 2004; Slobodan *et al*., 2011; WB, 2012). The content of completed and ongoing research projects in which these objectives are in contribution to the improvement of decision-making process to guide Ho Chi Minh City towards aspired benefits (Nguyen, 2010).

A future climate scenario is a plausible representation of future climate that has been constructed for explicit use in investigating the potential impacts of anthropogenic climate change. Climate scenarios often make use of climate projections by manipulating model outputs and combining them with observed climate data.

Besides that, there are some construction system will be constructed which its impact to infrastructure will be changed in relevant regions involving flow regime, flooding inundation, drainage system, etc (Veerbeek *et al*., 2008; Klinke and Renn, 2006).

The simulated scenarios in this study are consisted of combining the changes of future climate and anticipated building constructions. These anticipated scenarios are referred to the key project in national level of Kim (2013) entitled “Study on integrated measures for flood control in the

downstream area of Dong Nai – Saigon River Basin and vicinities", shown in **Table 5-2, 5-3** and **5-4** as bellows:

Table 5-2: Simulated Scenarios

No.	Scenario	Infrastructure Conditions	Hydrological conditions
1	HT_B1	Baseline	B1
2	HT_B2	Baseline	B2
3	T2_B1	Baseline+VT_GC	B1
4	T2_B2	Baseline+VT_GC	B2
5	T1547_B1	Baseline+QĐ1547	B1
6	T1547_B2	Baseline+QĐ1547	B2
7	DT_dambreak	Dautieng dambreak	HT2000
8	TA_dambreak	Trian dambreak	HT2000

Table 5-3: Abnormal hydrological conditions

No.	Notation	Hydrological conditions (Frequency of Flood discharge)
1	B1	Dautieng P=0.02%, Trian P=0.1%, Phuochoa P=0.5%
2	B2	Dautieng P=0.1%, Trian P=0.02%, Phuochoa P=0.5%
3	DT_DB	Dam faifure of Dautieng Reservoir
4	TA_DB	Dam faifure of TriAn Reservoir

Table 5-4: Infrastructure conditions

No.1	Notation	Infrastructure conditions
1	HT	Infrastructure in 201 + JICA 2001
2	T1547	Infrastructure in 2010 + Project 1547/QĐ-TTg
3	T2	Infrastructure in 2010 + Sea Dyke Project

5.3. Methods

The proposed approach quantifies the expected flood risk derived from various flood defense alternatives. It takes into account uncertainties resulting from non-systematic data included in hazard analysis. The conceptual framework is shown in **Figure 5-9**. Flood risk is evaluated in terms of the expected annual flood damage, expressed as: $E_{\text{expose}}(D_{\text{damage}} / x_{\text{event}})$, where D_{damage} is the damage caused by a specific flood event (x_{event}) in a specific location (Tung, 2002).

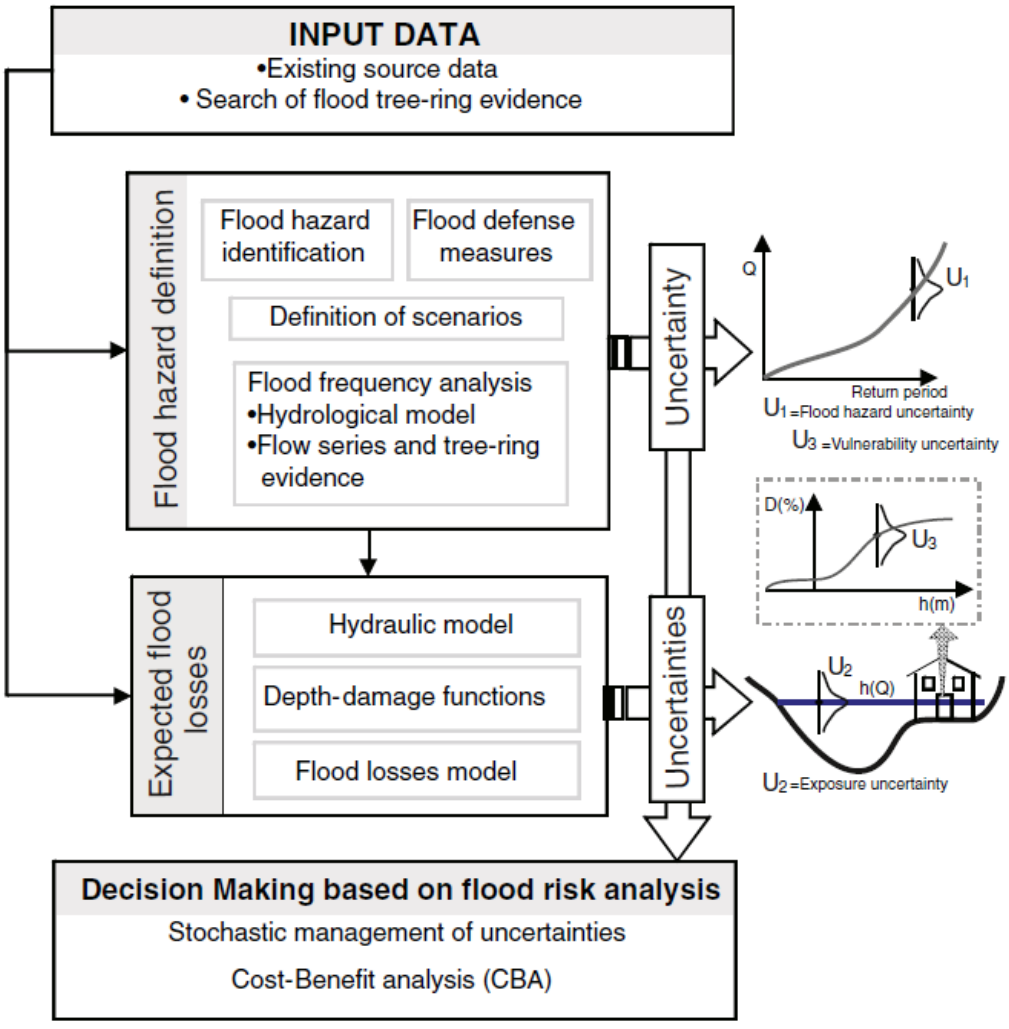

Figure 5-9: Methodological diagram used in flood estimate and decision-making process

Empirical flood depth-damage curves were used to evaluate the economic losses for each return period (USACE, 1992). The 1D/2D coupled numerical hydrodynamic flow model MIKE FLOOD (DHI, 2007b) was used to obtain the water depth. This model is based on numerical equations of conservation of mass/momentum (Chow, 1959) and is run with the required input data and parametrization including bathymetry and topography of the floodplain, geometry of hydraulic infrastructures, roughness value, eddy viscosity parameter, computational time step and boundary conditions.

Finally, a cost-based analysis was carried out to estimate the expected cost of each defense alternative considered (Tung, 2002). Although similar decision-based risk approaches have been proposed and used (Merz *et al*., 2002; Tung, 2002; Faber 2006; Dietrich *et al*., 2009), as far as the authors are aware this is one of the first examples of applied flood risk analysis where evidence from past flood tree-rings (i.e. non-systematic data) has been included in a flood hazard definition.

The methodology of this research is the ideal of proposing a coupled 1-2D hydro-hydraulics models for simulating inundation of Ho Chi Minh City area under hydrological variation scenarios involving climate change, sea level rise, etc.., and the map layers of land use, urban residents, and infrastructure are overlaid into inundated areas with clarified levels in spatial and temporal variation. The vulnerable formula is designed to estimate flood damage to separate area types. The **Figure 5-10** shows the flowchart of methodology structure.

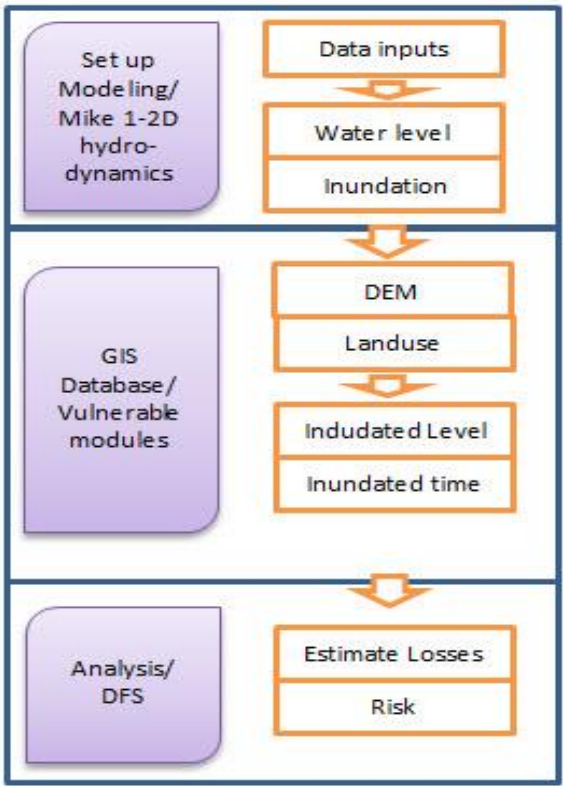

Figure 5-10: Methodology of this research

5.3.1. Hydraulic modeling

Among other commercial hydraulic models for a dam break event simulation as TELEMAC, SOBEK, DAMBRK and HEC-RAS, DHI MIKE is considerably high precision as it is used in a great number of similar research and consult projects (Arjan 2010; Ciria 2007; Defra 2005; Hallengatte 2008). This research would employ MIKE FLOOD which is a combination between one-dimensional flow in rivers and two-dimensional overflow on ground. This model has been showed to be capable of dealing with actual dam break events involving supercritical, subcritical, trans-critical, overland and overtopping flows as well as being able to simulate the wetting and drying processes which may occur. In addition, this model has the advantage of the 1-D model since it could accelerate the hydraulic model by emulating non-overbank rivers in a one-dimensional network (see **Figure 5-11**).

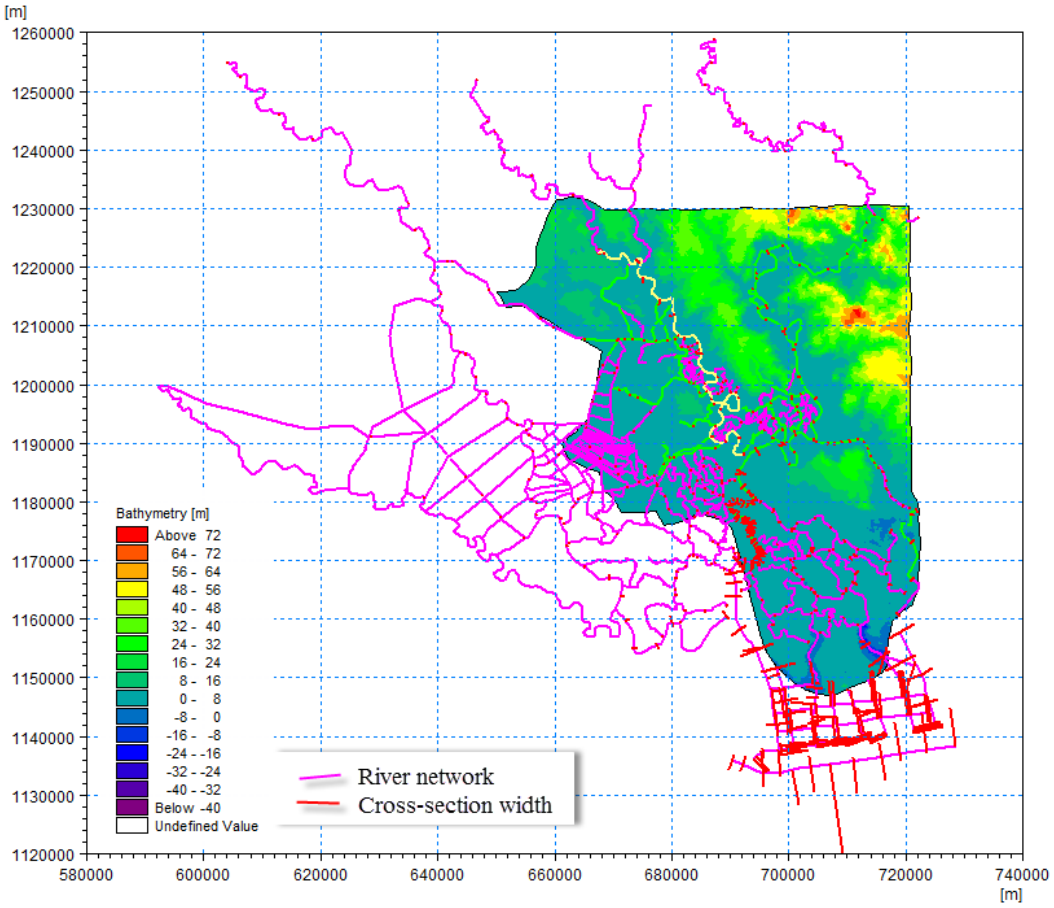

Figure 5-11: the coupled one-two dimensional hydraulic MIKE FLOOD model

5.3.2. Grid-Based GIS modeling

The main idea of "grid-based GIS" method is that a research area is divided into small cells with determined dimensions. According to Su *et al.* (2005), risk for each cell that is defined as the "possibility of loss or injury" is expressed as the following equation:

$$R_{risk} = H_{hazard} \times V_{vulnerable} \times E_{expose} \quad (6\text{-}1)$$

Where:

R_{risk} : Risk, exposure to the chance of injury or loss;

H_{hazard} : Hazard, something causing unavoidable danger, peril, risk, or difficulty;

$V_{vulnerable}$: Vulnerability, capable of or susceptible to being wounded or hurt due to a natural phenomenon of certain intensity;

E_{expose}: Exposure, the condition of being exposed without protection to the effects of harsh weather.

Flood hazard maps are clearly needed to be done first in flood risk assessment process. Normally, flood hazard can be assessed by field survey, remote sensing or computer modeling (WB, 2012). This research will employ the computer modeling method due to the fact that dam failure of Dautieng, Phuoa Hoa, Tri An as well as extreme flood events have never happened in the past.

The stage-damage curve describes the relation of flood damages to flood depths. The stage-damage curves are related to a specific class of special human activities or land use categories. Although the stage-damage curve in general did not consider the effects of flow speed, period of inundation, and sedimentation load and may need improvements, these concepts were still used intensively for flood damage assessment (Kubal *et al.*, 2009)

Finally, hazards maps and vulnerability maps are combined to form risk maps. All of the mentioned process is summarized as the bellow in **Figure 5-12**:

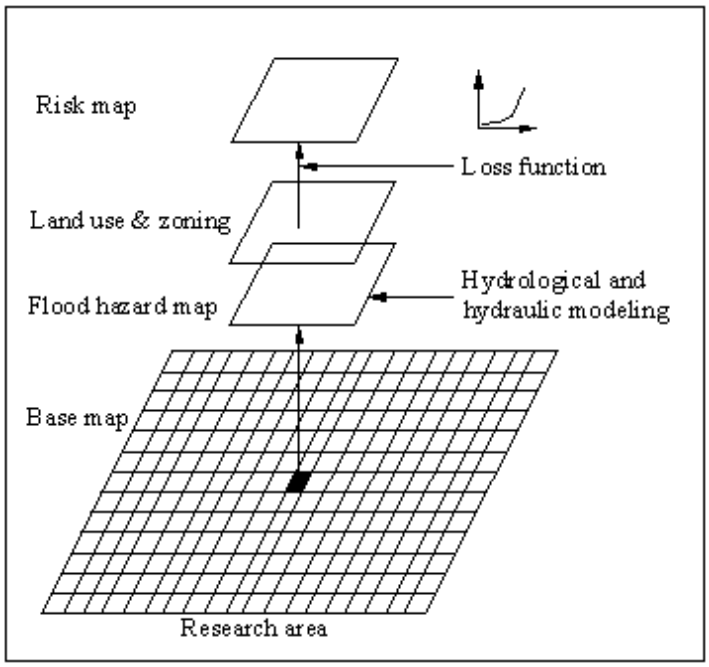

Figure 5-12: Flood damage analysis algorithm

5.3.3. Flood damage analysis

Hazard analysis is to derive the hazardous potentials under different scales of the event. In order to develop dam-break flood potential maps, it requires a two-dimensional distributed watershed model to estimate flood depths. Each watershed was divided into upstream highland catchments and a downstream alluvial plain with the assistance of geographical information systems (GIS). The upcoming flow of the upstream mountainous to the reservoir is collected from Chapter 3. According to the research, the MIKE NAM model of Denmark Hydraulic Institute was applied to compute the discharges catchments of the watershed from effective rainfall.

The movement of water at the downstream can be characterized by the two components: the land surface runoff component representing the movement of water over the land surface and into channels or flood plains, and the stream routing component denoting flood wave propagation in channels or flood plains. The surface runoff is calculated by NAM for rural areas and URBAN for urban areas. The research area was divided into 312 sub-regions based on topographic data. Meanwhile, the stream component is simulated by MIKE FLOOD. Basically, MIKE FLOOD dynamically couples 1D (MIKE11) and 2D (MIKE21) modeling techniques into one single tool. According to the manual guide of DHI (2012), the 1D part for rivers typically connects to the 2D part by the two kinds of links: standard and lateral links. For a standard link, a river discharges directly into a flood plain; when for a lateral link, there are connection between river banks and flood plain, and overtopping water would flow on the 2D region. A series of studies on the numerical flood model in the world have been conducted was concluded that a coupled 1-2D hydraulic model could accurately simulate the overland flow characteristics. Hence, this research would utilize MIKE FLOOD model already setup by Institute for Water and Environment Research

which used in emergency preparedness plan for the downstream of Dautieng reservoir.

In this model, the 1-D river network includes all the main rivers in Hochiminh city and neighbor areas, for example Lang The, Rach Tra - Thay Cai - An Ha, Tham Luong – Ben Cat – Rach Nuoc Len, Kenh Doi – Kenh Te – Tau Hu – Ben Nghe, etc. The discharges of Tri An and Phuoc Hoa reservoir and Vam Co rivers were set as the upstream boundary conditions for the model. The downstream boundaries made use of measured water level at Vung Tau station.

Meanwhile, the 2D MIKE 21 model uses a triangular grid structure to present the topography so it could imitate complex terrain areas by importing topographic data as digital elevation model (DEM). The flexible mesh of 2D model includes 163,352 nodes.

MIKE 11 and 21 are then coupled by the lateral link (showed in **Figure 5-12**). It was assumed that frictions of areas were chosen based on land use maps, and are imported into MIKE21 FM model in form of a friction matrix. Subsequently, the model was calibrated and verified for the flood season from 2000 to 2007. The time step and interval periods are chosen by the trial method from 10, 5 to 2 seconds in which 2 seconds is the most stable parameter.

To assess the flood risk for the study area, hazard analysis was first done and flood potential maps under different probabilities of occurrence were generated with a grid of solution of 5x5 meters.

Subsequently, these results are converted into grids presenting flooding depth in Arc ASCII format which is compatible to Visual Basic Application (VBA) input. This flow depth files provided the estimated water depths in meters at each grid cell location.

5.3.4. Vulnerability analysis

For assessment of the risk, loss or damage must be estimated after the hazard analysis is done. Stage-damage curves, also known as “flood loss

functions" were used for this purpose in this study. A stage-damage curve depicts the relationship of damage varied with the flood depth. Individual curves are usually built for different human activities. A loss function usually relates to a specific type of land use zoning or economic activity and presents information on the relationships of damages to the flood depths. In this paper, human activities were classified into road, settlement, aquaculture, agricultural land, plantation land, fruit tree, paddy field, tree, salt field, grass land and others in this study. In these, settlement consists of all kind of buildings as residential, industrial and economic sectors. Land use map is showed in **Figure 5-13**.

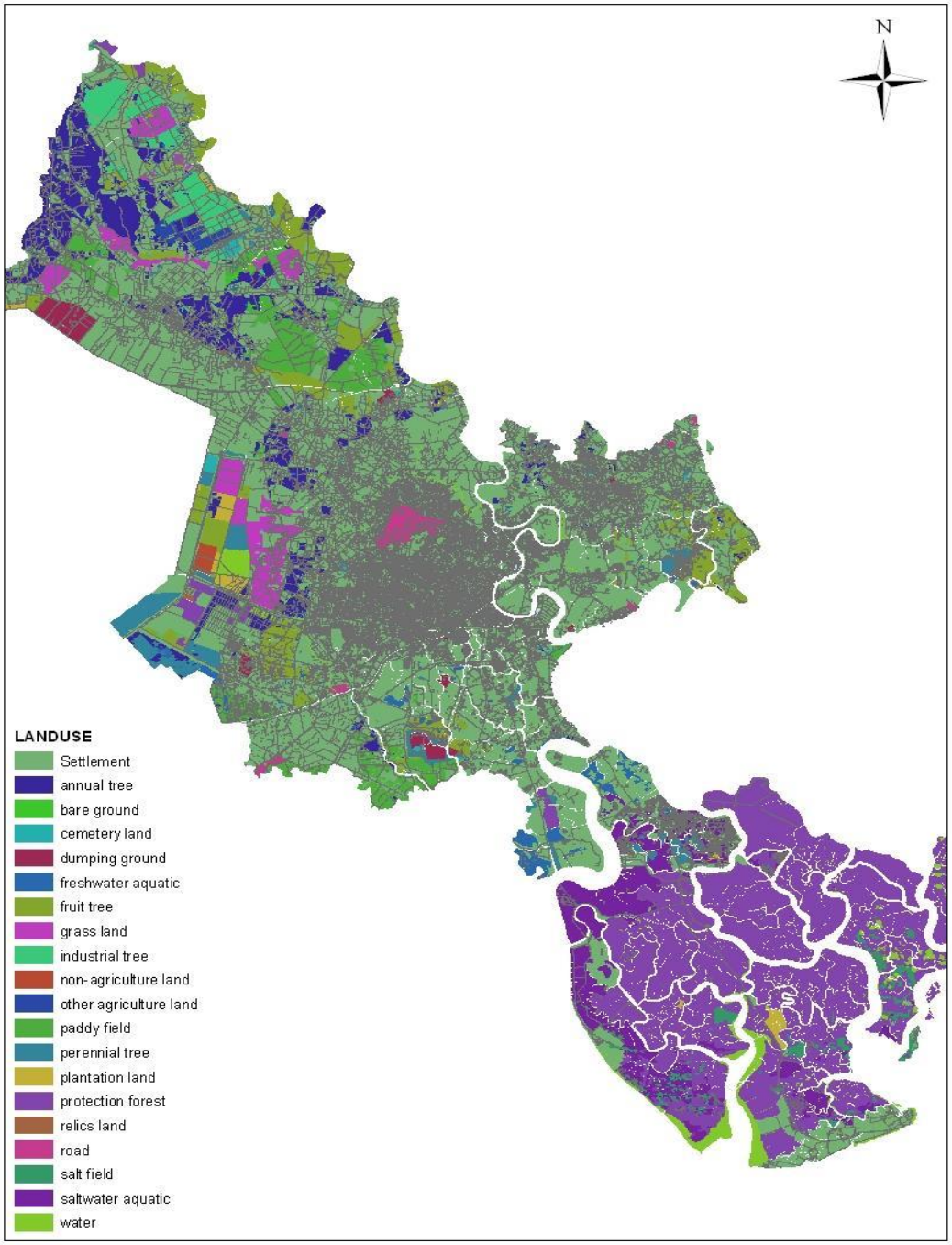

Figure 5-13: Landuse map of Hochiminh City

Curve for these different activity categories as shown in **Figure 5-14** was developed in the previous study of the authors (Nguyen, 2014)

The deterministic depth-damage functions considered here were derived from stream flooding caused by precipitation from intense thunderstorm activity

and long duration frontal activity. The typology of residential uses taken into account as in **Table 5-5**.

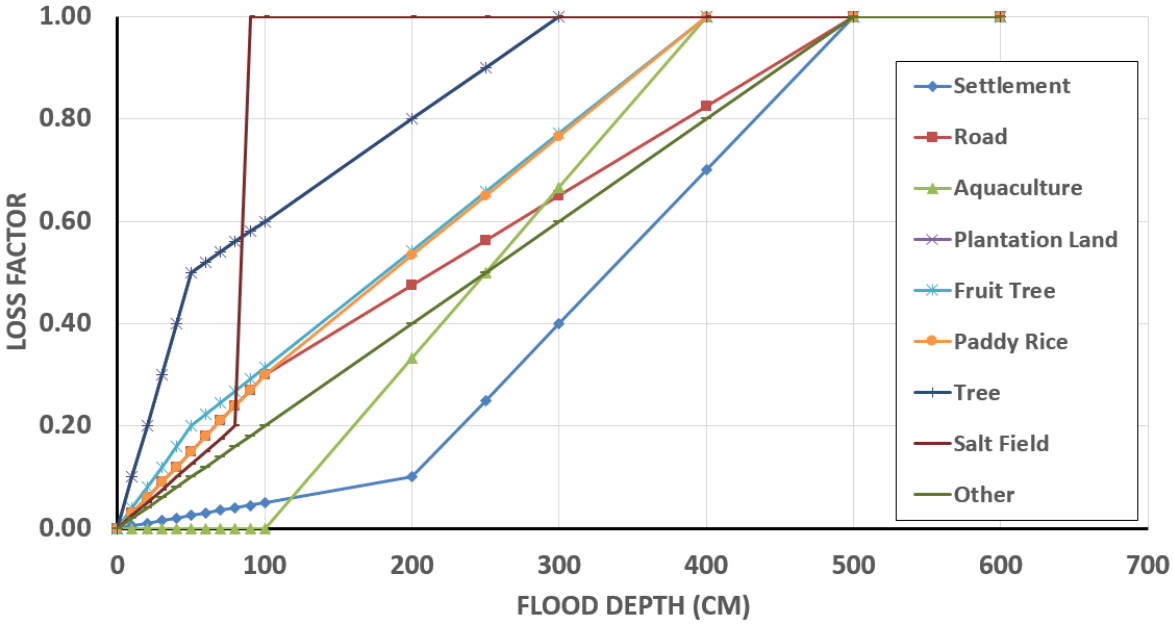

Figure 5-14: Loss functions

Table 5-5: Property of landuse class per m^2

Landuse class	Property (USD/m^2)
Settlement	1000
Road	100
Aquaculture	14.2
Plantation Land	5.8
Fruit Tree	3.6
Paddy Rice	2.7
Tree	1.5
Salt Field	0.97
Other	0.02

5.4. Results and discussion

5.4.1. Results

By applying the 1-2D Mike Flood coupled, this study simulated and estimated for 8 designed scenarios. **Figure 5-15** to **5-22** show the results of the maximum inundated depth based on the simulated scenarios:

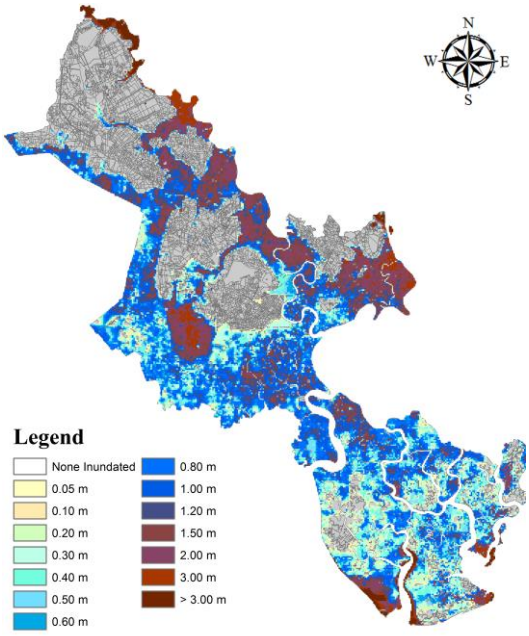

Figure 5-15: Max inundation map – HT_B1

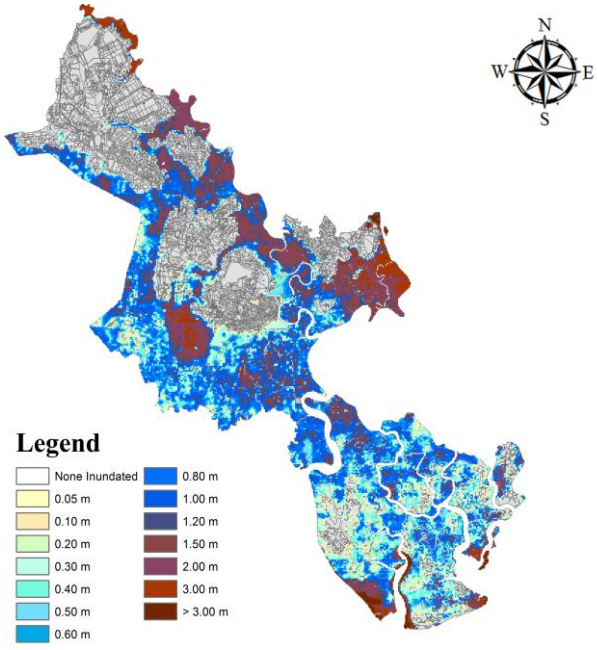

Figure 5-16: Max inundation map – HT_B2

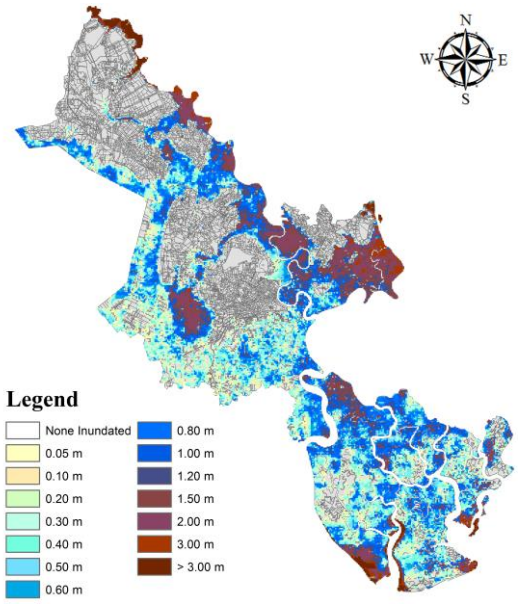

Figure 5-17: Max inundation map - 1547_B1

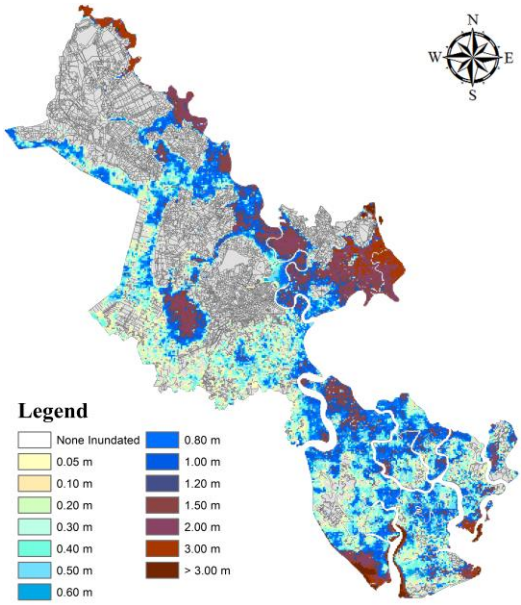

Figure 5-18: Max inundation map - 1547_B2

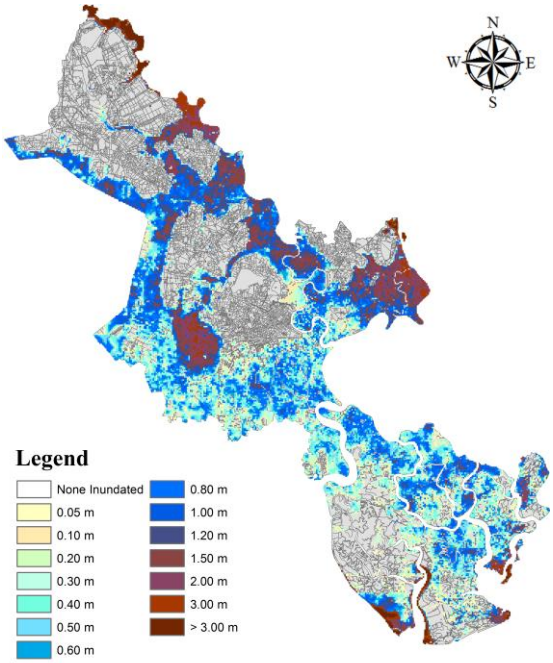

Figure 5-19: Max inundation map - T2_B1

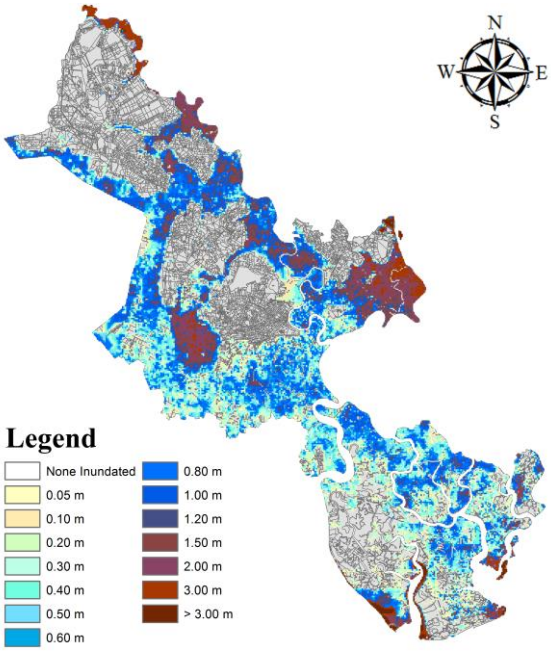

Figure 5-20: Max inundation map - T2_B2

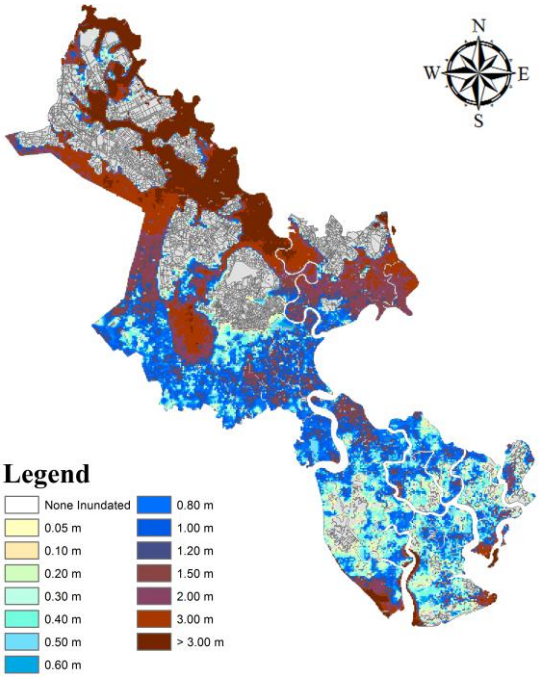

Figure 5-21: Max inundation map - Failure of Dautieng dam

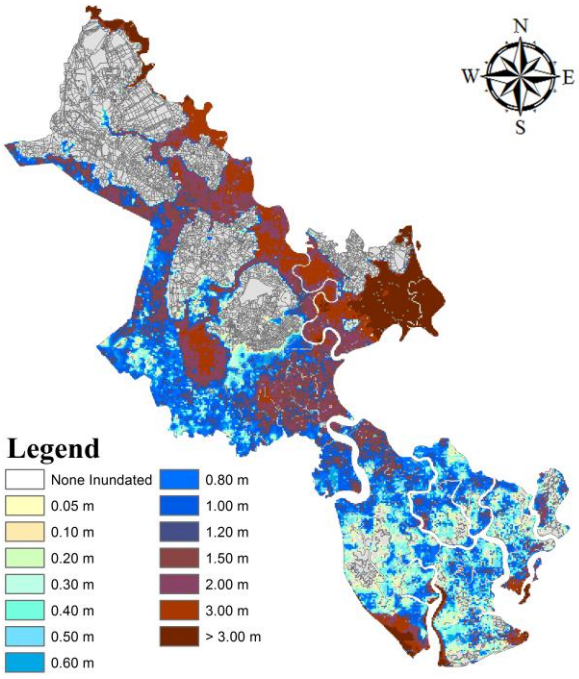

Figure 5-22: Max inundation map - Failure of Trian dam

Next, results of the inundated water depth extracted from hydrodynamic model are input to the flood risk analysis model (GIS-based Modeling) and simulated and accessed flood risk in HCMC. The obtained results of flood risk maps based on proposed scenarrios show from **Figure 5-23** to **Fiure 5-30**:

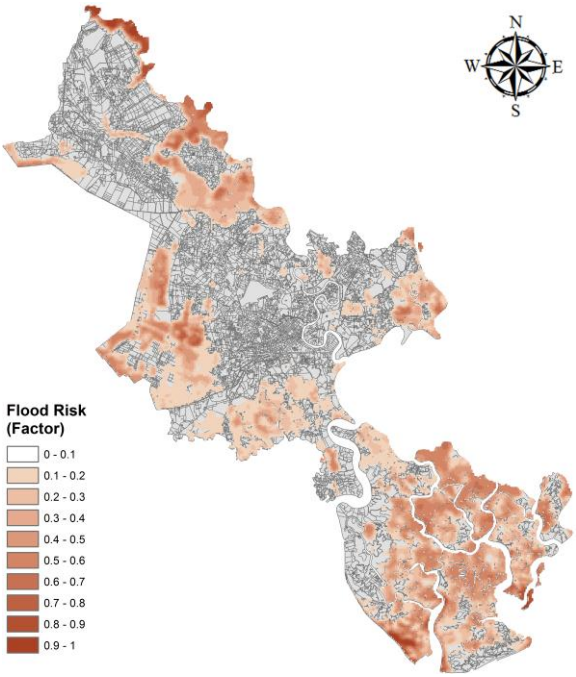

Figure 5-23: flood risk map – HT_B1

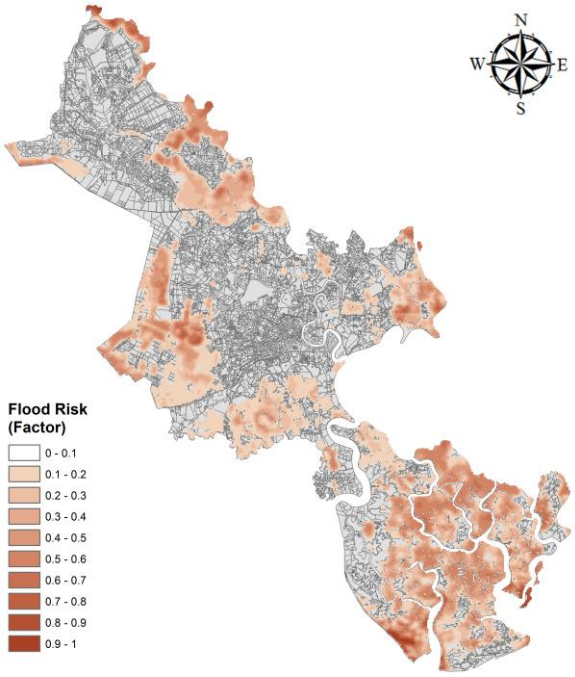

Figure 5-24: flood risk map – HT_B2

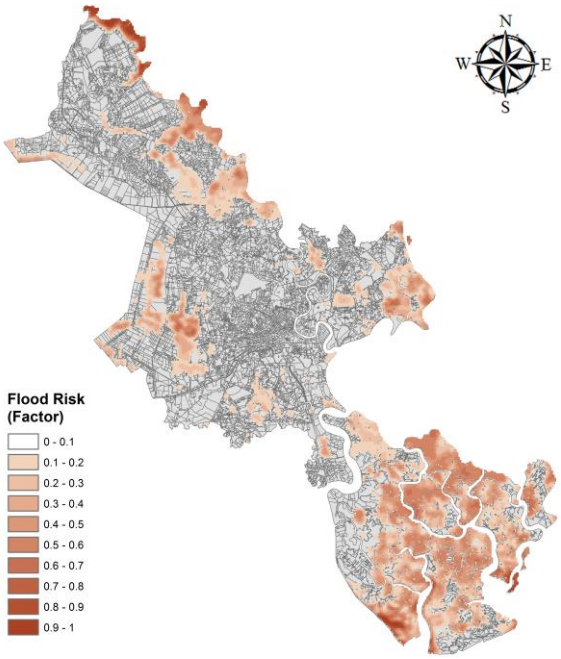

Figure 5-25: flood risk map – 1547_B1

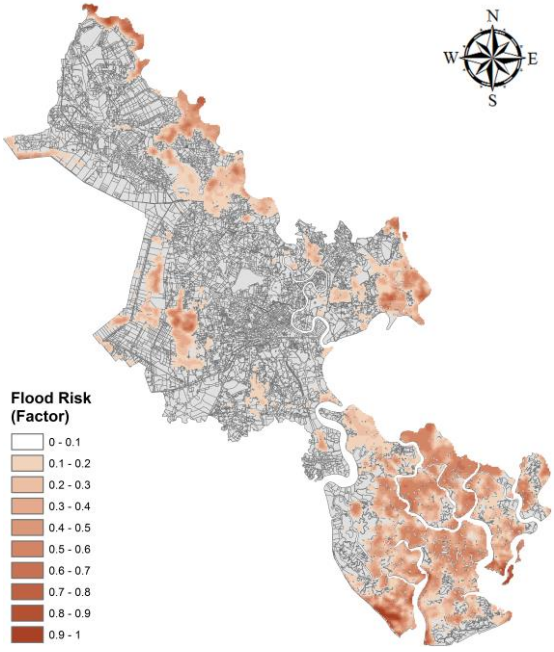

Figure 5-26: flood risk map – 1547_B2

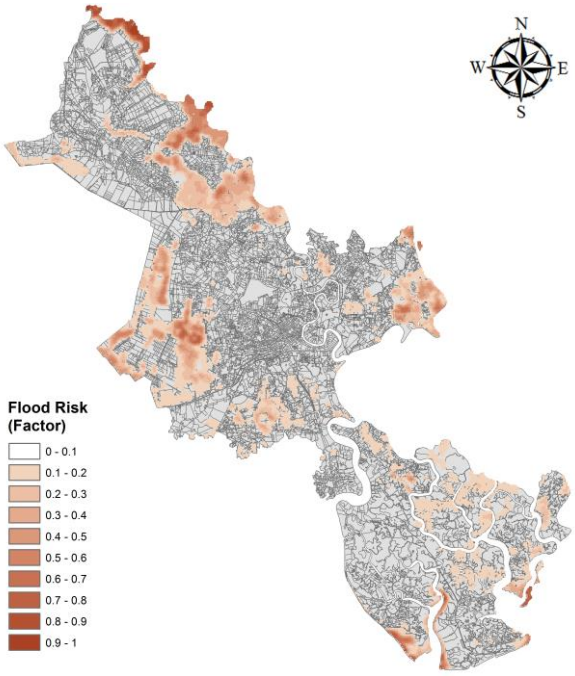

Figure 5-27: flood risk map – T2_B1

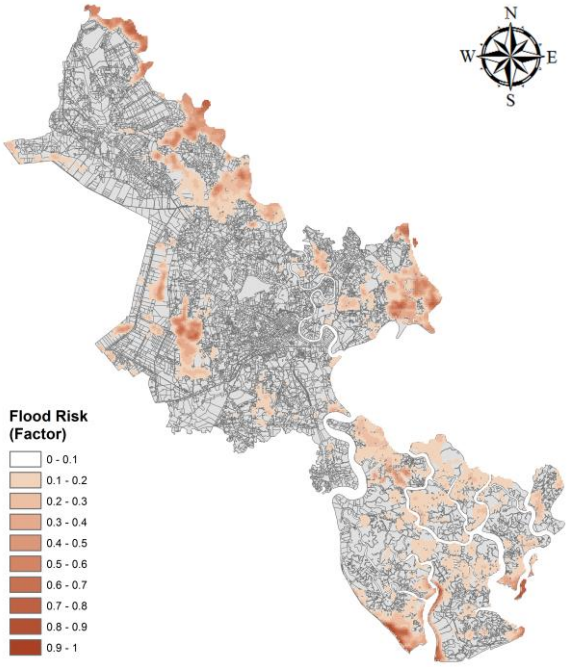

Figure 5-28: flood risk map – T2_B2

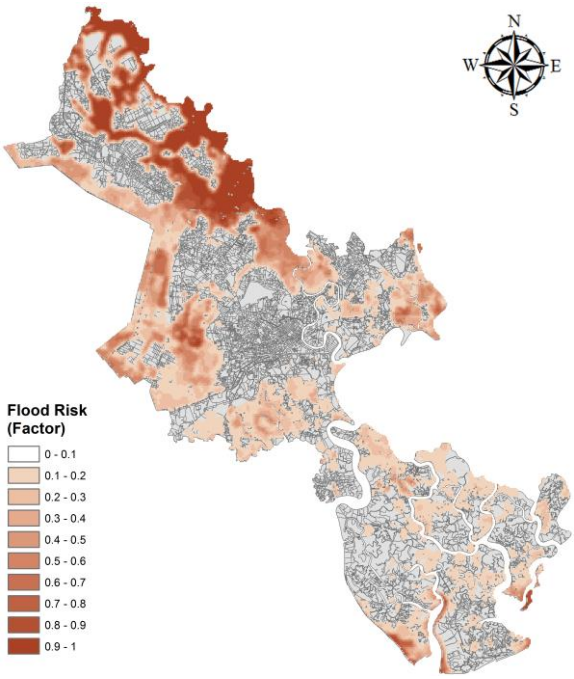

Figure 5-29: flood risk map – Failure of Dautieng dam

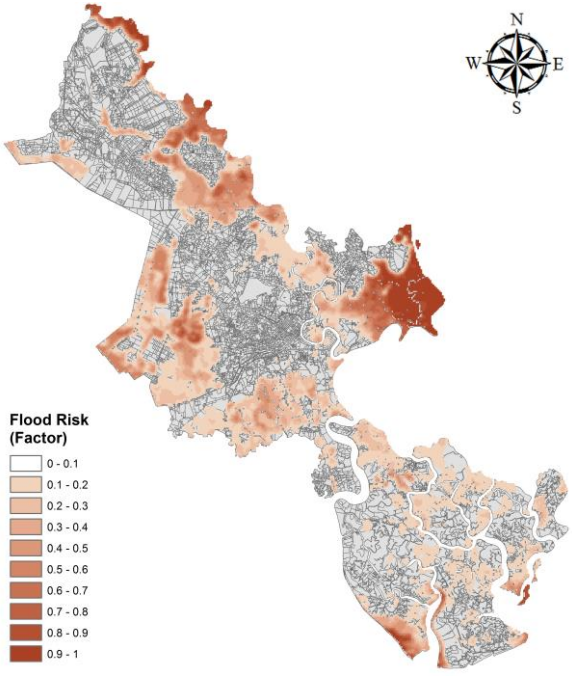

Figure 5-30: flood risk map – Failure of Trian dam

Then, the curves of depth-damage function were designed and applied to GIS-based modeling for estimating the damage losses based on the land use classes. The obtained results of damage maps show in **Figure 5-31** to **5-38**:

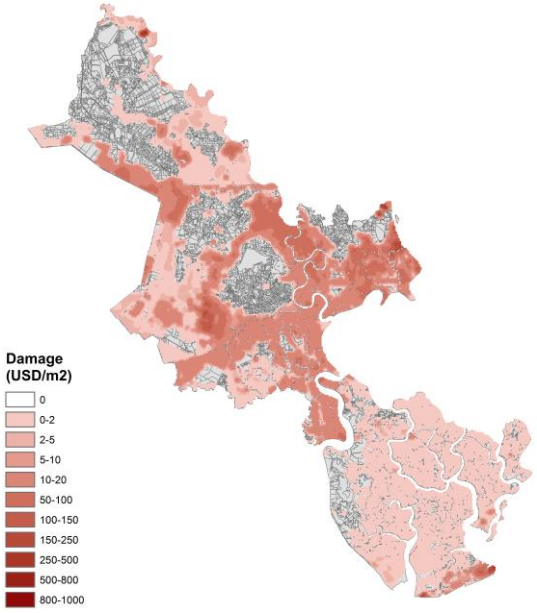

Figure 5-31: Map of estimated damage – HT_B1

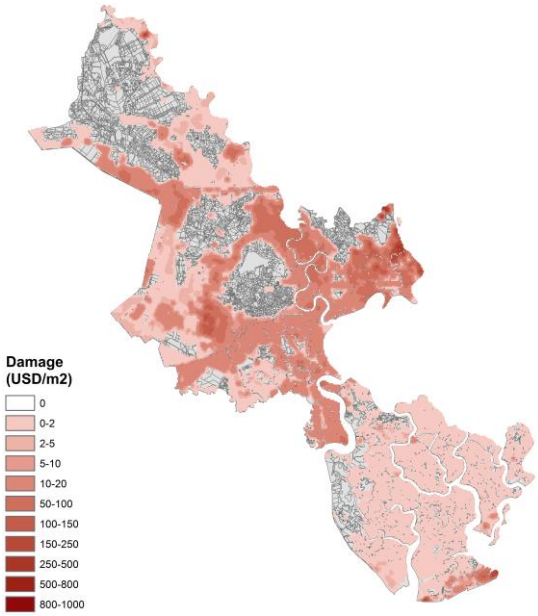

Figure 5-32: Map of estimated damage – HT_B2

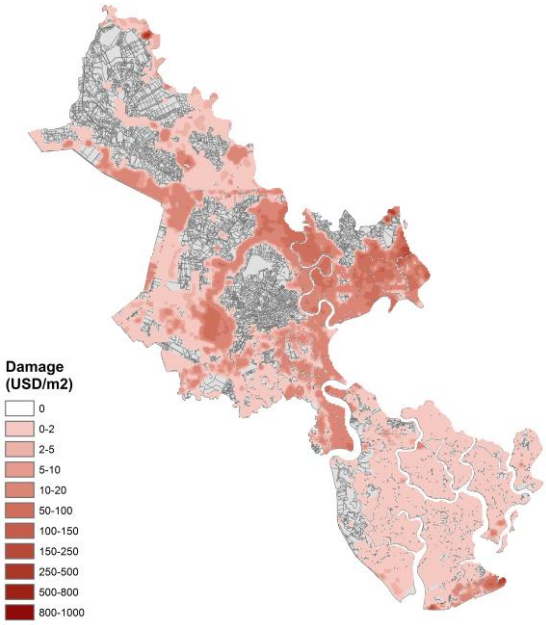

Figure 5-33: Map of estimated damage – 1547_B1

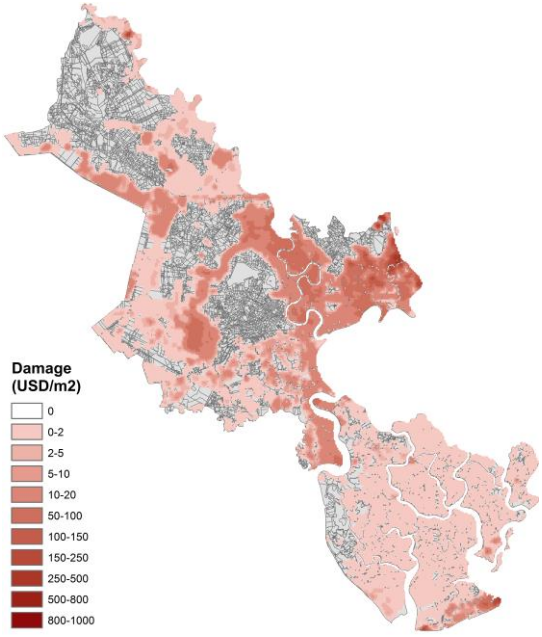

Figure 5-34: Map of estimated damage – 1547_B2

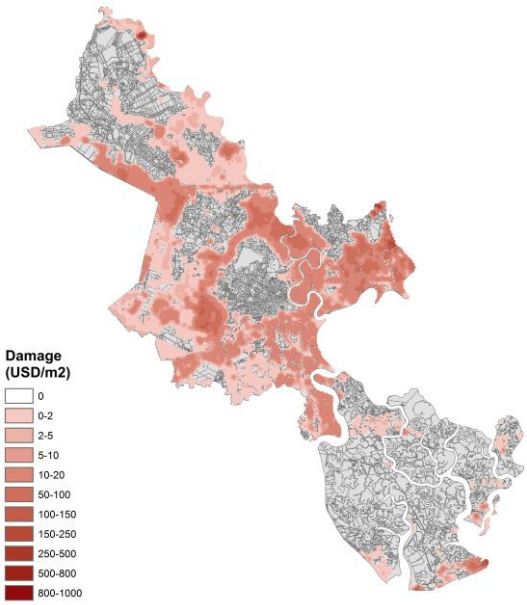

Figure 5-35: Map of estimated damage – T2_B1

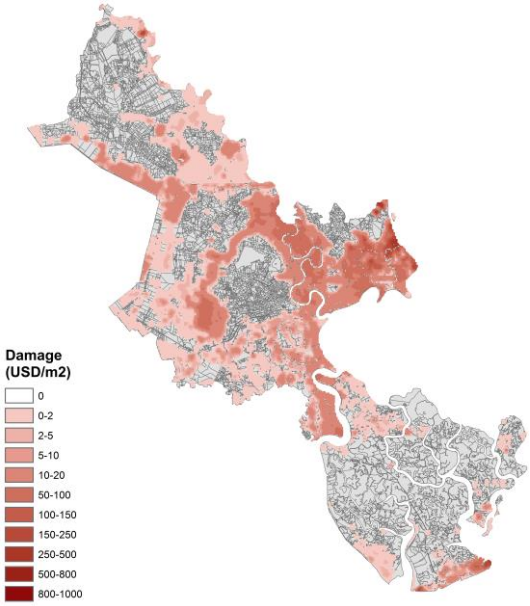

Figure 5-36: Map of estimated damage – T2_B2

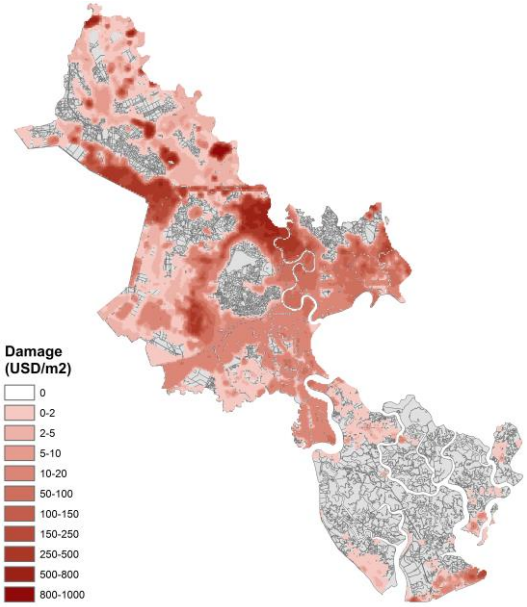

Figure 5-37: Map of estimated damage – Failure of Dautieng dam

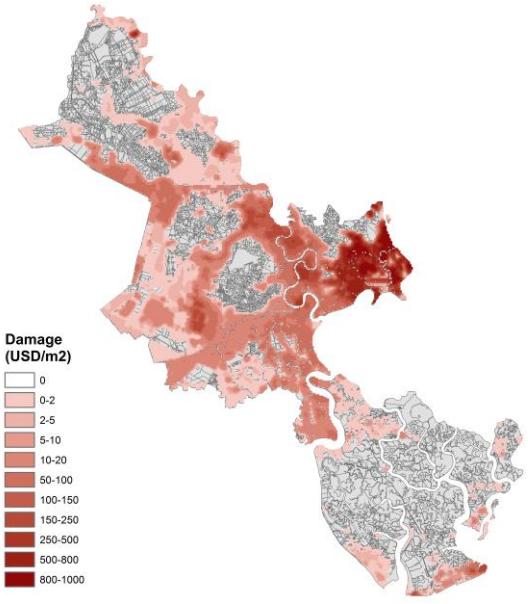

Figure 5-38: Map of estimated damage – Failure of Trian dam

Table 5-6: Estimated damage based on type of lands

Landuse	**Estimated damage based on type of lands (Mil. USD)**									
Scenarios	Settlement	Road	Aquaculture	Plantation	Fruit	Paddy rice	Tree	Salt Field	Other	Total
HT_B1	1,033.14	2.79	9.59	28.93	41.36	7.62	13.96	0.70	102.55	1,241
HT_B2	1,074.41	3.16	10.00	28.69	45.73	7.13	13.91	0.71	108.15	1,292
1547_B1	751.48	1.88	6.86	19.82	38.90	3.81	12.76	0.70	76.89	913
1547_B2	790.43	2.18	7.01	19.00	42.88	3.52	12.44	0.71	80.82	959
T2_B1	750.98	2.00	4.94	22.95	36.61	5.67	3.01	0.26	72.77	899
T2_B2	790.38	2.18	6.59	18.97	42.85	3.52	3.11	0.44	79.72	948
DT_Dambreak	3,390.68	3.50	12.58	97.96	95.42	45.08	5.63	0.47	290.11	3,941
TA_Dambreak	3,646.86	10.65	27.31	69.52	280.01	10.82	5.50	0.66	321.54	4,373

Table 5-7: Summarized results

Scenarios	% Max water depth	Estimated damage (Mil. USD)
HT_B1	66.11	1,240.66
1547_B1	59.65	913.09
T2_B1	55.92	899.19
HT_B2	65.84	1,291.89
1547_B2	56.93	958.98
T2_B2	55.87	947.77
DT_dambreak	74.48	3,941.42
TA_dambreak	68.61	4,372.86

5.4.2. Analyzing hydrological conditions

In case of baseline scenarios:

- When flood discharge of the upstream reservoirs exceeds the designed frequency as hydrological condition B1 - Dautieng reservoir releases the discharge exceeding flood frequency of P = 0.02%, then the flooded area) is 66.11%, and total damage is estimated at $ 1.24 billion, including damage on houses – construction which occupies with the largest proportion of 1,03 billion.

With hydrological conditions B2 - Tri An reservoir releases the flood discharge exceeding the flood frequency of P = of 0.02%, then the flooded area1 is 65.84%, and the total estimated damage is 1.29 billion which is larger than the HT_B1 $ 50 million, and the biggest damage is urban housing - construction (1.07 billion dollars).

In case of completing construction according to Decision No. 1547/QD-TTg:

Estimated damage according to hydrological conditions B1, inundated area accounted for 59.65%, and total loss in 1547_B1 is 913 million, which

reducing 341 million compares with HT_B1, most damages which are reduced in the inner region - construction of buildings (751 million USD).

With the hydrological condition B2, the flooded area is reduced in proportion (56.93%). This is understandable because the total amount of flood discharge in Trian reservoir is bigger than Dautieng reservoir, and the inner area is protected by dikes and flood contruction control, so the total amount of water poured in lower areas and the downstream of the watershed. Under this scenario, the total loss was 959 million which reducing 344 million as compared to HT_B2 and most damages reduced by protecting the inner urban area (from 1.07 billion USD with the HT_B2 dropped to 790 million USD in 1547_B2).

In case of constructing the sea dyke connecting Vung Tau to Go Cong:

Hydrological conditions B1: average total flood area of Ho Chi Minh City occupied 55.92%. Total losse were estimated at 899.2 million USD, where the damage on housing sector accounted for 751 million.

Hydrological conditions B2: average total flood area of Ho Chi Minh City occupied 55.87% less than B1, which are explained similarly with HT_B1 and HT_B2. Regarding to the loss, B2 scenario causes more damage than B1 scenario with the total damage of 959 million USD and damage on houses and buildings accounted for the highest rate of 790 million USD, the remaining loss of other industries accounted for 151 million USD.

5.4.3. Analyzing effects of construction on damages

By hydrological conditions B1: with according to Decision No. 1547/QD-TTg, the ability to control flooding inner region is best, reducing flood area approximately 13.1% compared with the status scenario HT_B1, and 2.9% with T2_B1. However, with 1547_B1, most reduced flood area was the area inside embankments to control the water level in center of Ho Chi Minh city, while other areas aren’t not only reducing flooded but also increasing the flood area than current. On damages, loss result of HT_B1 is greatest damage at $ 1.24

billion USD, and the 1547_B1is 913 million USD, and the lowest damage as T2_B1 is 899 million USD.

By hydrological conditions B2: the flood area also reduced similarly with trend of the hydrology condition B1, in case of calculation for hydrological conditions B2 - Tri An releases the flood discharge exceeding the flood frequency of P = of 0.02%, the construction solution under Decision No. 1547/QD-TTg likely the best flood control for inner areas of city center. But in terms of overall ability to control the flood under construction solution, T2_B2 brings greater efficiency, particularly flooded area in the city is 55.9% according to T2_B2, 56.9% by 1547_B2, and 65.8% by HT_B2. Total estimated value of damage with HT_B2 was 1.29 billion USD, and T2_B2 were is 948 million USD.

5.5. Conclusion

Increased frequency and intensity of flooding events, combined with trends in growing urban population in most countries have led to the need for increased and internationally coordinated efforts to enhance technologies and policies for dealing with floods. A number of national and international research programs have made good progress in this respect, but much more is needed in order to improve flood management strategies. This research has adopted an original approach that aims to quantify the cost-effectiveness of resilience measures and integrative and adaptable flood management plans for different scenarios.

To access the max inundated water depth in HCMC, the 1-2D MIKE FLOOD Molde was applied for simulating inundated water depth. The map results of inundation indicated that the JICA-2001 could not protect HCMC even only center of urban from flood and tide. Moreover, the inundation caused by flood increased significantly urban center under flood scenarios.

With the project 1547/QD-TTg, almost area in city urban could be protected from the upstream flood and tide. However, the suburbs of the city was trend of increasing flood inundation. It was explained that the project

1547/QD-TTg protect inner of HCMC by preventing over-land flows from flood, and total amount of flood water volume was entered to smaller areas. As comparison of inundated results between JICA-2001 and Project 1547/QD-TTg, total inundated area of Cangio Mangroves forest in Project 1547/QD-TTg had slightly higher than in JICA-2001.

By the Project of sea dike, inundated area inner of HCMC was slightly decrease as compared to JICA-2001. But total inundated area of whole HCMC was dramatically reduced as compared with JICA-2001 and Project 1547/QD-TTg. Depending on goals to flood control in HCMC, scenarios of Project 1547QD-TTg and Sea Dike were considered.

In economic aspect, the results of flood risk and damage analysis showed that the project of JICA-2001 for protecting HCMC from rainfall was not appreciate in context of increasing of sea level and upstream flood. Total economic losses was estimated around 1,240.66 milion USD, 1,291.89 million USD, 3,941.41 million USD and 4,372.89 milion USD in B1, B2, Dau Tieng dam failure and Trian dam failure, respectively.

By the Project 1547/QD-TTg, total losses were 913.09 milion USD and 958.89 milion USD in B1 and B2 hydrological conditions, respectively. It showed that total losses in Project 1547/QD-TTg siginificanly reduced as compared to the project of JICA-2001.

Project of Sea Dike was also estimated the damage losses, and total losses in this scenarios was smallest as compared to other scenarios. The results of damaged losses were 899.19 milion USD in B1 hydrological condition and 947.77 milion USD in B2 hydrological condition.

Although sea dike project was better to reduce the damaged losses, Project 1547/QD-TTg was better to flood control in urban center of HCMC. Furthermore, the cost for construction also a important factor to be considered, but this was not analyzed in this research.

CHAPTER VI

EFFECTS OF CLIMATE CHANGE AND DEVELOPMENT ON SEDIMENTATION IN PLAIN OF REEDS

6.1. Background

The suspended sediment load in the MRD plays an important role in carrying contaminants and nutrients to the delta and changing the geomorphology of the delta river system. In recent decades, it is generally perceived that the flow and sediment transport in the Mekong River have changed due to climate change and development activities, but observed sediment data are lacking. Moreover, after natural floodplains, the sediment deposition have replaced by dense river systems as resulting in floodplain compartments protected by embankments.

In recent years, the Mekong Basin has undergone significant hydropower development. Pre-1990, most hydropower development in the Mekong was publically funded, but this new wave of development has generally been led by commercial partnerships between private sector developers and host governments. In the Lower Mekong Basin, at least twelve potential mainstream hydropower developments are currently being considered by private sector developers (MRC, 2010). Ten of these proposed projects are planned for Lao PDR, and the other two for Cambodia (**Figure 6-1**). Site preparation for the first of these projects, Xayaburi, is underway. The Lao government and its Thai developer are beginning preparatory earth works and resettlement plans for those whose land is needed for the dam's construction.

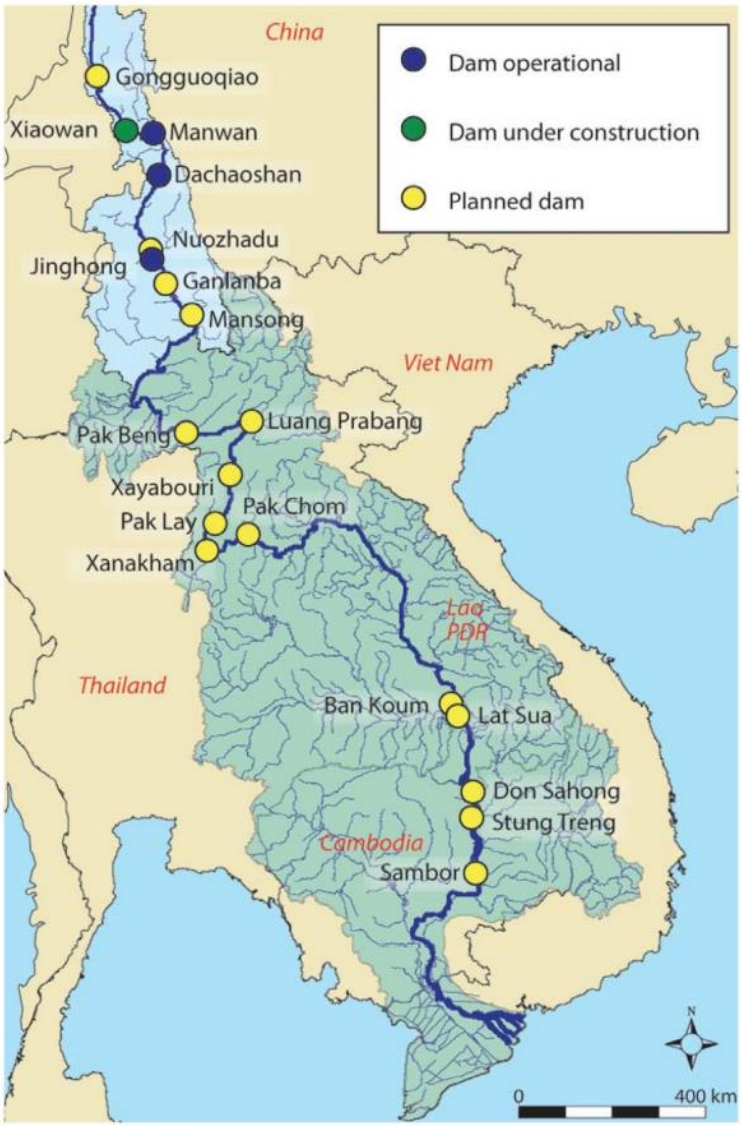

Figure 6-1: Map Showing Current and Proposed Mainstream Mekong Hydropower Dams

Several studies (Lu and Siew, 2006; Liu and He, 2012; Liu *et al.*, 2013) showed that these dams reduced the sediment delivery from the Lancang River to downstream Mekong. Some studies reported that, total suspended sediment (TSS) discharge from the Chiang Saen branch reduced from mean annual 75 million m^3 (during the period of 1962-1992) to 35 million m^3 (during the period of 1993-2003). Similarly, in the Khong Chaim branch, reduced from 180 million

m^3 (1962-1992) to 100 million m^3 (1993-2003) and in Pakse reduced from 160 million m^3 (1962-1992) to 120 million m^3 (1993-2003) (MRCS/WUP-FIN, 2007).

This study is aimed to investigate impacts of water availability and sea level rise on sediment transport under anticipated scenarios. Therefore, the hydrodynamic model and sediment transport model – Mike 11 are applied for simulating sediment load processes on the Mekong Rivers in order to quantify spatial variability of sediment floodplain deposition in the Lower Mekong Delta (LMD), as well as a strategy to quantify the uncertainty of sediment loads based on anticipated scenarios associated with various upstream discharges (hydropower dams development) and sea level rise (climate change). The findings of outcomes is able to contribute to the debate on the economic value of floodplain deposition in terms of nutrients, which is a hot topic in the Mekong Delta, as well as are the concrete basis in contribution to propose sustainable measures for improving positive effects and restricting negative impacts on cultivation.

6.3. Data setting and Methodology

6.3.1. Study area

Within the LMD our study area is located in the Dong Thap Muoi (DTM), which is also called the Plain of Reeds (see **Fiure 6-2** and **Figure 6-3**). The DTM has an area of 7,081 km^2 and is shared between three provinces: Long An, Tien Giang and Dong Thap. Approximately 70% of the total area is used for agriculture, while DTM accounts for 36.7% of the LMD. In its upstream section, the Tien River carries about 80% of the total discharge of the Mekong River. In addition, a significant flood discharge transfers along Cambodia border into DTM via horizontal canals causing serious flood inundation and affects to agricultural cultivation and human activities. To strengthen the stability and economic development in DTM, the governmental authority has been investing huge budget for improving irrigation and drainage systems in order to control

water sources at compartments by low dikes for crops and high dikes for flood protection. The man-made channel and dike systems have greatly altered the natural hydrodynamic conditions in the Vietnamese part of the delta. In combination with the extensive development of dike systems in the last decades, especially after the devastating flood in 2000, the floodplains are increasingly cut off from the natural inundation regime. With characteristics of particular DTM, the channel density of 11.6 m/ha is comparable to the average density of the Delta. About 67% of the dikes in the study area are low dikes, with average crest levels of about 2.5 m, and 33% are high dikes for flood protection, with average crest levels of about 4.5 m.

6.3.2. Data used

Hourly discharge and water level data from all the available hydrological stations located in the LMD were used (**Table 6-1**) for calibration and validation of Mike 11 hydrodynamic and sediment transport models. The simulation period was chosen from July to December, which covers the entire flooding season (August–October). Rainfall data (daily time series) from 13 stations were used for the NAM hydrological model which was integrated with the Mike 11 model to take into account the runoff generated within the LMD. The Thiessen polygon method was use to obtain sub-catchment rainfall from the 13 stations rainfall (Figure 6-2). At the upstream boundary at Kratie (**Figure 6-2**), the suspended sediment data are unavailable. Hence, we derived the sediment discharge boundary condition at Kratie using the relationship between water discharge and suspended sediment concentration (Eq. 6-1) developed by Manh *et al*. (2014).

$$SSC_t^{\text{Kratie}} = 10^{\left(-494.02 \log\left(Q_t^{\text{Kratie}}\right)\right)^{-4.52}} + 2.88 \quad (6\text{-}1)$$

Where, SSC_t^{Kratie} is suspended sediment concentration [mg/L] at time *t* at Kratie, Q_t^{Kratie} is water discharge [m^3/s] at time *t* at Kratie.

The sediment discharge is calculated by using the following equation:

$$SSD_t^{\text{Kratie}} = 2.65 \times 10^{(-3)} \times SSC_t^{\text{Kratie}} \times Q_t^{\text{Kratie}} \quad (6\text{-}2)$$

Where, SSD_t^{Kratie} is sediment discharge [m^3/s] at time *t* at Kratie.

The hydrodynamic model was calibrated and validated with the observed discharge and water level data from the year 2000 and 2002. The year 2000 can be considered as a big flooding year and the 2002 as a normal flooding year. The sediment transport model was calibrated validated using the data of sediment discharge data from 2002. These data were collected by the Division of Science and Technology, Thuyloi University, Vietnam (former Water Resources University). The locations of the data stations are shown in the **Figure 6-2** and **Figure 6-3**.

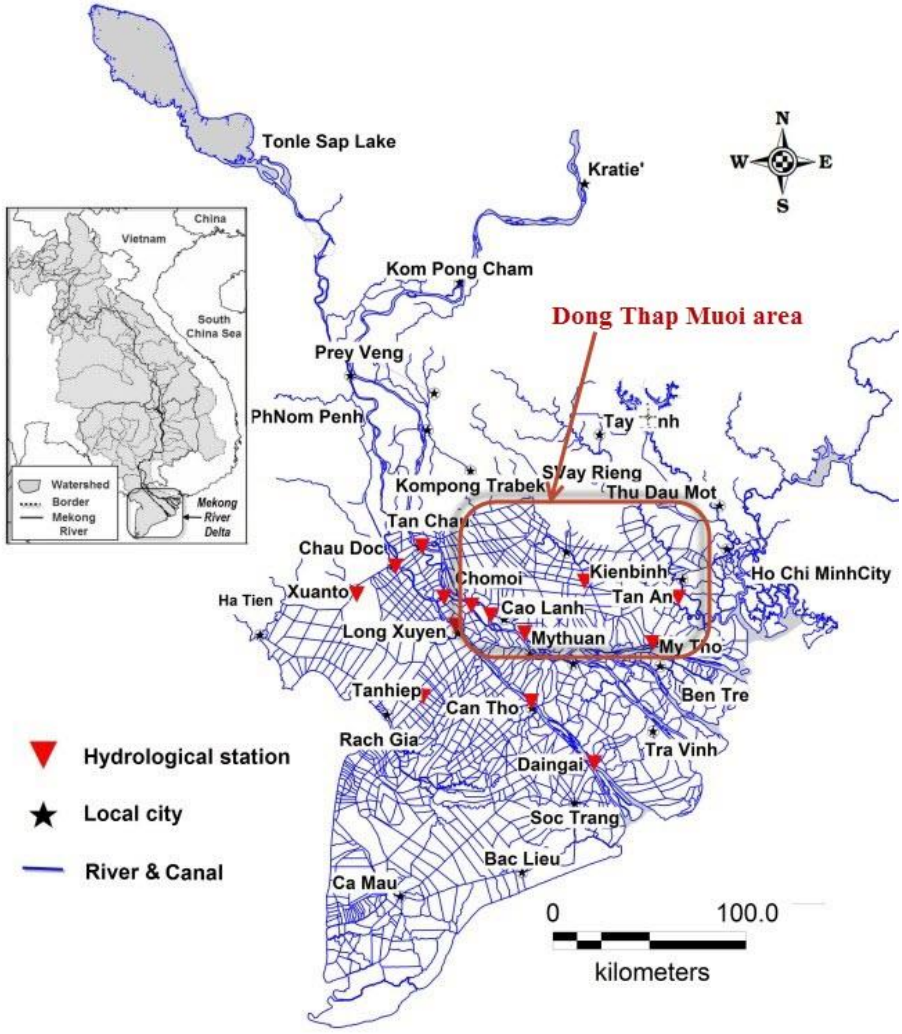

Figure 6-2: Lower Mekong River and location of hydrological stations

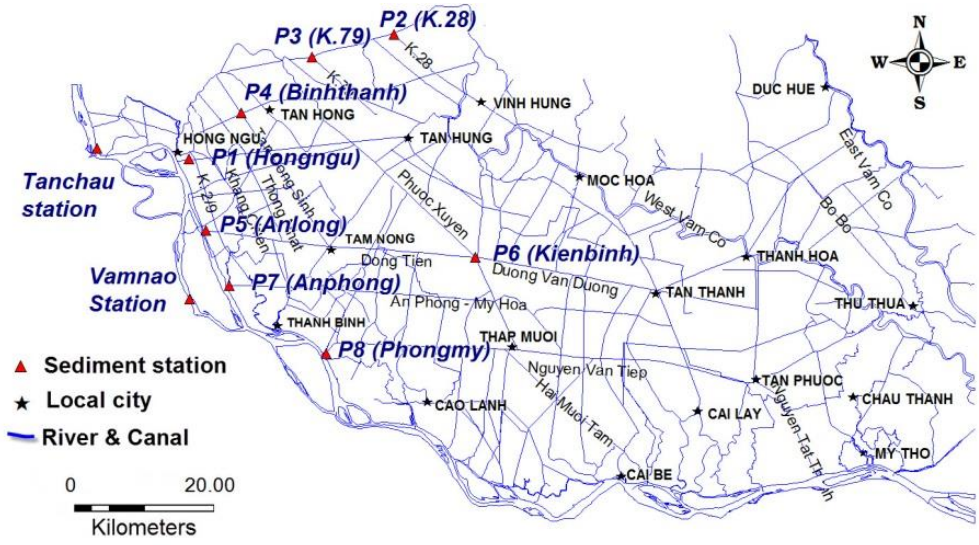

Figure 6-3: Study area and location of sediment mobile stations

6.3.3. Mike 11 model

Mike 11 model, developed by DHI, is a modeling system for simulating water flow, water quality and sediment transport in estuaries, rivers, irrigation channels and other water bodies (DHI, 2012). It comprises of a number of modules, such as Hydrodynamic (HD), Rainfall Runoff (RR), Advection Dispersion (AD), Water Quality (ECOLab), Sediment Transport (ST) etc. We used the HD module with its fully hydrodynamic method based on Saint-Venant equations for the river flow. The RR and ST modules will be discussed separately below. The MLD is a very complicated network of rivers and channels. All rivers and channels in the LMD and Dong Nai-Saigon River system are represented in the model with 4,110 branches and reaches with a total length of 24,200 km and 39,780 cross sections. Three types of river structures are represented, which are 19 free overflow weirs (broad-crested), 14 culverts (rectangular section) and 2,429 underflow control structures (see **Figure 6-4**). The control structures are treated as automatic with upstream/downstream water level control. To prevent the flow of sea (saline) water into the paddy fields, the

control gates will be closed if the water level in the rivers due to tidal effects is higher than the upstream water level in the paddy fields. .

The model consists of 22 upstream inflow boundaries (discharge time series), 58 downstream water level boundaries and 22 sediment inflow upstream boundaries, and rainfall-runoff links to 1,682 sub-basins. The upstream model domain was extended up to Kratie, downstream of the Cambodia border and Tonlesap Lake. The Manning's roughness values were set by calibration. In most river sections a value of 0.028 was use and in channel reaches the values varied from 0.025 to 0.1.

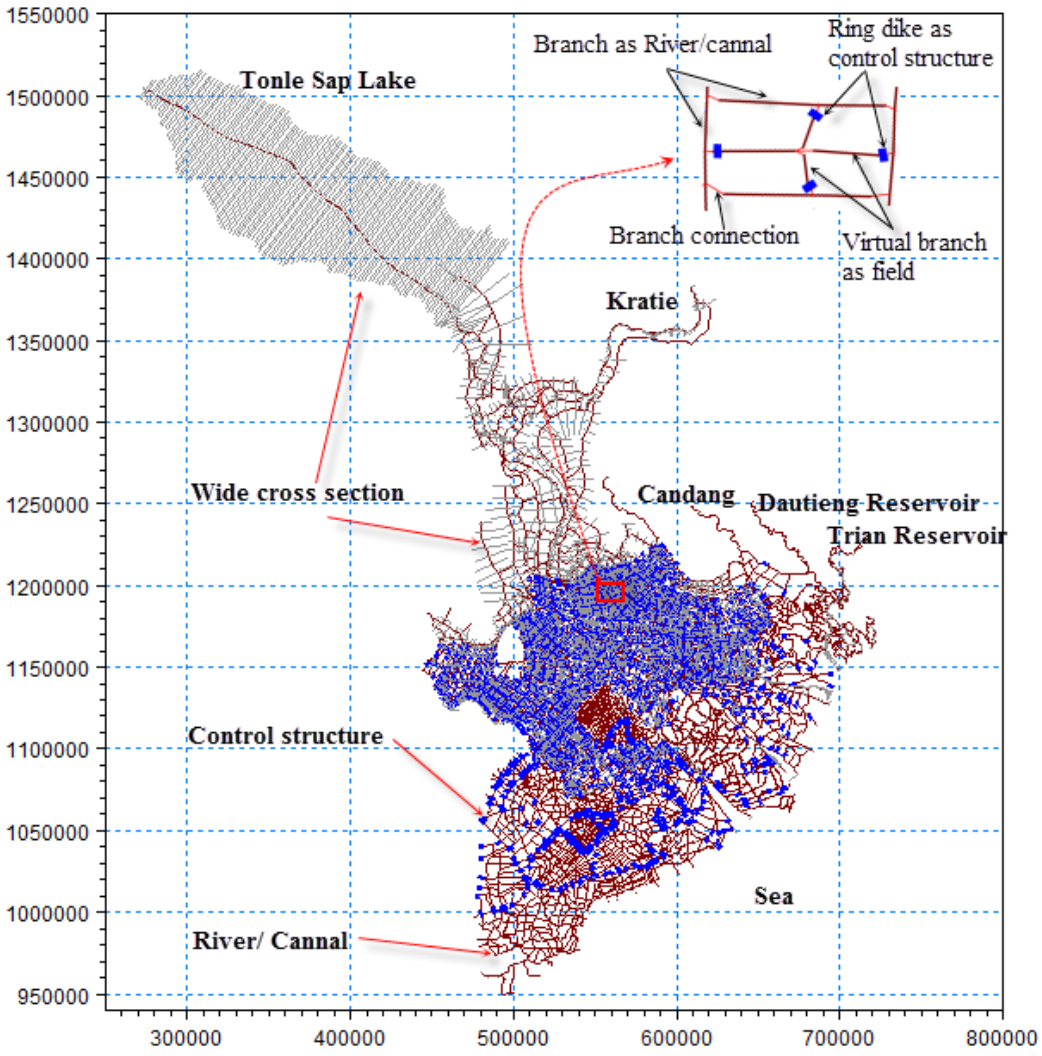

Figure 6-4: Modeled river network in Mike 11

6.3.4. Mike 11 NAM model

The NAM is a conceptual RR model (Havnø *et al.*, 1995; Nielsen *et al.*, 1973). It can be integrated with the Mike 11 HD model for computing discharge time series input to the HD model that is generated within the model domain. The model domain can be divided into a number of units or subbasins. NAM treats each subbasin as a lumped unit with 10 main parameters that need to be calibrated. There are 1,682 subbasins in our model. For the calibration purpose they were grouped into two types: those in the delta area and those in the upstream of the deltas (**Figure 6-5**). The parameters we used are established in earlier studies by Ngoc *et al.* (2011, 2013a).

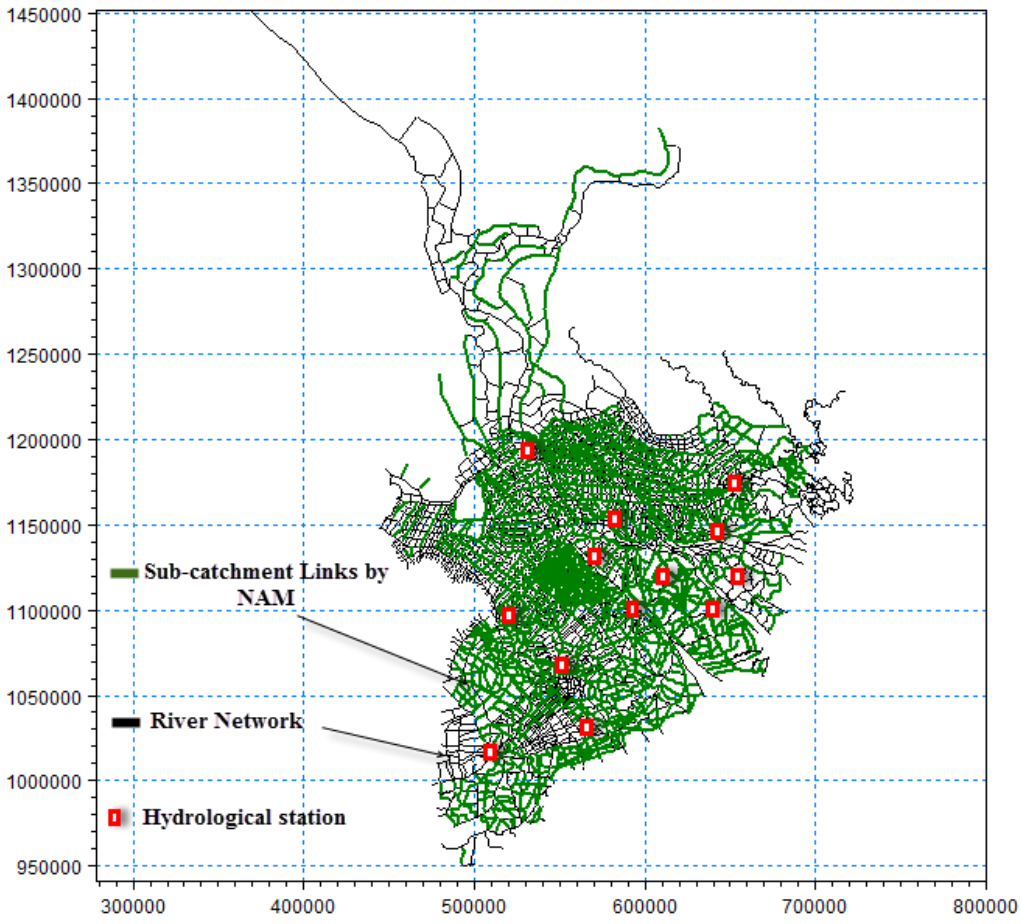

Figure 6-5: Sub-catchments links in Mike 11 NAM model

6.3.5. Mike 11 ST model

The ST model used in Mike 11 is based on Van Rijn model in which the sediment load is divided into bed load and suspended load according to the relative magnitudes of bed shear velocity and particle fall velocity (Van Rijn, 1984). When the bed shear velocity exceeds the fall velocty, sediment is transported as both suspended sediment and bed load. The parameter set in sediment transport model is referred to a report of. The sediment properties specified in the model are based on a number of previous studies (Hung *et al.*, 2014b; Manh *et al.*, 2014; Ngoc *et al.*, 2013b; MRC/DMS, 2010).

Most suspended sediment in the LMD is fine-grained (Hung *et al.*, 2013a). MRC/DMS (2010) pointed out a d_{50}=3-8μm in the Tonle Sap River. Sediment analysis from 11 trap sites over large area of the LMD found that grain size of deposited sediment are uniformly distributed with a dispersed grain size distribution of 41% clay (grain size <2μm) and 51% silt (grain size 2-63μm) (Manh *et al.*, 2014). Hung *et al.* (2014b) reported that the average flock size determined for floodplains of the DTM is d_{50}=35μm, which dominates the sediment deposition over 12 trap sites measured on floodplain of the DTM. They also indicated that range of dispersed and flocculated grain sizes is d_{50}=2.5-80 μm, which were extensively used to evaluate a calibration range of $W_0=1\times10^{-5}$ – 7×10^{-3} m.s-1, where W_0 is the free settling velocity based on the Stoke's law (Manh *et al.*, 2014; Hung *et al.*, 2014b). (see detail in **Table 6-1**)

Table 6-1: Sediment transport parameter set

No.	Item	Value	Description
1	Relative density	2.65	Specific gravity
2	Kinematic viscosity	1.5	x 10^{-6} m^2/s
3	Global grain diameter	35	μm
4	Grain diameter in border of Cambodia	10-35	μm
5	Grain diameter in Tien River	40-65	μm
6	Grain diameter in DTM	10-40	μm

6.4. Proposed modeling scenarios

We base our analysis on a baseline scenario and eight future scenarios (**Table 6-4**). The year 2002 is considered as the baseline scenario and the future scenarios are based on different levels of dam development and projected climate change in the region. Three levels of dam development are considered, namely low development (LDD), low development plus the Xayaburi dam (XDD) and high development (HDD). The HDD scenario includes all the dams considered in the LDD, the Xayaburi and some additional dams. The reservoir storage capacity of the LDD scenario in the Lower Mekong is almost double of the BL scenario (**Table 6-3**). With addition of the under construction highly controversial Xayaburi, the storage capacity in the lower Mekong will be added by about 10% of the LDD scenario, but it is not estimated to increase the water demand and irrigation area. The HDD scenario almost doubles the storage capacity in the Lower Mekong as well as in the Upper Mekong in China from that of the XDD scenario. For climate change, we based on the report of the Vietnam Ministry of Natural Resources and Environment (MONRE, 2012), and we considered two future periods, 2050 and 2100. The estimates of the change in rainfall, temperature and sea level rise are for these time periods are presented in **Table 6-2**).

Table 6-2: Scenarios of climate change and sea level rise

Climate change to study area (unit)	**Period**		
	2020	2050	2100
Rainfall (%)	1	2.8	5.2
Sea Level Rise (cm)	9-10	25-30	62-82
Temperature (^{0}C)	0.4	1.3	2.5

Table 6-3: Upstream development in irrigation and hydropower dams

Anticipted Scenarios	**Total water demand (10^6 m^3)**	**Irrigated area (1,000 ha)**	**Total reservoir capability (10^6 m^3)**	
			Lower Mekong	China
Baseline in 2002	1,620	7,422	6,185	-
Low dam development	3,109	8,316	12,443	10,300
Xayaburi dam development	3,109	8,316	13,743	10,300
High dam development	4,194	11,349	26,778	22,700

Table 6-4: Proposed modeling scenarios

No.	**Scenarios**	**Description**	**Climate Change**	**Upstream Development**
1	BL	Baseline	2002	2002
	BL2050	Baseline+CC2050	2050	2002
3	BL2100	Baseline+CC2100	2100	2002
4	HDD	BL+HDD	2002	High dam development
5	HDDCC2100	BL+HDD+CC2100	2100	High dam development
6	LDD	BL+LDD	2002	Low dam development
7	LDDCC2100	BL+LDD+CC2100	2100	Low dam development
8	XDD	LDD+Xayaburi	2002	Xayaburi constructed
9	XDDCC2100	LDD+Xayaburi+CC2100	2100	Xayaburi constructed

6.5. Results

6.5.1. Model verification

To evaluate the performance of Mike 11 model, the coefficients of Nash-Sutcliffe (E_2), Root Mean Square (R_2) and Root Mean Square Error (*RMSE*) (see in Eqs. 3-17, 3-16 and 3-19 in Chapter 3) were used to express the model's ability to simulate hydrodynamics and sediment transport.

The hydrodynamic model (HD) simulated the period July 1st to December 30th 2000 with a time step of 10 minutesl and output was stored hourly. Observed water levels at 14 hydrological stations during the year 2000 were used for model verification. (Locations of data collection sites are shown in **Figure 6-2**).

Table 6-5: Coefficients of Nash-sutcliffe, R^2 and *RMSE* between observed and simulated water levels

No.	Station	Nash-sutcliffe (E_2)	R^2	RMSE
1	Tanchau	1.000	1.000	0.002
2	Chaudoc	0.997	0.997	0.038
3	Vamnao	0.975	0.984	0.088
4	Longxuyen	0.933	0.937	0.112
5	Chomoi	0.966	0.967	0.103
6	Caolanh	0.926	0.930	0.133
7	Xuanto	0.978	0.985	0.130
8	Kienbinh	0.911	0.927	0.224
9	Tanhiep	0.940	0.970	0.144
10	Mythuan	0.912	0.933	0.131
11	Mytho	0.938	0.957	0.170
12	Cantho	0.914	0.953	0.138
13	Daingai	0.950	0.958	0.166
14	Tanan	0.918	0.929	0.191

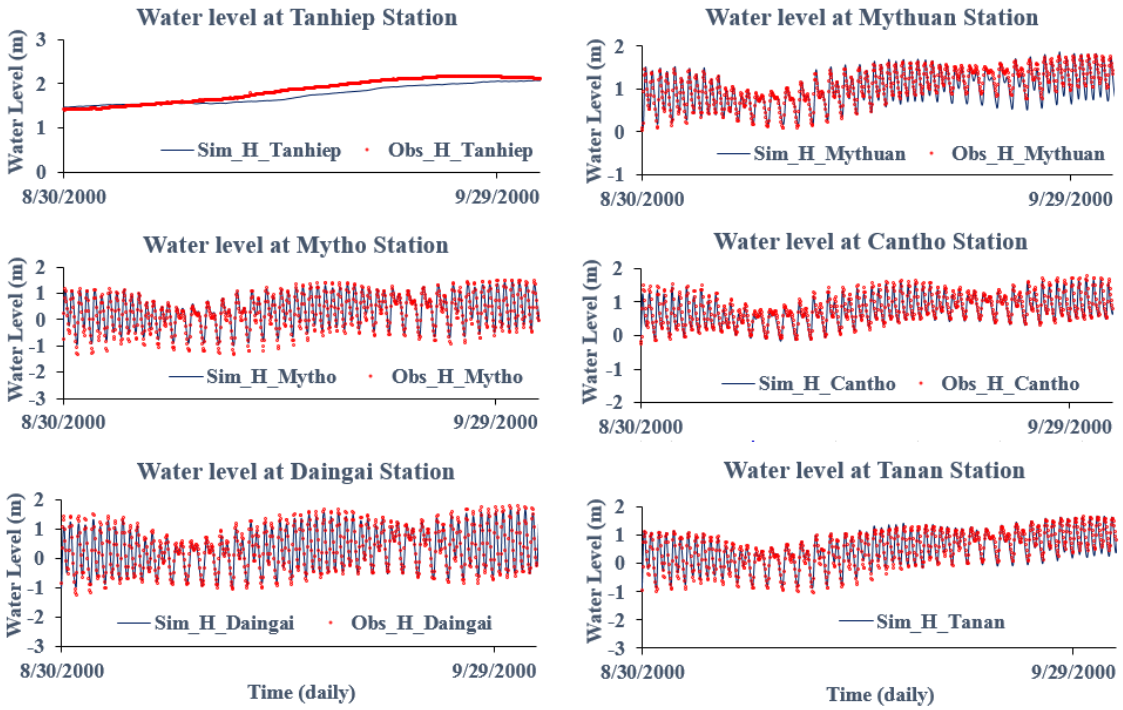

Figure 6-6: Calibration of observed and simulated water level for some stations in 2000

The modelled and observed water level comparison (**Table 6-5** and **Figure 6-6**) indicate that the model achieves a greater precision at hydrological stationlocated along the main branches of the Lower Mekong River (Hau and Tien Rivers) than at those located in the secondary canals. This is probably because the complex of river network system, as well as many flood control structures along the main river branches will invariably have a significant effect on the hydrodynamics in the secondary canals. However, the model shows very good agreement with data at most stations with R^2 values close to unity Nash-sutcliffe coefficients (E_2) higher than 0.91. This provides sufficient confidence in the ability of the model to simulate river hydrodynamics.

Next, the model was verified for sediment transport using data obtained in September 2002 using 10 mobile stations (see **Figure 6-3** for locations). The model/data comparisons are shown in **Table 6-6** and **Figure 6-7**.

Table 6-6: Coefficients of Nash-sutcliffe, R2 and RMSE between observed and modelled daily sediment discharges

No.	Station	Point	Nash-sutcliffe (E_2)	R^2	RMSE	No.	Station	Point	Nash-sutcliffe (E_2)	R^2	RMSE
1	Tanchau		0.634	0.842	1.369	6	Binhthanh	P4	0.703	0.898	0.011
2	Vamnao		0.575	0.734	0.541	7	Anlong	P5	0.561	0.904	0.040
3	Hongngu	P1	0.604	0.928	0.050	8	Kienbinh	P6	0.764	0.928	0.050
4	K28	P2	0.595	0.741	0.010	9	Anphong	P7	0.392	0.735	0.005
5	K79	P3	0.642	0.909	0.006	10	Phongmy	P8	0.290	0.818	0.032

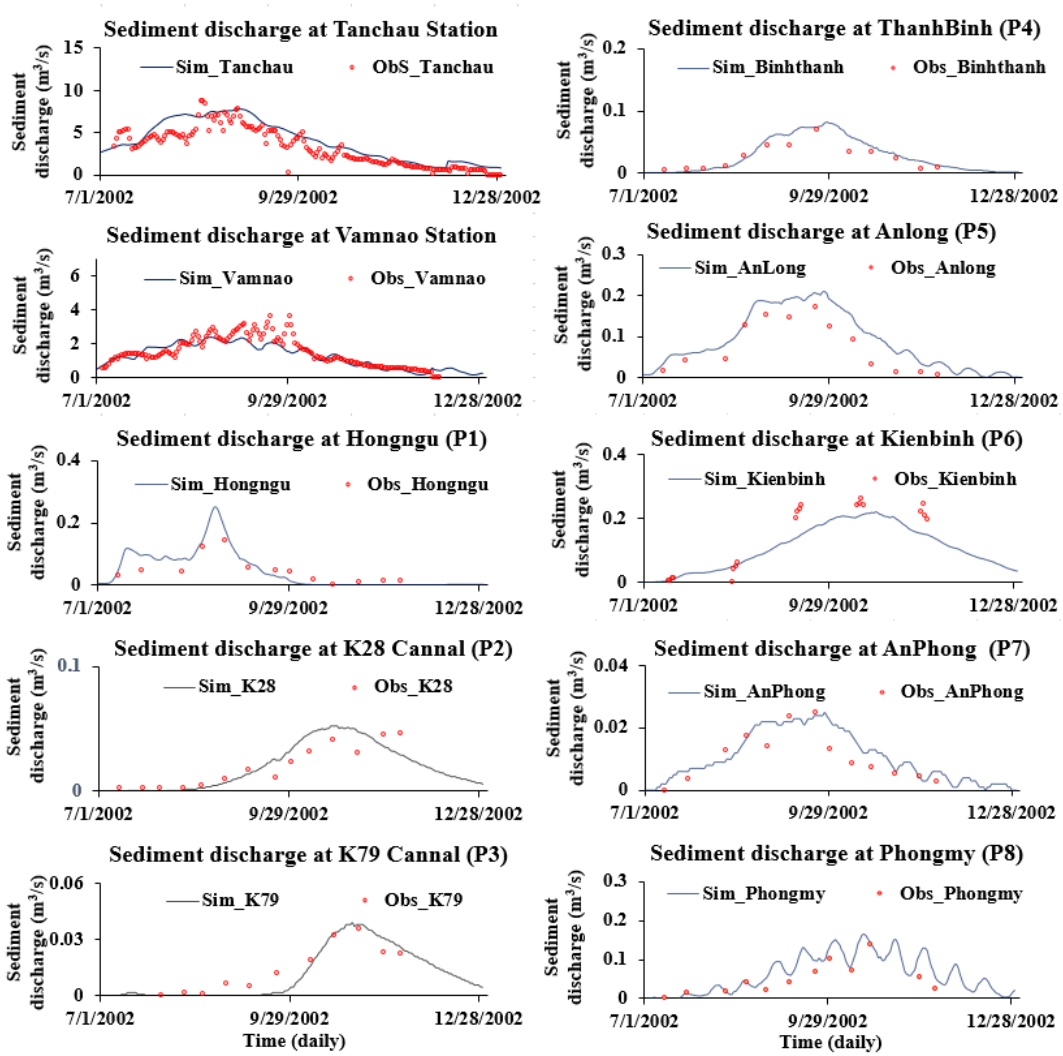

Figure 6-7: Observed and simulated sediment discharge in 2002

In general, there is good agreement between the modelled and measured sediment fluxes. The error statistics show that model/dta comparisons are very good upstream of the LMD (Tanchau and Vamnao stations) and at the Cambodia border (K28 (P2), K79 (P3), Hongngu (P1), Binhthanh (P4) canals)). In addition, the R^2 values are much higher than E_2 values indicating that the model reproduces the trend in observations better than the magnitudes. It should, however, be taken into account that the accuracy of sediment transport measurements is relatively low (compared for e.g. to water level measurements) and therefore, the achieved model/data comparisons provide sufficient confidence in the model to proceed with scenario modelling described as above-metionted.

Figure 6-8 shows the modelled flood and sediment discharge at the main stations for the baseline scenario (July-Dec 2002). In the event of 2002, the volume of flood discharge in Tien River is about three times higher than in Hau River at the upstream of the LMD and it transfers much volume of flood from Tien River to Hau River at the junction of Vamnao, which connects the Tien River and Hau River together. However, sediment discharge at Chaudoc is not much smaller than sediment discharge at Tanchau. It seems to say that the total sediment delivery is not only transferred from Tien River to Hau River at Vamnao Junction, but also depended on the hydrodynamics on river.

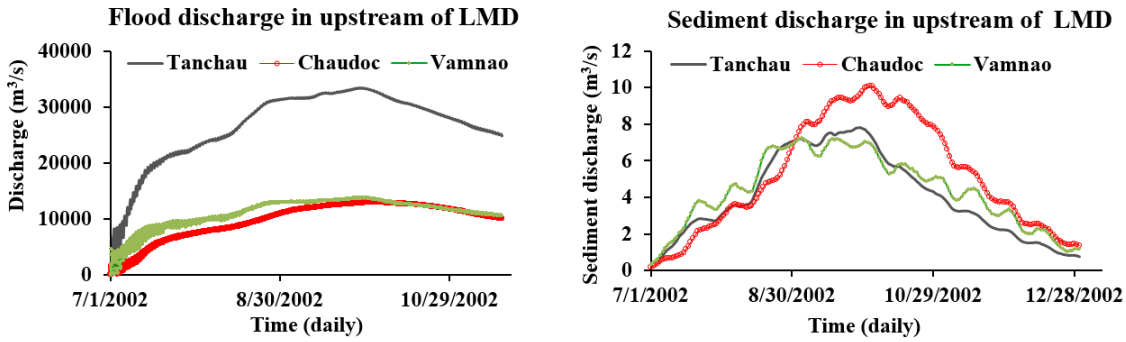

Figure 6-8: Flood discharge and sediment discharge at upstream of LMD in 2002

6.5.2. Changes in sediment transport based on upstream dam development scenarios

Figure 6-9 shows the total sediment discharge transports via Tien River and Cambodia border to the DTM floodplains affected by upstream development of hydropower dams. The results show that during the 2002 flood season, that sediment would have been brought into the DTM through overbank flow over floodplains at the Cambodia border. As expected, increased water storage in hydropower reservoirs leads to a reduction in the r total sediment transport to the LMD.

The effect of further developing hydropower reservoirs on sediment transport into the DTM floodplains via Tien River and Cambodia border is illustrated in **Figures 6-10** and **6-11**. Along the Cambodia border, the associated decreases in sediment transport into the DTM floodplains varies from Tanchau to West-Vamco River. The sharpest drop (about 50% of the baseline transport) is at P3 (K79) closer to West-Vamco River (**Figure 6-10**). Sediment discharge also decreases by abot 50% at P2 (K28), and, to a lesser degree, at P4 (Binhthanh) closer to Tanchau station.

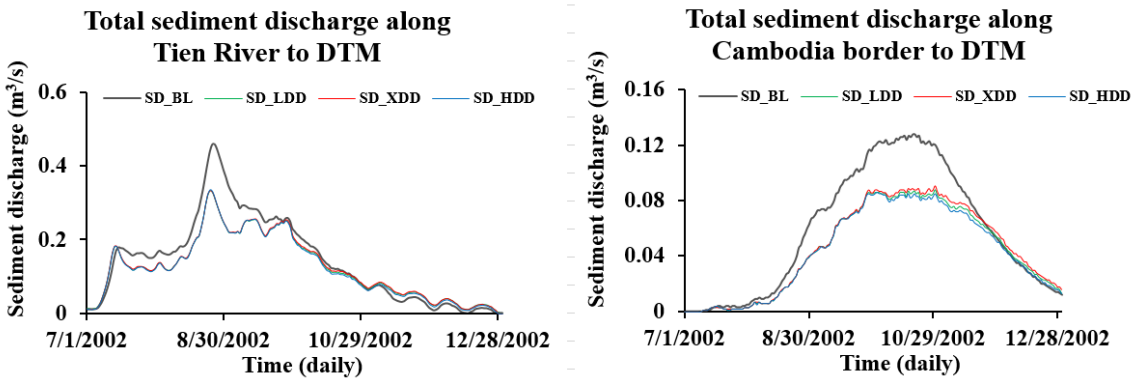

Figure 6-9: Total sediment discharge delivery to DTM via Tien River and Cambodia border based on hydropower dam development scenarios: a) Total sediment discharge delivery to DTM via Tien River; b) Total sediment discharge delivery to DTM via Cambodia border

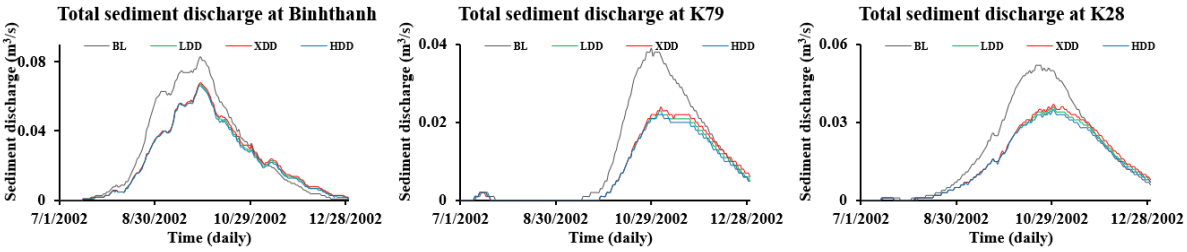

Figure 6-10: Total sediment discharge delivery to DTM via Cambodia border based on scenarios of hydropower dams: Total sediment discharge delivery to DTM via a) Binhthanh; b) K79; c) K28

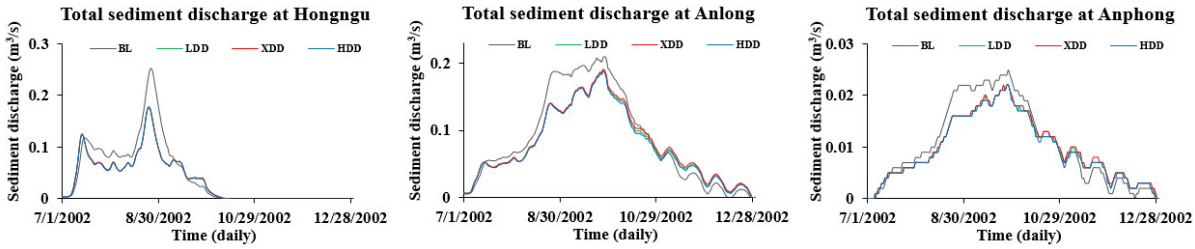

Figure 6-11: Total sediment discharge delivery to DTM via Tien River based on scenarios of hydropower dam development: Total sediment discharge delivery to DTM via: a) Hongngu; b) Anlong; c) Anphong

Similarly, **Figure 6-11** (and **Figure 6-9a**) shows that the sediment supply to the DTM from the Tien River would also be reduced by further development of hydropower reservoirs. In general, therefore, it can be concluded that the further development of reservoirs in the upper Mekong will inevitably reduce sediment delivery to the LMD as well as the DTM floodplains. However, at the end of flooding season (from November to December), the sediment discharge was slightly increased for all stations. This is an answer for regulation/operation of hydropower dams at the upstream, flooding discharge is partially stored in wet season and released in dry season for electricity generation.

The above results also show that the reduction in sediment supply to the DTM will be practically the same for LDD, HDD and XDD scenarios, with the reduction associated with the former being slightly smaller than the others.

As above-analyzed, the DTM floodplains is located in the eastern upstream of the LMD in which the northern direction of DTM is adjacent to the

border of Cambodia and the west is along the Tien River. Consequently, DTM floodplains obtained sediment from two sources, i.e. via main canals connecting to the Tien River, and via canals collecting overland flood flow from the border of Cambodia. The sediment discharge delivered to DTM floodplains from Cambodia through overland flood flow depends on the magnitude of the overflow, however, it is still smaller in comparison to the sediment delivery from the Tien River (Manh *et al*., 2014). Sediment dynamics in DTM floodplains from sources of overflow from Cambodia border is slightly smaller than the sediment discharge from the Tien River. For more details, the following parts will show the changing of sediment discharge and accumulative sediment in spatial of DTM floodplains.

6.5.3. Changes in sediment transport based on climate change scenarios

Under climate change (CC) scenarios considered here, annual precipitation was increased by 2.8% (in 2050) and 5.2% (in 2100), while sea level was raised by 30 cm in 2050 and 82 cm in 2100. **Figure 6-12a** shows that the simulated flood discharges under climate change scenarios is smaller compared to the present, especially much smaller in the July wet season. This is probably because the increase in sea level at the diwnstream boundary is sufficient to impedee the flood discharge from upstream, even with CC increased precipitation. This effect is clearly visible in **Figure 6-12a**, around July, when flood discharge is small and fluctuates with the tide and rising sea level. Following this future decrease in flood discharge, the sediment discharge at Tanchau also shows a reductioncompared to the present. The results (**Figure 6-12b)** also show that as the CC signal increases in time, sediment discharge to the LMD will reduce further.

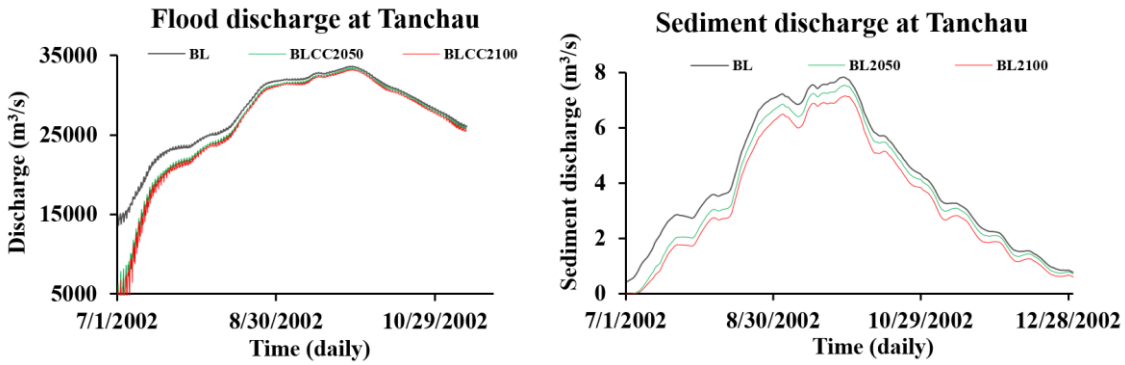

Figure 6-12: Flood and sediment discharge at Tanchau based on climate change scenarios: a) Flood discharge at Tanchau; b) Sediment discharge at Tanchau

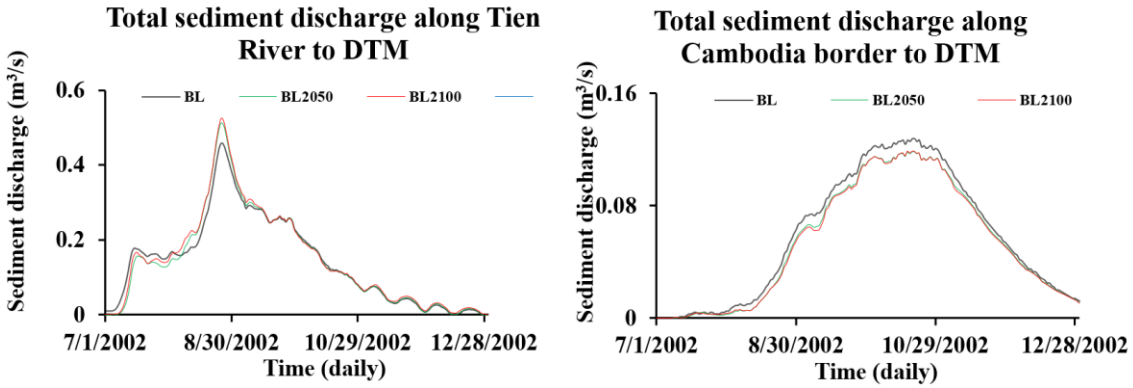

Figure 6-13: Total sediment discharge delivery to DTM via Tien River and Cambodia border based on climate change scenarios: Total sediment discharge delivery to DTM via: a) Tien River; b) Cambodia border

At the Cambodia border, the total sediment discharge delivery via Cambodia floodplains to the DTM also shows a future decrease (**Figure 6-13b**). Along Tien River, an increase of total sediment discharge via main gates of Tien River is shown underCC, increasing in time as CC signals become stronger (**Figure 6-13a**).

When the effect of hydropower dam development scenarios (see in **Figure 6-9**) and climate change (**Figure 6-13**) are compared, the former appears to result in a much higher reduction in sediment discharge to the DTM.

6.5.4. Sediment distribution in DTM floodplains

Table 6-7 shows the changes in cumulative sediment at Tanchau station and DTM floodplains where they are affected by low/high dam development and climate change conditions at the upstream of the LMD in comparison to the baseline scenario.

The total sediment transport at Tanchau station is decreased from 62.78 to 52.57 million m^3 depending on anticipated scenarios. The development at the upstream will lead to the increase in water demand and completed hydropower dams in the upstream of the Mekong Basin, total sediment transport is strongly declined to 57.03 million m^3 under HDD scenario. The total sediment transport is also decreased for the cases of LDD and XDD by 57.72 and 58.56 million m^3, respectively. Accordingly, the total sediment transport rate, which is delivered to the DTM floodplains, is also reduced significantly from 2.14 million m^3 (DTM/Tanchau 3.41%) under the baseline scenario to 1.73 million m^3 (3.04%), 1.76 million m^3 (3.05%) and 1.79 million m^3 (3.06%) under HDD, LDD and XDD scenarios, respectively. Hence, high development with increasing water demand and water storage is a key factor to restrict volume of sediment delivered to the LMD floodplains of Vietnam.

Sediment delivery to the DTM floodplains is originated from 2 main sources, i.e. along the Tien River and overflow from the border of Cambodia floodplains. The amount of sediment delivered to the DTM via along the Tien River is about 1.23 million m^3 (57.66% of total sediment in the DTM) and via the border of Cambodia is about 0.91 million m^3 (42.34% of total sediment in the DTM). The upstream development has dramatically been affected the amount of sediment delivery as well as the proportion of main sediment sources to the DTM. The above impacts is presented through the fluctuation in total sediment transport at Tanchau station, main canals connecting to the Tien River and over the border of Cambodia floodplains. The achieved results pointed out that total sediment delivery to the DTM floodplains went down drastically when comparing

development scenarios of hydropower dam with baseline (in **Table 6-7**). The proportion of transported sediment to the DTM floodplains via Tien River and the border of Cambodia showed a little change, i.e. the total transported sediment via along the Tien River to the DTM floodplains is raised from 57.66% to 61.45% in HDD, 61.00% in LDD and 60.50% in XDD. This may indicate that the development of hydropower dams and irrigation areas at the upstream of the LMD tend to decrease the total transported sediment not only from Tanchau to the LMD floodplains but also via the border of Cambodia to the DTM floodplains.

In order to quantify the total cumulative sediment floodplain under CC scenarios, the total average amount of sediment deposition rate that is delivered into the DTM floodplains in wet season is also compared in these columns 2-4 of **Table 6-7**. Under the impact of CC conditions, the sea level is also raised which impedes the water flowing downstream into the sea. The total sediment discharge at Tanchau station tends to decrease from 62.78 million m^3 in baseline to 56.96 million m^3 under BL2050 and 52.57 million m^3 under BL2100. Although the total cumulative sediment delivery to Tanchau following the CC scenarios declined stronger than development scenarios of hydropower dams, total cumulative sediment delivery to the DTM floodplains gained much higher in comparison with development scenarios of hydropower dams, and even larger than that in baseline. In details, the total cumulative sediment that delivery to the DTM floodplains had ongoing upward trend from 2.14 million m^3 in baseline to 2.26 and 2.42 million m^3 in BL2050 and BL2100, respectively. On the contrary, the total cumulative sediment coming to the DTM tended to be low in the development scenarios of hydropower dams. The columns 5-7 of **Table 6-7** proved that a decrease from 2.14 million m^3 in baseline to 1.79, 176 and 1.73 million m^3 in XDD, LDD and HDD scenarios, respectively.

Table 6-7: Cumulative sediment distribution in the DTM floodplains based on upstream development and CC scenarios

	Cumulative sediment distribution (10^6 m^3/ flood season)								
Zone	BL	BL+ CC2050	BL+ CC2100	LDD	XDD	HDD	LDD+ CC2100	XDD+ CC2100	HDD+ CC2100
Tanchau	62.78	56.96	52.57	57.72	58.56	57.03	51.32	52.32	50.66
% DTM/Tanchau	3.41 %	3.96 %	4.61 %	3.05 %	3.06 %	3.04 %	203.93 %	3.58 %	3.81 %
DTM	2.14	2.26	2.42	1.76	1.79	1.73	1.96	1.87	1.93
-Along Tien River	1.23	1.42	1.60	1.07	1.09	1.06	1.27	1.16	1.25
% of DTM	57.66 %	63.08 %	65.89 %	61.00 %	60.50 %	61.45 %	64.56 %	61.88 %	64.94 %
-Along border	0.91	0.83	0.83	0.69	0.71	0.67	0.69	0.71	0.68
% of DTM	42.34 %	36.92 %	34.11 %	39.00 %	39.50 %	38.55 %	35.44 %	38.12 %	35.06 %

Moreover, looking at the rows 7 and 9 of **Table 6-7**, it pointed out that stronger occurrence in CC may lead to higher increase in proportion of cumulative sediment distribution in the DTM floodplains via along the Tien River and greater decrease via the Cambodia border. By development scenarios of hydropower dams, the same tendency was also found but slightly changed smaller in magnitude. Specifically, total sediment accumulated in the DTM floodplains via along the Tien River counted for 57.66% in baseline, it increased to 63.08% in BL2050 and reached to 65.89% in BL2100. This slight increase also had in development scenarios, cumulative sediment contribution to the DTM floodplains via along the Tien River count for 60.50%, 61.00% and 61.45% in XDD, LDD and HDD, respectively.

Combination of development scenarios and climate change conditions also simulated in this research. It indicates that trends of changing cumulative sediment distribution to the DTM floodplains were the same as compared to CC scenarios, but the increase in values was smaller. The last three columns of **Table 6-7** outlined quite clearly the above-stated.

To clearly have a virtual vision about spatial sediment distribution in the DTM floodplains, the simulated cumulative sediment results in the 1-D hydrodynamics model are interpolated by using Kriging methods in ArcGIS to make maps of annual deposition rate based on the anticipated scenarios.

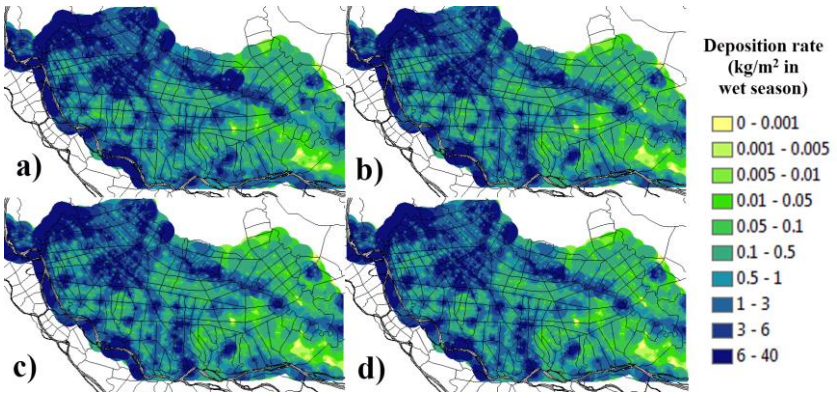

Figure 6-14: Maps of sediment distribution in the DTM floodplains: a) Baseline; b) HDD; c) LDD; d) XDD.

Figure 6-14 shows maps of the annual deposition rate for the simulated flood events based on baseline and development scenarios of hydropower dams. In the big flood of baseline 2002, the inundated area in DTM floodplains was much larger, while the sediment deposition rate was higher. A higher amount of sediment deposition delivered from the Tien River bring sediment into secondary canals and deposited in central DTM floodplains which far away from the Tien River about 40-60 km, with a high deposition rate in a range of 3-40 kg.m^2/wet season. Sediment delivery from the overland flood flow at the border of Cambodia obtained a high sediment concentration which also cumulated in the upstream of DTM floodplains and faraway from the Cambodia border about 30-50 km, with the deposition rate of 6-40 kg.m^2/wet season (see **Figure 14a**). However, some areas located near the Tien River and the Cambodia border, sediment was not deposited as it may be because of the flood flow was enormous and the flow velocity was much higher than the settling velocity of sediment.

Figure 6-15 spatially depicts the deviation of sediment deposition in DTM floodplains as compared to scenarios of developing construction in hydropower dams and irrigation area.

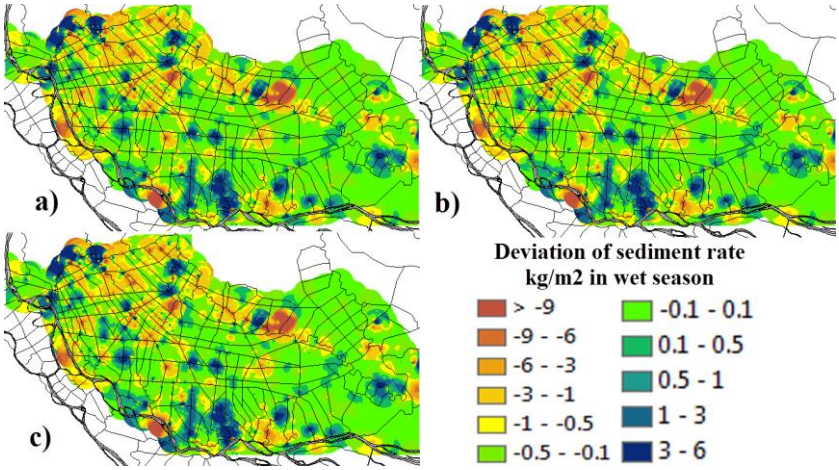

Figure 6-15: Deviation maps of sediment distribution in the DTM floodplains between development scenarios and baseline: a) HDD-Baseline; b) LDD-Baseline; c) XDD-Baseline

At the main gates along the Tien River, transported sediment to DTM (as Hongngu (P1), Anlong (P5), Phongmy (P8)) decreased (the same as other sediment stations). In addition, the reduction in transported sediment occurred inside the DTM floodplains, while its amount is also dependent on the distance from the upstream of the main river to secondary canals (see **Figure 6-15**).

The achieved results indicated that, by upstream development of hydropower dams, the deposition rate was significantly declined in inundated areas located near the Cambodia border (about 3-6 kg.m^2/wet season) and the central DTM floodplains (about 1-3 kg.m^2/wet season). The effect of decrease in sediment deposition was higher in HDD and smaller in LDD and XDD scenarios. **Figure 6-15a** presents the changes in deposition rate as a result of HDD scenario in comparison to baseline, and **Figure 6-15b** and **Figure 6-15c** show the deviation in deposition rate of LDD and XDD scenarios in comparison to baseline.

The spatial distribution of the cumulative sediment and sediment deviation in the DTM floodplains under impacts of CC showed in **Figure 6-16** and **Figure 6-17**. These maps depict that CC conditions significantly affected to sediment deposition in the DTM. The stronger accumulation of sediment occurred along Tien River and the downstream of the DTM floodplains. This deposition occurred descending depended on distance from Tien River and the downstream of the DTM. Nevertheless, deposition decreased in some places but increased in others.

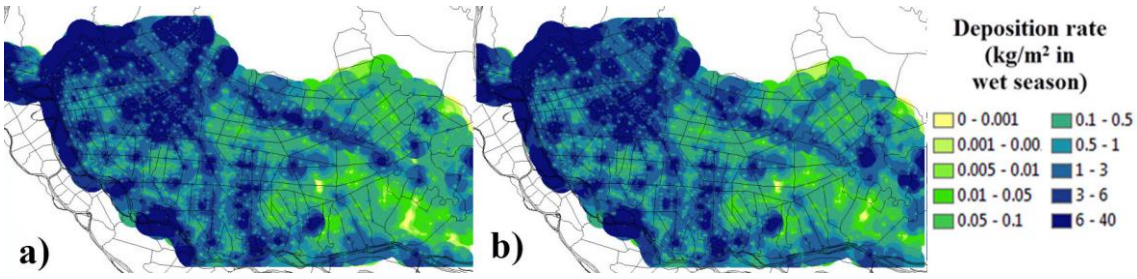

Figure 6-16: Maps of sediment distribution in the DTM floodplains based on the climate change scenarios: a) BL2050, b) BL2100

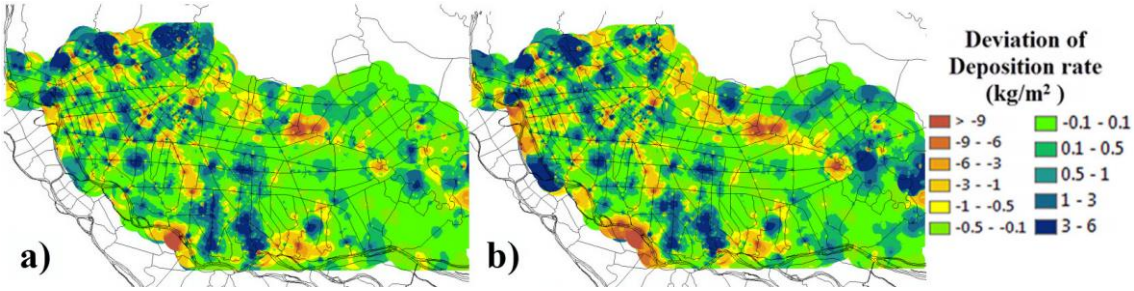

Figure 6-17: Maps of deviation of sediment distribution in the DTM floodplains based on the climate change scenarios: a) BL2050-BL; b) BL2100-BL

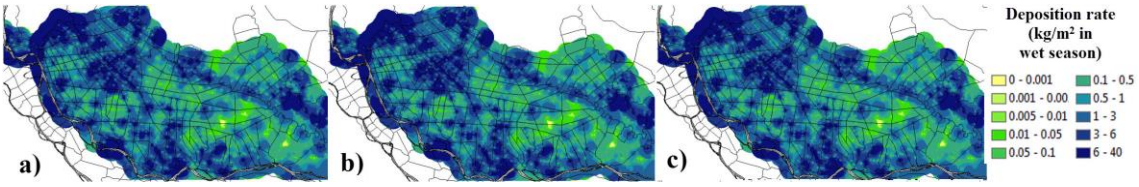

Figure 6-18: Maps of sediment distribution in the DTM floodplains based on development scenarios under climate change impact with: **a)** LDDCC2100; **b)** XDDCC2100; **c)** HDDCC2100

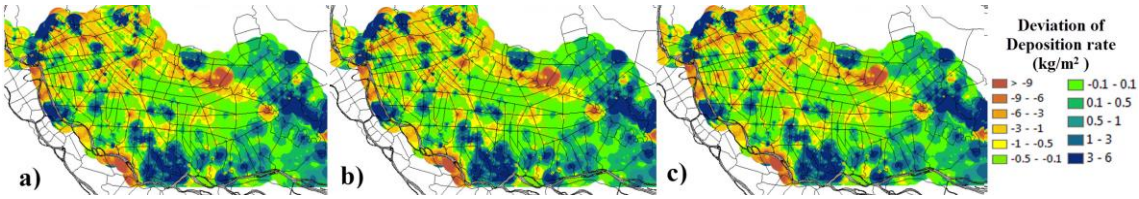

Figure 6-19: Maps of deviation of sediment distribution in the DTM floodplains based on development scenarios under climate change impact with: a) LDDCC2100-BL; b) XDDCC2100-BL; c) HDDCC2100-BL

The modeled results also evaluate spatial variations of sediment deposition following development scenarios under impacts of climate change. **Figure 6-18** and **Figure 6-19** image the maps of sediment deposition impacted by development and climate change. It also expresses the deviation of sediment deposition rate between climate change and development scenarios.

By high development of hydropower dams under climate change impact (HDDCC2100), it was dramatically affected to spatial distribution of sediment

deposition. The sediment deposition at the upstream of DTM floodplains was significantly declined while it was highly increased at the downstream (see **Figure 6-19**). These figures show that climate change mostly affected the downstream of DTM floodplains, and it was partly affected the upstream area between the Tien River and the Cambodia border.

The changes in sediment in DTM floodplains under the low and Xayaburi dam development scenarios combined with CC conditions (LDD+CC2100 and XDD+CC2100) signified in **Figures 18a** and **18b**. The changes in sediment deposition have also the same tendency to high development scenario but smaller in magnitude of deposition rate and affected area (see **Figure 6-19**).

The results basically represented effects of development in ascending water storage capability and sea level rise on sedimentation in the DTM floodplains. These above-mentioned maps and tables depicted that sediment delivery from overflow at the border of Cambodia floodplains was not as much as the influence from the sea level rise. It may have a partial impact in rising the annual precipitation from the upstream of the LMD. Sediment delivery via the border of Cambodia to DTM floodplains is slightly inclined in high dam development (HDD) at the upstream of the Mekong River. In addition, it has almost no change in sediment transport at the Cambodia border under low and Xayaburi dam development (LDD and XDD) scenarios due to climate change. Furthermore, the sediment delivery from the upstream along the Tien River was significantly affected by upstream development and climate change, but it has less influence to the overflow in Cambodia floodplains.

6.6. Conclusion

Sedimentation on floodplains in the Lower Mekong Delta is very important, but knowledge about sediment transport is limited. Based on the collection of historical sediment observation in Dong Thap Muoi (DTM), this study improves the understanding of quantitative sediment deposition processes

on floodplains under the impacts of climate change and various developments at the upstream of the Mekong Basin.

According to the findings of this research, the simulated model evaluated the quantity of sediment deposition in spatial DTM floodplains from Kratie and overflow from the border of Cambodia. In general, higher deposition rate was occurred in closer distances to the two main sediment sources, i.e. along the Tien River and the border of Cambodia floodplains. The high sediment deposition was also found in central DTM floodplains where confluence of discharge from the Tien River and the overflow from the Cambodia border.

The deposition rate may decrease by the distance from the Mekong River and the secondary channels, while the source of the floodplain sediments also decrease by the distance to the main river. Deposition rate in the study area is quite high as compared to the other regions, and it is expected that the deposition rate will change when the hydrological conditions changed. The above results indicate that deposition processes will increase, especially in the downstream of the DTM floodplains if climate change occurs, and the deposition increases significantly when the sea level is raised greatly.

Besides that, the development in the upstream is one of the major factors leading a decrease in sediment discharge as well as sediment deposition in the downstream. To be specific, once the upstream of the Mekong Basin develops under the high/low development scenarios, deposition processes will significantly reduce in floodplains located close to the Cambodia border and the center of DTM.

Based on the present results, it may be helpful to contribute more details in understanding the sediment transport in LMD floodplains. In addition, it can be argued that natural or man-made actions that change floodplain inundation, e.g. sea level rise, the complete compartments or construction of dams along the upstream of the Mekong River may change the sediment delivery and also spatial sediment deposition in DTM floodplains.

CHAPTER VII

THE EFFECT OF SEA LEVEL RISE ON THE SEDIMENTATION OF MEKONG RIVER ESTUARIES, SOUTHERN VIETNAM

7.1. Introduction

The processes of erosion and deposition in a river estuary are extremely complex (Holeman, 1968; Teisson *et al.*, 1991; Van Leussen, 1994). Evolution of the morphology of the estuary results in both positive and negative contributions to the environment and economy, such as the development of agriculture and aquatic products such as shellfish and other fish. Erosion may decrease the fertility of the land and even damage the livelihoods of local people, whereas the deposition of sediment can form new alluvial land or expand existing islets, dunes, and sandbars. However, such deposition may also cause serious problems for navigation, such as closing of the river or estuary. It is therefore important to recognize that deposition processes pose significant challenges for the sustainable management of water resources. Sedimentation is a vital concern for the conservation, development, and utilization of soil and water resources (Van Leussen, 1994).

Vietnam is well known as a country with numerous rivers and has two large deltas created by two of the longest rivers in Asia: the Red River and the Mekong River. The Red River forms the northern delta, while the Mekong River with its main distributaries, the Tien River and Hau River, creates the southern delta. The Mekong River Delta (MRD) is flat, low-lying, and fertile and has hence contributed significantly to the development of the social economy, supporting 16 million inhabitants (approximately 22% of the total population of

Vietnam), providing more than 27% of the country's GDP and about 50% of the annual rice production (Gottschalk, 1977; DHI, 2007b). From the last decades of the 20th century to date, the MRD has been affected by concentrated human activities, rapid economic development, and climate change in particular, resulting in major land and water resource problems such as acute flooding during the wet season, seawater intrusion in the lower delta during the dry season, and sedimentation and erosion. The complex morphological evolutions of the Mekong River Estuaries are among the most serious influences.

In recent decades, a number of studies have provided new and interesting results. These noteworthy publications include Wolanski *et al*. (1996, 1998), Nguyen (1995), Nguyen *et al*. (2000), Ta *et al*. (2001), Nguyen (2007), Tamura *et al*. (2010) and Mikhailov and Arakelyants (2010). It was pointed out that most of the suspended sediment (SS) is fine silt and that sediment transport is influenced by many factors, particularly river currents, sea currents (monsoon currents), tidal currents, and wave-generated currents. Furthermore, the combination of meteorological and oceanic effects produces strong variations in coastal areas, mainly at seawater level and coastal currents.

According to the Intergovernmental Panel on Climate Change (IPCC, 2007), the coastal countries of Southeast Asia are highly vulnerable to climate change. Of these, Vietnam ranks first in terms of population among ten countries and territories that could be impacted by sea-level rise (SLR). Global climate change and SLR could alter the hydrodynamic characteristics of low-lying coastal areas such as the MRD. Hence, the morphological evolution of the Mekong River Estuaries is related to urgent challenges of sustainable development and protection of human society (Julien, 1998). In this study, we simulated erosional and depositional processes in the Tien River Estuaries, Mekong River System, including the effects of SLR.

7.2. Model application

7.2.1. Model setup

Two models were developed: a regional model covering the South China Sea in southern Vietnam (**Figure 7-2**) and a local model of the Mekong River Estuaries (**Figure 7-3**). The boundaries of the regional model are specified as from the Mekong River mouths to the Bachho and Condao hydrographic stations (**Figure 7-2**), where limited wave data are available. The local model covers a region from the Mythuan and Cantho (**Figure 7-3**) to the nearshore zone of the Mekong River Estuaries. The local and regional models covered a mesh area sufficient to ensure that the impacts of the main factors on the wider area were fully considered. To link up the local and regional models, the downstream boundary conditions of the local model, such as water level and waves, are extracted from the large regional model.

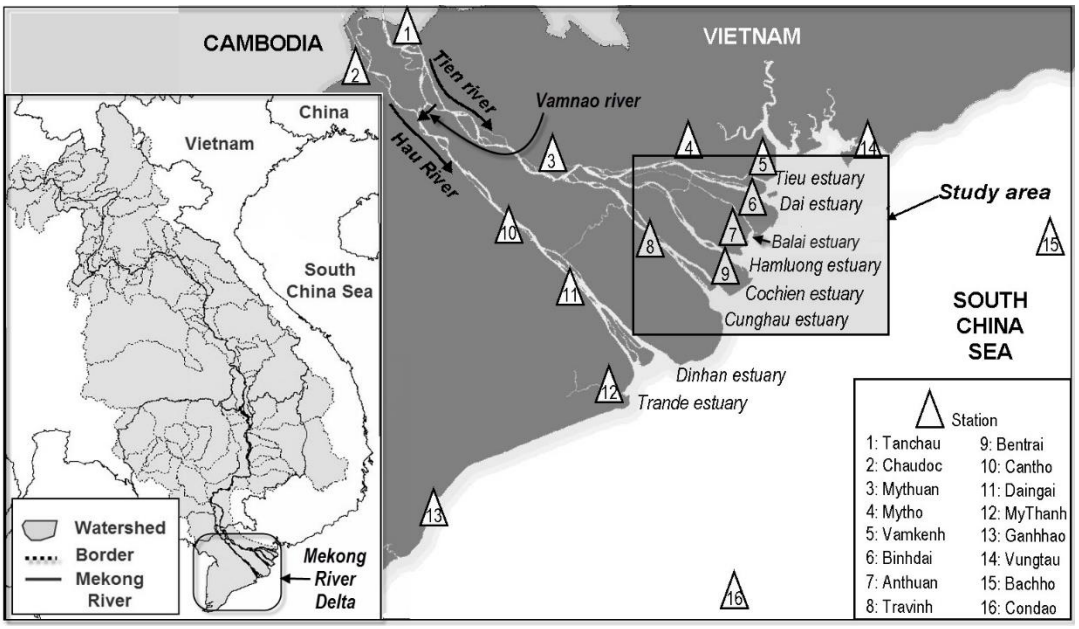

Figure 7-1: Location of Lower Mekong River and hydrological stations in southern Vietnam

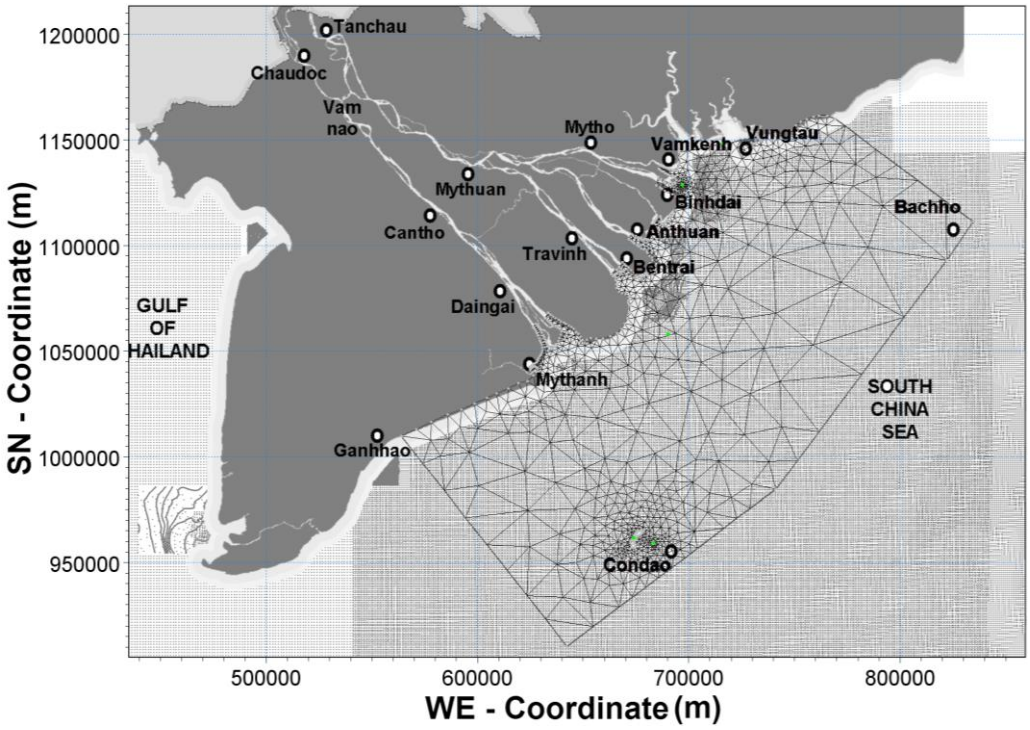

Figure7-2: Regional model with unstructured mesh

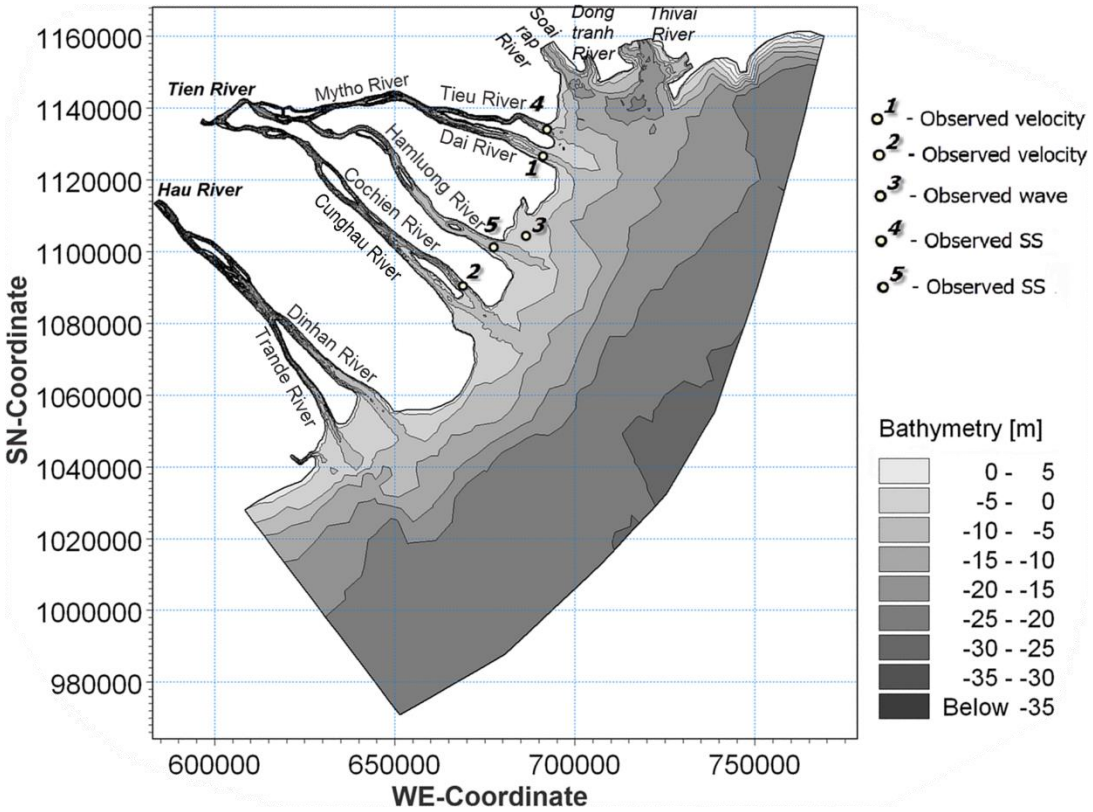

Figure 7-3: Bathymetric of local model covering the Mekong River Estuaries

7.2.2. Boundary and initial conditions

The monsoon wind and waves are two other important factors affecting the water level, current at the sea and sediment transport. The input data of wind speed and wind direction also are based on the measured data of Vungtau hydrological station. Whereas, the spectral wave results of the regional model is chosen for the wave boundary condition. The mean value of salinity in the sea 32‰ is set at the sea boundary conditions (Thanh Letrung *et al.*, 2016). The upstream boundary salinity is very small, and it is approximate 0‰, throughout the year. In additions, from the temperature is shot-range of 24^{o}C to 28^{o}C in whole area, so the value 26^{o}C is chosen. For sediment boundaries, the mean seasonal values of suspended sediment concentration at Mythuan and Cantho are used as the upstream boundaries and the downstream boundaries in South China Sea is chosen with an average suspended sediment concentration of 0.0001 kg/m^3. (Ngoc *et al.*, 2013b)

7.2.3. Calibrating model

These two models of the Tien River Estuaries were first calibrated with the observed water level, velocity, wave, and suspended sediment (SS) data, in September 2009. In the regional model, the upstream boundary conditions were the water level series of the hydrological stations at the Mekong River mouths (e.g. Vungtau, Vamkenh, Binhdai, Anthuan, Bentrai, Mythanh, and Ganhhao), whereas predicted tidal elevations were used for the downstream boundaries. The monthly input data of wind speed and direction were based on data measured from the Vungtau meteorological station. The monthly average wave data from the Bachho station were specified for the offshore wave boundary conditions. The two hourly upstream discharge boundaries in the local model were the Mythuan and Cantho hydrological stations. At the downstream end, the water level and spectral wave boundaries in the sea were obtained by results from the regional model. In the upstream area, salinity boundaries were set at 0‰ year-

round. In the coastal zone, these boundaries were 32‰, except in January and February when the boundaries were set at 35‰ (Ngoc *et al.*, 2013b; Thanh Letrung *et al.*, 2013). In addition, since the temperature ranged from 24 to 28°C over the whole area, the value of 26°C was selected.

The calibrated parameters of the Mike 21 HD, Mike 21 SW, and Mike 21 MT models were fixed to gain appropriate results. In Mike 21 HD, density was considered a function of temperature and salinity, and the Manning value is within the range 20–40 $m^{1/3}/s$ by variation in the water depth. The time step was from 0.1 to 30 s and defined by separation of the Courant–Friedrich–Levy (CFL) stability criterion; the CFL number was 0.9. The Eddy viscosity was specified by the Smagorinsky formulation with a Smagorinsky coefficient value of 0.28 (Nguyen, 2007). In Mike 21 SW, the decoupled parametric formulation was selected to simulate waves by Nikuradse roughness and the JONSWAP formulation (DHI, 2007b).

In Mike 21 MT, after trial-and-error processing, the achieved fall velocity of suspended sediment was 0.2 mm/s. According to analysis of the bed parameter of the Mekong River Estuaries, the model bed was described by four unique layers: a surface mud layer as a mobile fluid mud with low critical shear stress of erosion, a second mud layer as partly-consolidated mud, a third consolidated mud layer with high-density sediment, and a fourth hard mud layer. Erosion was calculated using an equation originally proposed by Parchure and Mehta (1985), which is given below:

$$S_E = E \times e^{\left[\alpha \times \sqrt{\tau_b - \tau_{cre}}\right]} ,$$

where S_E is the erosion rate (g/m^2), E is the erodibility of the bed ($kg/m^2/s$), α is the erosion coefficient ($m/N^{1/2}$), τ_b is the bed shear stress (N/m^2), and τ_{cre} is the critical bed shear stress for erosion (N/m^2).

Table 7-1: Bed parameters in Mike 21 MT

Layer number	Mud Type	Wet Density of bottom sediment (g/L)	Critical shear stress for Erosion τ_{cre} (N/m^2)	Erosion coefficient E ($kg/m^2/s$)	Coefficient α ($m/N^{0.5}$)	Initial thickness (m)
1	Mobile fluid mud	120	0.17-0.20	0.000005	5	0.05-0.3
2	Partly consolidated mud	300	0.35-0.40	0.000001	4	1-2
3	Partly consolidated mud	450	0.55-0.60	0.000001	4	4-6
4	Hard mud	600	1.50	0.0001	1	10

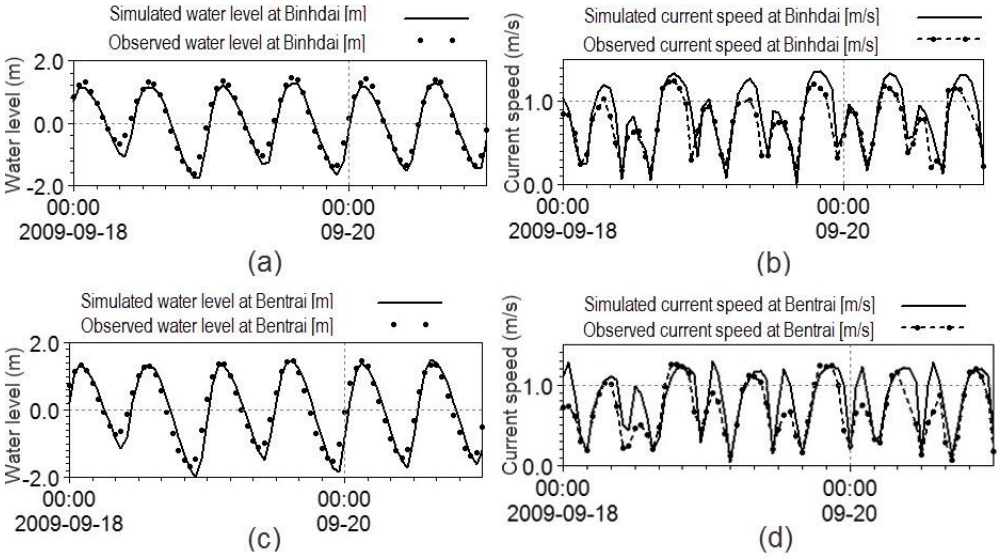

Figure 7-4: Calibration of water levels and current speeds simulated by Mike 21 HD

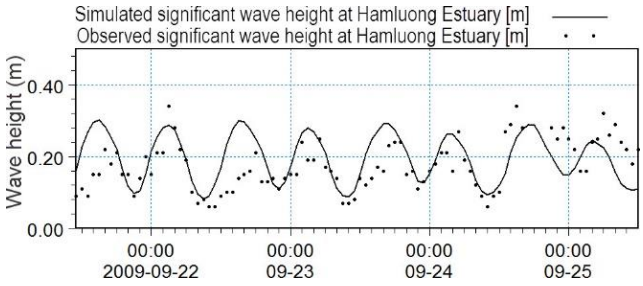

Figure 7-5: Calibration of significant wave heights simulated by Mike 21 SW at point 3 in Fig. 7-3

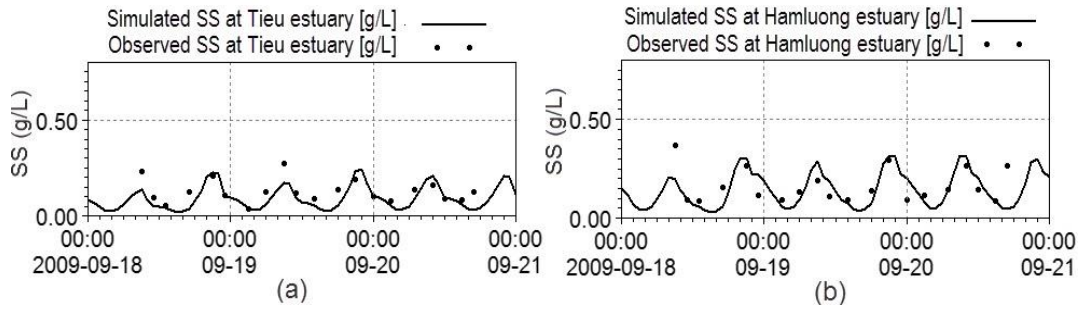

Figure 7-6: Calibration of suspended sediment concentrations simulated by Mike 21 MT

The parameter values of each layer were based on the results of Ngoc *et al.* (2013b), as shown in **Table 7-1**. For sediment boundaries, the mean seasonal SS values at Mythuan and Cantho were used as upstream boundaries and downstream boundaries in the South China Sea with an average SS of 0.0001 g/L.

Figure 7-4 shows the calibrated results from September 18–21, 2009, in the Dai and Cochien Estuaries of the Tien River. **Figures 7-4a** and **7-4c** show a comparison between simulated water levels and observed data (Binhdai and Bentrai) with very little deviation (less than 5%) and similar fluctuations in variation. Simulated current speed results show good agreement with observed data, as shown in **Figures 7-4b** (point 1 in **Figure 7-3**) and **7-4d** (point 2 in **Figure 7-3**). These two figures delineated the same order between simulated velocity results and observed data, and there was no noticeable difference between the series. **Figure 7-5** shows the simulated result and observed data north of the Hamluong Estuary (point 3 in **Figure 7-3**). This figure indicates that the two series were close and that the simulated results were satisfactory. In general, the simulated results virtually replicated the particularity of waves in the study area, despite small discrepancies in the observed data.

The calibrated SS results from the mud transport module and observed data of the Tieu and Hamluong estuaries, shown in **Figure 7-6**, were obtained for the same calibration time with hydrodynamics. Those figures showed that the

simulated results and observed data for each estuary were similar and concurrent. Although the maximum observed data exceeded the simulated results, this was to an insignificant extent, whereas the minimum survey data and simulated results had the same value.

7.3. Proposing model scenarios and simulated results

7.3.1. Proposed modeling scenarios

The Vietnamese Ministry of Natural Resources and Environment (MONRE, 2009) reported that the sea level may rise by 28 to 33 cm in 2050 and about 65 to 100 cm in 2100, relative to the baseline period of 1980–1999 (**Table 7-2**). SLR will tend to exacerbate the effects of coastal erosion and deposition. In addition, it may cause the river's discharge to vary, resulting in strong sea-current domination at the river mouth, which could aggravate the problem of salt intrusion. In this study, two scenarios, low- and high-SLR, designed with increases in sea level of 30 cm (in 2050) and 100 cm (in 2100), respectively, were used to simulate morphological processes in the Tien River Estuaries.

Table 7-2: Sea level rise (cm) relative to the period 1980–1999

Scenario	2020	2030	2040	2050	2060	2070	2080	2090	2100
Low SLR scenario	11	17	23	28	35	42	50	57	65
Medium SLR scenario	12	17	23	30	37	46	54	64	75
High SLR scenario	12	17	24	33	44	57	71	86	100

7.4.2. Simulating the SLR scenarios and results

Comprehensive calibrations between simulated results and observed hydrodynamics data (i.e. water level and current speeds), waves, and movement of sediment in September 2009 conducted through simulation by the Mike 21 Coupled FM achieved appropriate results and indicated that the selected parameters were reasonable. Next, the two models were simulated for three cases: the baseline and the low- and high-SLR scenarios. These scenarios were computed for a decade from January 1, 2010 to January 1, 2020.

The computed astronomical tide and resulting time series of water levels were used for upstream (river mouths) and the sea boundaries of the regional model in the baseline, whereas the boundary conditions in the two SLR scenarios were based on the results obtained in the key projects of Nguyen (2010), Letrung (2011, 2012). Next, the results of the regional model were extracted and set as the downstream boundary conditions of the local model. The time series of the mean hourly discharge of the Tien (My Thuan hydrological station) and Hau Rivers (Can Tho hydrological station) were the upstream boundary conditions for the local model.

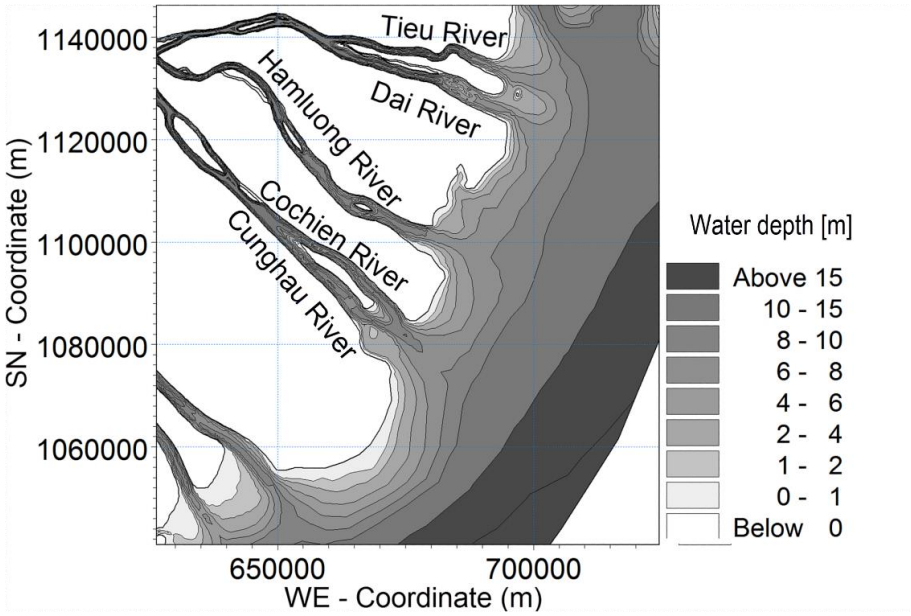

Figure 7-7: Water depth simulated in the baseline at 18:00 (GMT +7) on January 20, 2012

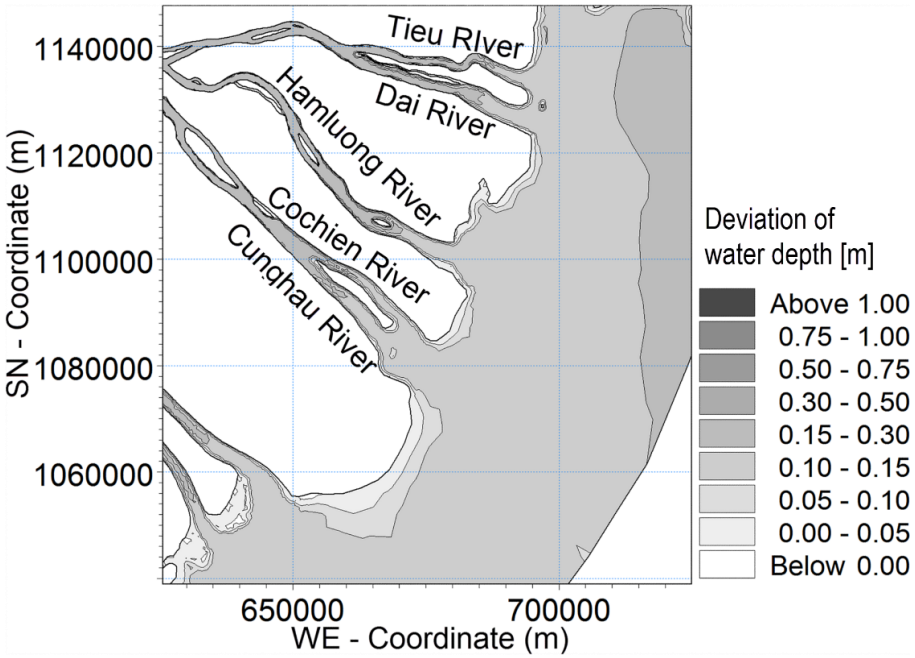

Figure 7-8: The deviation of simulated water depth between the low-SLR scenario and the baseline at 18:00 (GMT +7) on January 20, 2012

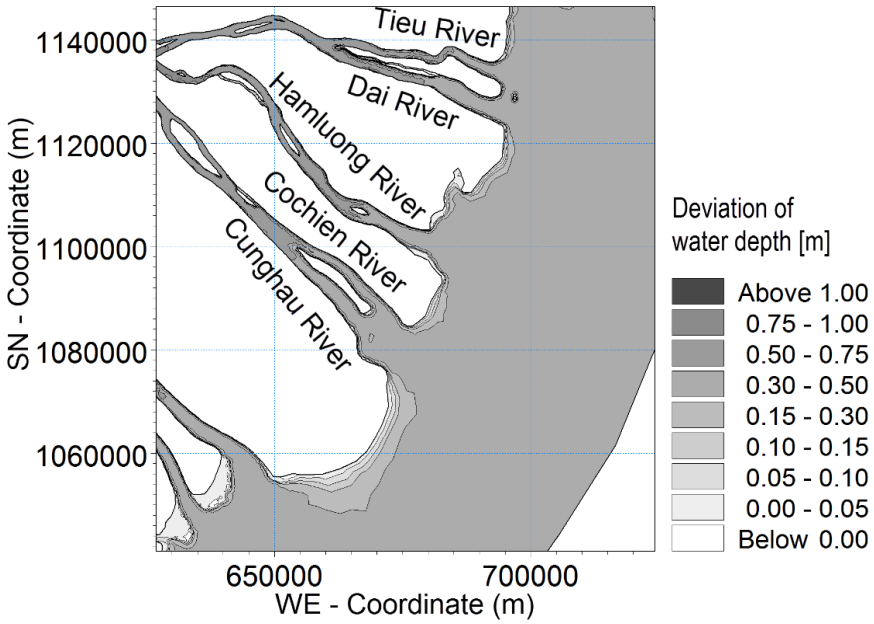

Figure 7-9: The deviation of simulated water depth between the high-SLR scenario and the baseline at 18:00 (GMT +7) on January 20, 2012

Table 7-3: Summary of surface level (m) results in the decade

Scenario	Items	Vamkenh (Tieu River)			Anthuan (Hamluong River)			Bentrai (Cochien River)		
		Min	Max	Mean	Min	Max	Mean	Min	Max	Mean
Baseline	Surface level (1)	-2.58	1.86	-0.02	-2.60	1.90	-0.01	-2.95	1.97	-0.03
Low SLR	Surface level (2)	-2.47	2.30	0.28	-2.50	2.34	0.29	-2.85	2.42	0.27
	ΔH [(2)-(1)]	0.11	0.44	0.30	0.11	0.44	0.30	0.09	0.44	0.30
High SLR	Surface level (3)	-2.25	3.33	0.95	-2.28	3.36	0.96	-2.68	3.45	0.94
	ΔH [(3)-(1)]	0.33	1.47	0.97	0.33	1.46	0.98	0.27	1.48	0.98

The hydrodynamic modeling results indicated marked differences among the three simulation scenarios and significant influences of SLR on the currents of the Tien River Estuaries. The water depth of the baseline ebb tide and the deviation of water depth in the low- and high-SLR scenarios compared with the baseline are shown in **Figures 7-7**, **7-8**, and **7-9**, respectively, for the dry season of 2012 at 9:00 A.M. on 20 January. When the sea level rose, the inundation area expanded. Dunes and sandbars were almost submerged in the high-SLR scenario. Table 7-3 shows the water level results at three hydrological stations (Vamkenh, Anthuan, and Bentrai) in three main distributaries (Tieu River, Hamluong River, and Cochien River) of the Tien River. The mean water level rose 30 and 97-98 cm in the low- and high-SLR scenarios. The maximum water level increased by 44 and about 147 cm in the low- and high-SLR scenarios, but minimum water level values were about 9–11 and 27–33 cm, respectively.

Rising seawater and changes in upstream flow made the current in the study area more complex and led to noticeable current speed increases. In the low-SLR scenario, the Tieu, Dai, Cunghau, and Cochien Rivers had current speed increases of 4–6%, while the highest current speed increase of more than 7% occurred in the Hamluong River. However, in the high-SLR scenario, these values were larger and more dissimilar. The current speeds of the Tieu and Dai

Rivers increased by 13 and 15%, while increases in the Hamluong and Cunghau Rivers were 19 and 20%, respectively. The values peaked at 21% in the Cochien River.

According to the results obtained for the two SLR scenarios, the simulated current was stronger and SS transport was higher than in the baseline. The strong currents increased erosion of the river bed, and the eroded sediment increased SS transport in the distal zone of the Tien River Estuaries. The SS was transported out of the river mouth. There was also an increase in SS transfer between the estuaries of the Mekong River in the coastal zone. This point is illustrated in **Figure 7-10**. The SS in the Tien River as a result of the baseline (**Figure 7-10a**) was about 0.2 g/L. Outside the Tien River mouths, the SS decreased below 0.075 g/L, while in the nearshore zone, the obtained SS was within the range 0.05 to 0.075 g/L. However, the SS reached only 0.025 g/L in the coastal region between the Tien River Estuaries and the Hau River Estuaries.

The result of the low-SLR scenario (**Figure 7-10b**) indicated increased SS in the Tien River Estuary area, and the region in which SS exceeded 0.2 g/L was extended into the sea. Although there was an increase in sediment distribution in the coastal zone near the Tien River mouths, the SS did not change noticeably. In the high-SLR scenario (**Figure 7-10c**), the SS was diffused significantly and its isoline was within the range 0.075–0.1 g/L, encompassing virtually the whole of the Tien River Estuary area. Remarkably, the obtained SS value exceeded 0.25 g/L in the area of the Tien River mouth. Furthermore, the region in which the SS value exceeded 0.2 g/L extended into the sea more than twice as much as the baseline. SS also increased in the area of the Hau River month with the maximum value exceeding 0.25 g/L. (See details in **Table 7-4**).

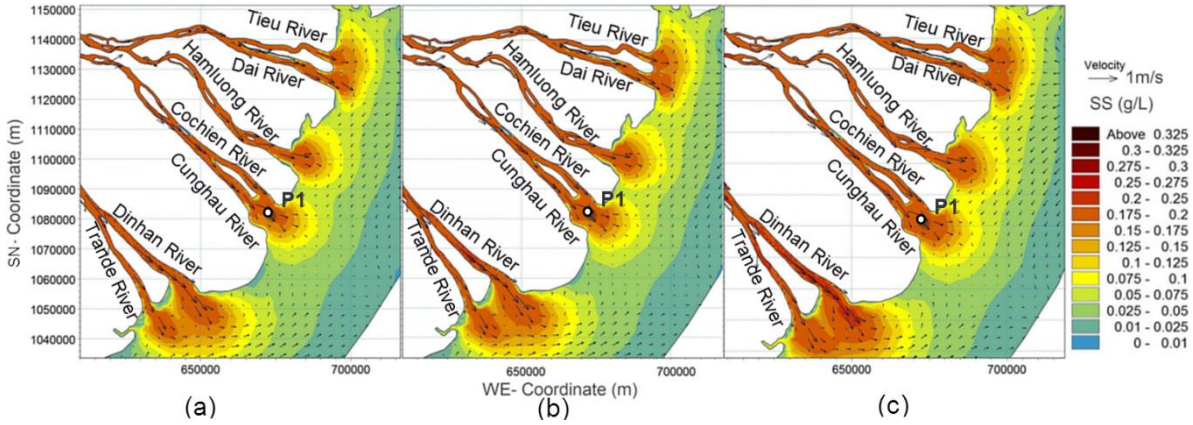

Figure 7-10: Movement of suspended sediment at 15:00 (GMT +7) on September 6, 2010, (a) in the baseline; (b) in the low-SLR scenario; and (c) in the high-SLR scenario.

Table 7-4: Mean SS of Baseline as compared to SLR scenarios

Simulation Case	Suspended sediment concentration	Hamluong (CR2)	Tieu-Dai (CR3)	Cochien-Cunghau (CR5)
Baseline	Mean SS (mg/l)	86.46	83.22	89.06
Low SLR	Mean SS (mg/l)	87.99	84.08	90.84
High SLR	Mean SS (mg/l)	95.01	90.91	95.17

The river bed showed different erosion and deposition characteristics between flood and dry seasons. During the flood season, a high-velocity river current carried SS out of the river mouth and the sediment consolidated the sandbars, islets, and alluvial grounds of the Tien River Estuaries. Concurrently, this current was a major cause of erosion, rapidly eroding the river bed. During the dry season, the cold sea current dominated the Tien River Estuary area (see **Figure 7-11**). In all SLR scenarios, the sea current accelerated and moved a portion of the sediment that had been deposited during the flood season southward. Furthermore, the strong cold current disrupted the weak foundation of the shoreline.

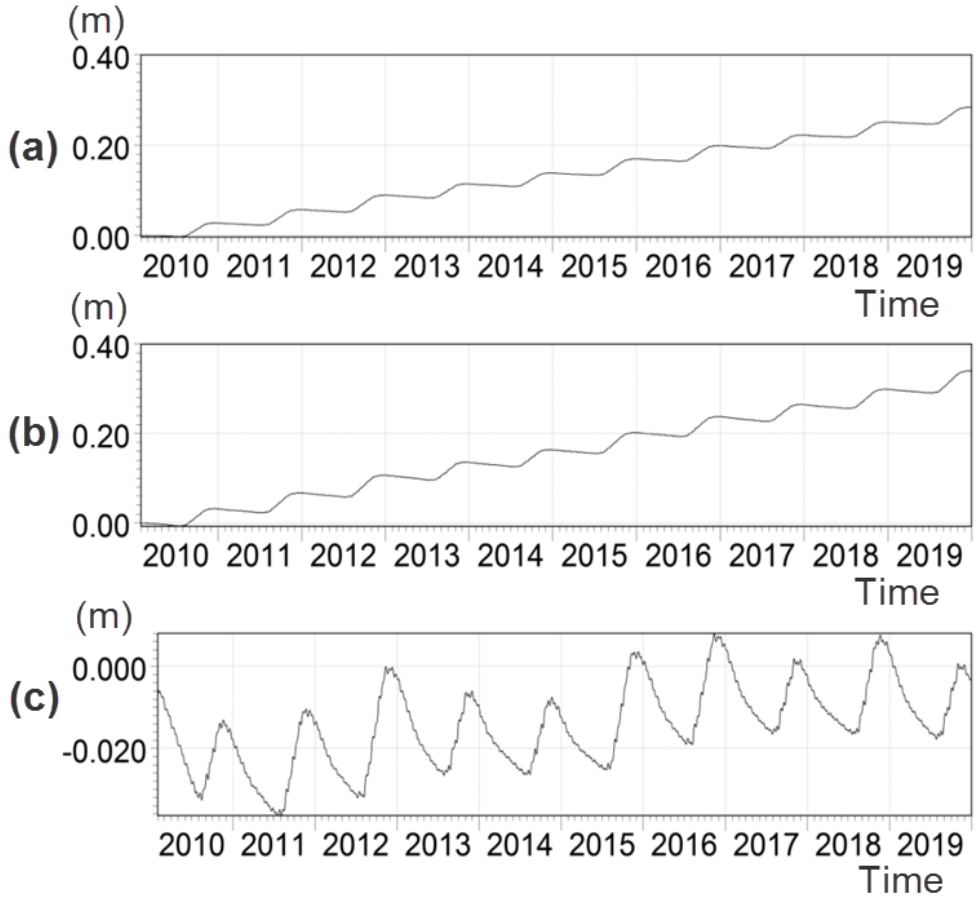

Figure 7-11: Bed change at P1, shown in Figure 7-10, in different seasons in baseline (a); in the low-SLR scenario (b); in the high-SLR scenario (c)

Figures 7-12, **7-13**, and **7-14** illustrate further details of the erosion and deposition results for the Tien River Estuaries in the baseline, showing low- and high-SLR scenarios, respectively, for the decade from 2010 to 2020. Deposition and erosion processes of the SLR scenarios occurred to a far greater extent compared with those of the baseline. Long-term simulated results for the baseline of morphological evolution of the Tien River Estuaries showed that while the river bed was eroded, river banks were mostly consolidated. However, because of the strong cold sea current of the dry season, river shore degradation occurred sporadically where the foundation was weak. Sandbars were built and fortified during the flood season but later carved and moved slightly into the mainland (as illustrated in **Figure 7-14**).

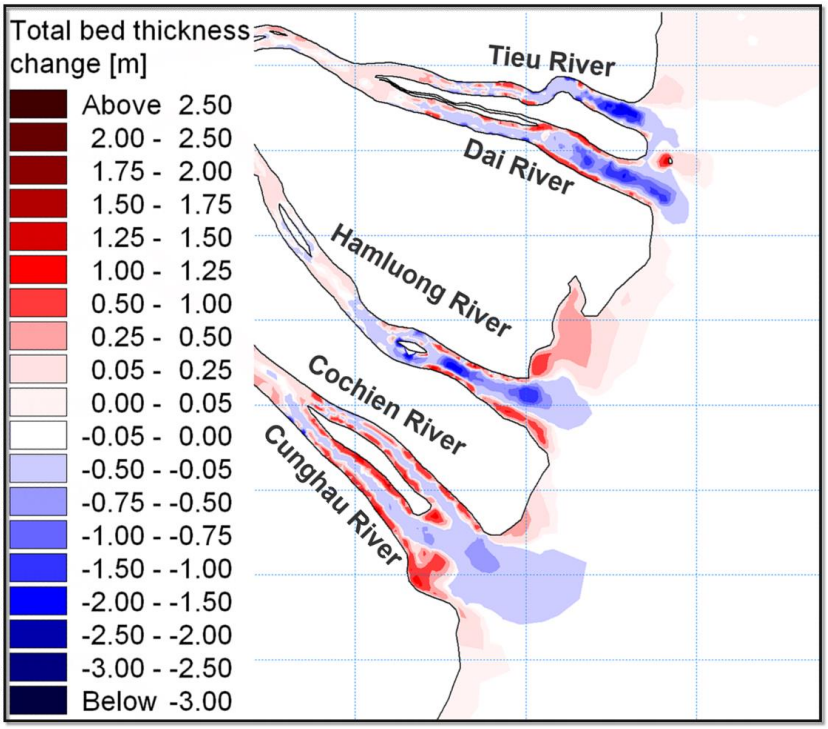

Figure 7-12: Total change in bed thickness from 2010 to 2020 in the baseline

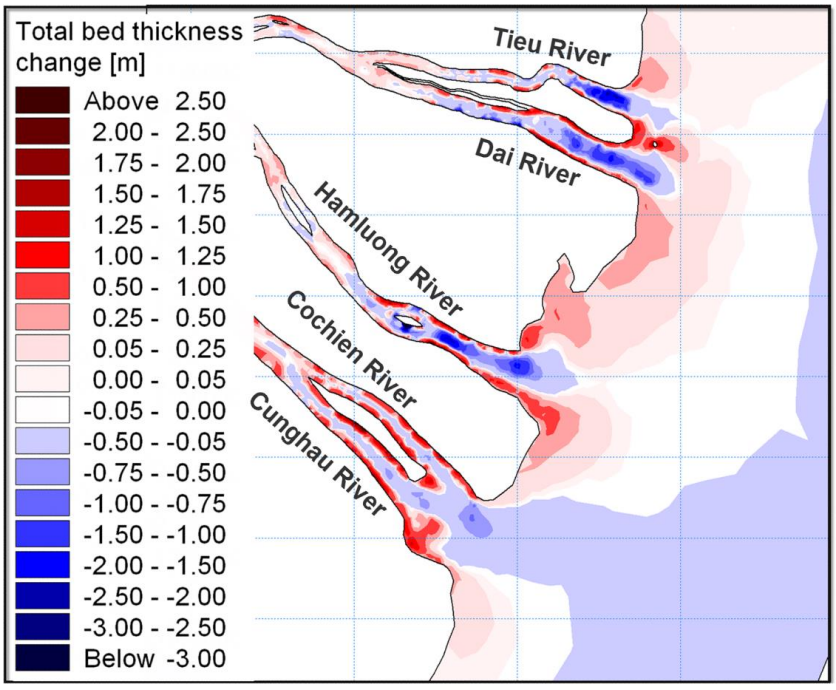

Figure 7-13: Total change in bed thickness from 2010 to 2020 in the low-SLR scenario

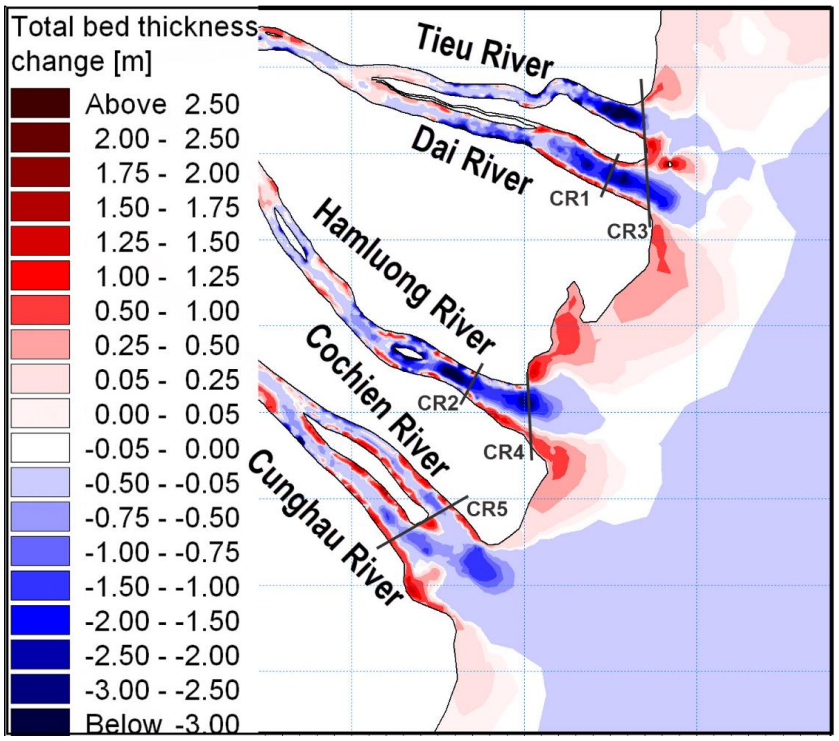

Figure 7-14: Total change in bed thickness from 2010 to 2020 in the high-SLR scenario

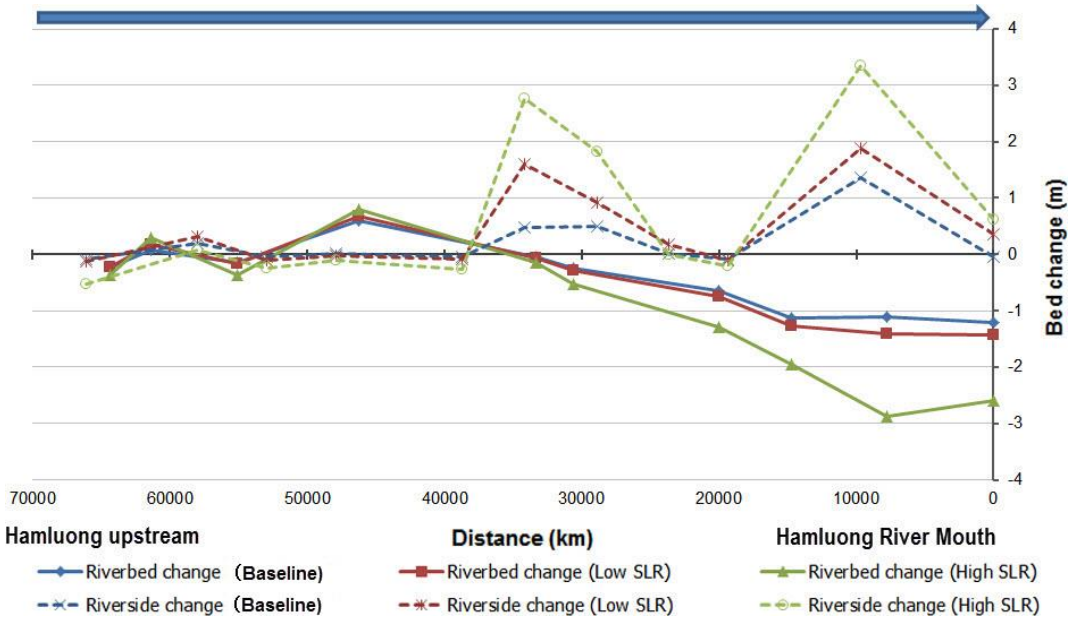

Figure 7-15: Change in bed elevation along the Hamluong River

In the low-SLR scenario (**Figure 7-13**), erosional processes intensified, causing Mekong River cross-sections to narrow and deepen. In the river, the depositional and erosional processes had trends equivalent to those in the baseline. River bed levels decreased and river banks aggraded significantly, although erosion alternated with deposition in some places. In the nearshore zone, SS settled easily while the sea bed was more eroded than in the baseline. In the high-SLR scenario (**Figure 7-14**), although the bed of the Mekong River was strongly eroded, the shoreline of the Mekong River Estuaries was remarkably aggraded.

The results of bed thickness changes in the rivers and estuaries are shown in **Figure 7-15**. Erosion in the high-SLR scenario was several times higher than in the baseline. The bed and sea bed were eroded by strong river and sea currents. In addition, although the river banks were virtually accreted, considerable erosion occurred at a few places along the Mekong River banks, such as along the Tieu, Dai, and Hamluong Rivers. Because tidal effects reach farther into the mainland with increasing sea level, associated erosion and deposition occurred not only at the river mouth area but also in the mainland. Tidal currents were most important among the erosion and deposition problems and tended to become more serious and complex (**Figure 7-13**). These were the cause of the serious erosion in the Mekong River. The strong degradation of the bed caused the river banks to become unstable and prone to collapse easily at places where the river cross-section was narrow (**Figure 7-14**).

7.5. Conclusions

Long-term simulation results of the baseline show that the factors contributing to the morphological evolution of the Tien River Estuaries are mainly natural. The influences of semidiurnal macro-tides, tidal asymmetry, river currents, sediment discharges, saline intrusion, and geological structure on the river's topography are considerable. The erosion of the Tien bed is very serious

with a decrease of 0.5 m every year. The Tien River cross-section has narrowed and deepened due to erosion, while accretion of river banks and shorelines leads the Tien River to extend into the South China Sea. With high river discharge during flood season, suspended sediment is deposited in the distal zone, creating sand barriers and strengthening existing islets.

Influenced by SLR, current and sediment transport changed significantly in the Tien River Estuaries. The magnitude of the velocity values also increased slightly within the range 5–7% in the low-SLR scenario but increased considerably up to 21% in the Cochien and Cunghau Rivers in the high-SLR scenario. The strong current carried more SS out of the mouths of the Mekong River. In the two simulated SLR scenarios, SS was much higher in the estuarial area and led to consequent aggradation of the coastline in the Mekong River Estuaries, while the sea bed was degraded and the bathymetry of the coastal zone became a slope. However, the tidal influences differ between each estuary and distributary of the Mekong River. Tidal currents under the impact of the SLR scenarios largely intruded into the mainland leading to noticeable erosion and deposition in the Mekong River.

The results of this study suggest that, in the near future, after the sea level rises slightly (the low-SLR scenario), the morphological evolutions of the Tien River Estuaries will have the same trend as existing processes in the baseline, but erosion and deposition will intensify. However, a sea level increase of 1 m (high-SLR scenario) will significantly complicate the erosional and depositional processes. The influence of tidal activity will be extended further into the mainland and will cause deposition and erosion in both the river mouth and upstream river areas. River bed erosion will occur rapidly, and the bed level will rapidly decline, damaging river bank stability.

CHAPTER VIII
GENERAL CONCLUSIONS

8.1. General conclusions

The downstream of the Dong Nai - Saigon River Basin spreads over a wide area, including Ho Chi Minh City (HCMC) and six provinces; Binh Duong, Dong Nai, Tay Ninh, Long An, Dong Thap and Tien Giang, with a total area of 10,805.2 km^2. This area is a low-lying land, adjacent to the East Vietnam Sea and about 15% of this area has been often an intertidal area (1,593.6 km^2). In general, this low-lying area is strongly influenced by the variation of two factors; river flow and tidal current.

In recent years, many large reservoirs have been constructed in the upstream area for multiple purposes of flood control, hydropower generation, irrigation and industrial usages. However, failure of equipment or mishandling of reservoir operation, it caused a huge disaster to the downstream of the Dong Nai – Saigon River Basin. Moreover, the impact of tidal current considerably increases, and salt water intrusion problems and lack of fresh water have been seriously happening on the Saigon River. Furthermore, climate change - rising sea level are also an important factor which govern increase of salinity intrusion, flooding, and hamper flood drainage in the Plain of Reeds (so-called Dong Thap Muoi area, a part of Mekong Delta) and HCMC. Extreme rainfall on the Dong Nai - Saigon River Basin in HCMC area combining the high tides and rising sea levels will progressively put pressure on the drainage system and increased flooding in HCMC in the near future.

This dissertation investigates the urgent problems in the Dong Nai – Saigon River Basin, in southern Vietnam, and various numerical models including hydrological models, reservoir operation models, flood vulnerability

assessment model and hydrodynamics models are established. The models cover whole the Dong Nai – Saigon River Basin. Four main objectives in this dissertation were studied and summarized as below:

In the first chapter, an overview of the Dong Nai – Saigon River Basin and urgent problems relating to water resources management were shown.

The theoretical underpinnings for the research aims were elaborated upon in a literature review by chapter II.

The hydrological models in chapter III were designed and simulated for inflow into the Dautieng Watershed. The numerical models for rainfall-runoff process using the Tank Model and the NAM Model incorporated with a parameter-optimization technique of Genetic Algorithm (GA) for the Dautieng Reservoir Basin. The simulated runoff results of two optimized hydrological models achieved a good performance as compared to observed data through two indicators of correlation coefficients and Nash-Sutcliffe coefficients which were 0.90 and 0.82 in the GA–Tank model and 0.90 and 0.80 in the GA–NAM model respectively. This result is very useful for restoration and prediction of inflow in the upper Saigon River Basin.

In chapter IV, the model of optimal reservoir operation using a constrained genetic algorithm (CGA) was also constructed for multi-use reservoir management of Dautieng Reservoir and the scenario analyses were conducted from the viewpoints of river ecosystem conservation and salt water intrusion from a river mouth. The optimal reservoir management simulated by the proposed CGA-optimization model showed the effective performance in comparison with the current operation in simulated 20 years (1999-2008). In addition to that, the results also indicated that water deficits in the scenarios reduced significantly in spite of ensuring adequate amount of environment base flow. Furthermore, the proposed model combined CGA method can handle large variety of practical aspects, such as supplied water precedence to sectors,

considering of inflow requirement for flushing salt intrusion, priorities to flood control and water storage, or combination of these.

In Chapter V, a tool of vulnerability assessment using a GIS-based hydraulic model, a depth-damage function and flood loss model was developed to estimate flood damage and discriminate land areas from the viewpoint of flood inundation damage in the downstream of the Dong Nai-Saigon River Basin. The obtained results of flood loss estimation showed the land areas with high/low vulnerability if extreme flood events would occur. This study gained an important outcome in contribution for decision-makers to urban management and disaster risk mitigation measures.

The one-dimensional model (MIKE 11 ST) described in chapter VI was applied to simulate the effect of climate change and upstream hydropower development in the Mekong River Delta (MRD). Based on the results, it is found that higher deposition rate was occurred in closer distances to two main sediment sources: along Tien River areas and border of Cambodia floodplains. Moreover, the development in upstream is one of major factors leading a decrease in sediment discharge as well as sediment deposition into downstream. But the sediment deposition significantly increased at downstream by SLR.

And the two-dimensional model (MIKE 21/3 coupled FM) in chapter VII was used to simulate the effects of SLR on sedimentation in Mekong River Coast. Results in chapter VI showed dramatic reduction of sediment discharge at upstream of MRD in simulated scenarios of climate change and upper hydropower development, while results in chapter VII revealed that sediment deposition occurred much higher in river mouths by simulated SLR scenarios.

In this dissertation, the deterministic approaches were proposed for modeling and solving urgent problems in water resources management. The empirical results indicated the applicable potential of numerical models for water resources management. The results also showed that SLR and development strategy are not only significantly impact on operation of reservoirs and

inundation in the downstream of the Dong Nai – Saigon River Basin, but also influence to sedimentation of the Mekong Delta estuaries. The aforesaid outcomes highlighted that the Dong Nai – Saigon River Basin is dramatically affected by climate change and rural development. This study is the key contribution to avoid the mistakes of past and building resilience into managing water sensitive cities, and improve decision-making process to guide Ho Chi Minh City towards aspired benefits in the coming decades.

8.2. Recommendations

The chapter I showed the current problems in the Dong Nai – Saigon River Basin involved hydrology, reservoir operation, inundation and erosion/ deposition, the chapter III, IV, V, VI and VII pointed out how they impact to study area as well as some suggestion to contribution in sustainable development of the Dong Nai – Saigon river Basin. However, the relative problems as indicated in this dissertation have not been entirely solved owing to the limitation in study period and available data. Hence, the recommendations for future research and development are:

1. Improvement of hydrological data for model input by investment of hydrological data in the Dong Nai – Saigon River basin.
2. Enhancement of genetic algorithm for improving efficiency in search of optimal solutions.
3. Development of hydrological models with hourly forecasting, reservoir operation model for daily simulation.
4. The influences of climate change and sea level rise on inundation of HCMC as well as the morphological evolutions of the Mekong River Estuaries are very serious; hence it is necessary to study those effects by simulation in longer time period and in detail to each smaller sub-basins.

ACKNOWLEDGEMENTS

I wish to express my sincere appreciation to the organization: Japan Society for the Promotion of Science (JSPS), and Thuyloi University (TLU), have support me to implement the planning study in Kyushu University, Japan under providing the RONPAKU scholarship.

I strongly express deep gratitude to my supervisor Professor, Dr. Kazuaki Hiramatsu, who spent much time for giving me most orientation, motivation, guidance, support and encouraged me to overcome difficulties and finish the study at Laboratory of Water Environment Engineering, Kyushu University.

I would like to express special appreciation to sub supervisors Associate Professor, Dr. Masayoshi Harada for his worth counseling and sharing experience during time of studying Japan.

I express special thanks to Professor Dr. Kyoichi Otsuki for valuable comments and contribution to complete my dissertation better.

I am very grateful to Professor Nguyen Quang Kim for all his tremendous helps and supports.

I also thank the following persons whose effort made this work possible: Mr. Le Trung Thanh and Mr. Nguyen Thai Quyet who help me to collect data related to my study area.

I am thankful to Graduate School of Bioresource and Bioenvironmental Sciences - Kyushu University, did help me to broaden my knowledge and useful for this research.

I specially thank to all Laboratory mates, Vietnamese friends in Fukuoka and Japan for sharing my trouble as well as my joys in my research process and my life.

Last but not least, a sweet word to all members of my family, they vitally encouraged and sympathized for my study plan.

REFERENCES

Abedian A., Ghiasi M.H. and Dehghan-Manshadi B., (2006) Effect of a linear-exponential penalty function on the GA's efficiency in optimization of a laminated composite panel, *Internaltional Journal of Computational Intelligence* 2(1): 5-11.

Afshar M.H., (2012) Large scale reservoir operation by constrained particle swarm optimization algorithms, *Journal of Hydro-environment Research* 6: 75-87.

Arjan W.J., Arie D.J., Joost M.K. and Jeroen P. S., (2010) Operationalising a resilience approach to adapting an urban delta to uncertain climate changes, *Technological Forecasting and Social Change*, 77:987-998.

Balasubramaniam A. S. and Uddin W., (1977) Deformation characteristics of weathered Bangkok clay in triaxial extension, *Géotechnique* 27: 75–92.

Chang F.J., Chen L., and Chang, L.C., (2005) Optimizing the reservoir operation rule curves by genetic algorithm, *Hydrological Processes* 19(11): 2277-2289.

Chang L.C., (2008) Guiding rational reservoir flood operation using penalty-type genetic algorithm, *Journal of Hydrology* 354: 65-74.

Chang L.C., Chang F.J., Wang K.W., and Dai S.Y., (2010) Constrained genetic algorithms for optimizing multi-use reservoir operation, *Journal of Hydrology* 390: 66-74.

Chaves P., and Chang F.J., (2008) Intelligent reservoir operation system based on evolving artificial neural networks, *Advances in Water Resources* 31: 926-936.

Chen L., and Chang F.J., (2007) Applying a real-coded multi-population genetic algorithm to multi-reservoir operation, *Hydrological Processes* 21(5): 688-698.

Chinh L. V. Hiramatsu K., Harada M. and Mori M., (2006) Optimal Gate Operation of a Main Drainage Canal in a Flat Low-lying Agricultural Area using a Tank Model Incorporated with a Genetic Algorithm, *Journal of the Faculty of Agriculture, Kyushu University* 51(2):351-359.

Chu-Tian C., Ming-Yan Z., Chau K. W. and Xin-Yu W., (2006) Using genetic algorithm and TOPSIS for Xinanjiang model calibration with single procedure, *Journal of Hydrology* 316: 129–140.

CIRIA (2007) Improving the Flood Performance of New Buildings, *Flood Resilient Construction. RIBA Publishing, London*.

Clark C. O., (1945) Storage and the unit hydrograph. Transactions, *ASCE* 110: 1419-1446.

Dawson R.J., Speight L., Hall J.W., Djordjevic S., Savic D. and Leandro J., (2008) Attribution of flood risk in urban areas, *Journal of Hydroinformatics* 10(4): 275–288.

DHI (2007a) Mike 21 Flow Model FM Hydrodynamic Module Scientific Documentation, *DHI Water and Environment, Denmark.*

DHI (2007b) Mike 21 Spectral Wave Module Scientific Documentation, *DHI Water and Environment, Denmark*.

DHI (2007c) *MIKE 11* user manual, *DHI Water and Environment, Demark*, pp. 229–244

DHI (2009a), *MIKE 11 user manual, Demark*.

DHI (2009b), *MIKE 11 reference, Demark.*

DHI (2012), *MIKE 11 reference, Demark.*

Dietrich J., Schumann A. H., Redetzky M., Walther J., Denhard M., Wang Y., Pfützner B. and Büttner U., (2009) Assessing uncertainties in flood forecasts for decision making: prototype of an operational flood management system integrating ensemble predictions, *Nat Hazards Earth Syst Sci* 9:1529–1540.

Faber R., (2006) Flood risk analysis: Residual risks and uncertainties in an Austrian context. Dissertation, *University of Natural Resources and Applied Life Sciences*

FLOODsite (2009) Flood Risk Assessment and Flood risk Management. An Introduction and Guidance Based on Experiences and Findings of FLOODsite (an EU-funded Integrated Project). *Deltares - Delft Hydraulics, Delft, the Netherlands*.

Gottschalk L. C., (1958) Predicting erosion and sediment yields. Intern. Union of Geodesy and Geophysics, *Association of Scientific Hydrology*. XI General Assembly, Toronto, Canada, Tome I, Vol. 1: 146–153.

Hallegatte S., (2008) Strategies to adapt to an uncertain climate change, *Glob. Environ. Change* 19(2): 240–247.

Hashemi S.R., Zulkifli I., Hair-Bejo M., Farida A. and Somchit M. N., (2008) Acute toxicity study and phytochemical screening of selected herbal aqueous extract in broiler chickens, *Int. J. Pharmacol*. 4: 352-360.

Havnø K., Madsen M. N. and Dørge J., (1995) MIKE–11 a generalized river modelling package. In "Computer Models of Watershed Hydrology" ed. by V. P. Singh, *Water Resources Publications*, Colorado: 733–782.

Hiramatsu K., Shikasho S., Kurosawa K. and Mori M., (2004) Drainage and Inundation Analysis in a Flat Low-lying Paddy-cultivated Area of the Red River Delta, Viet Nam, *Journal of the Faculty of Agriculture, Kyushu University* 49(2): 383-399.

Holeman J. N., (1968) The sediment yield of major rivers of the world, *Water Resour. Res.*, 4: 737–747.

Holland J. D., (1975) Adaptation in natural and artificial systems: An introductory analysis with application to biology, control, and artificial intelligence. *University of Michigan Press*, Ann Arbor, MI.

Honghai Q., Pu Q. and Altinakar M. S., (2013) GIS-Based Spatial Monte Carlo Analysis for Integrated Flood Management with Two Dimensional Flood Simulation, *Water Resour Manage* 27: 3631–3645.

Hormwichian R., Kangrang A. and Lamom A., (2009) A conditional genetic algorithm model for searching optimal reservoir rule curves, *Journal of Applied Sciences* 9 (19): 3575-3580.

Hsu N.S., and Wie C.C., (2007) A multipurpose reservoir real-time operation model for flood control during typhoon invasion. *Journal of Hydrology* 336: 282-293.

Hsu S.K., (1995) Shortage indices for water-resources planning in Taiwan. *Journal of Water Resources Planning and Management* 121: 119-131.

Hung N. M., Chinh L. V., Hiramatsu K., Harada M. and Dao N. T., (2011) Flood Inundation Analysis Using a Distributed Tank Model in an Urbanizing Agricultural Area of Song Nhue Hydraulic Structure Scheme in Hanoi, *Proceedings of the 5th International Symposium on the East Asian Environmental Problems (EAEP2011):* 235-240.

Hung N. N., Delgado J. M., Guentner A., Merz B., Bárdossy A. and Apel H., (2014a) Sediment in the floodplains of the Mekong Delta, Vietnam Part I: Suspended sediment dynamics, *Hydrol. Process*. 28: 3132-3144.

Hung N. N., Delgado J. M., Guentner A., Merz B., Bárdossy A. and Apel H., (2014b) Sediment in the floodplains of the Mekong Delta, Vietnam Part II: deposition and erosion, *Hydrol. Process*. 28: 3145-3160.

Hung N. N., Delgado J. M., Tri V. K., Hung L. M., Merz B., Bárdossy A. and Apel H., (2012) Floodplain hydrology of the Mekong Delta, Vietnam, *Hydrol. Process*. 26: 674–686.

IPCC (2007) Climate Change 2007: *Synthesis Report*.

Karamouz M., Kerachian R., Akhbari M. and Hafez B., (2009) Design of river water quality monitoring networks: a case study, *Environ Model Assess* 14(6):705–714.

Kim N. Q., (2010) Report on "Study on appropriate water exploitation solutions to drought and salt intrusion mitigation in Mekong Delta to adapt with scenarios of hydraulic work development in the upstream". *Granted in Aids by Key Project of State KC.08.06.10*

Kim N. Q., (2013) Report on "Study on integrated measures for flood control in the downstream area of Dong Nai – Saigon River Basin and vicinities". *Granted in Aids by Key Project of State 2014.*

Kim N. Q., Thanh Letrung, Ngoc T. A. and Quyet N. T., (2014) Assessing Inundation From Upstream Flooding and Sea Level Rise in The Downstream of The Dongnai-Saigon River. *Proceedings of the 19th IAHR-APD Congress 2014, Hanoi, Vietnam*, Paper number 263.

Kubal C., Haase D. and Scheuer S., (2009) Integrated urban flood risk assessment adapting a multicriteria approach to a city, *Natural hazard and earth system science* 9:1881-1895.

Li X., Guo S., Liu P., and Chen G., (2010) Dynamic control of flood limited water level for reservoir operation by considering inflow uncertainly, *Journal of Hydrology* 391: 124-132.

Liu C., He Y., Walling E. and Wang J., (2013) Changes in the sediment load of the Lancang-Mekong River over the period 1965– 2003, *Science China Technological Sciences* 56: 843–852.

Liu X., and He D., (2012) A new assessment method for comprehensive impact of hydropower development on runoff and sediment changes, *J. Geogr. Sci.* 22: 1034–1044.

Lu X. X., and Siew R. Y., (2006) Water discharge and sediment flux changes over the past decades in the Lower Mekong River: possible impacts of the Chinese dams, *Hydrol. Earth Syst. Sci.* 10: 181–195.

Madsen H., (2000) Automatic calibration of a conceptual rainfall runoff model using multiple objectives, *Journal of Hydrology* 235: 276–288.

Manh N. V., Dung N. V., Hung N. N., Merz B. and Apel H., (2014) Large-scale suspended sediment transport and sediment deposition in the Mekong Delta, *Hydrol. Earth Syst. Sci.* 18: 3033-3053.

Manh N. V., Merz B. and Apel H., (2013) Sedimentation monitoring including uncertainty analysis in complex floodplains: a case study in the Mekong Delta, *Hydrol. Earth Syst. Sci.* 17: 3039-3057.

Mekong River Commission (MRC/DMS) (2010) Origin, fate and impacts of the Mekong sediments, *Mekong River Comm.* 53, available from: http://www.mpowernetwork.org/Knowledge_Bank/Key_Reports/PDF/Research_Reports/DMS_Sediment_Report.pdf.

Merz B., Thieken A. and Blöschl G., (2002) Uncertainty analysis for flood risk estimation, Intern. Commission for the Hydrology of the Rhine basin, *Proc. Intern. Conf. on Flood Estimation*, Berne, CHR Report II-17: 577–585.

Ministry of Agriculture and Rural Development (MARD) (1995) "Handbook of guiding the reservoir operation rule curves for Dautieng reservoir", Tayninh.

Morita M., (2008) Flood Risk Analysis for Determining Optimal Flood Protection Levels in Urban River Management. *Blackwell Publishing Ltd*.: 142–149,

MRCS/WUP-FIN (2007) Final Report – Part 2: Research findings and recommendations. WUP-FIN Phase 2 – Hydrological, Environmental and Socio-Economic Modelling Tools for the Lower Mekong Basin Impact Assessment. *Mekong River Commission and Finnish Environment Institute Consultancy Consortium, Vientiane, Lao PDR*. Available on-line at http://www.eia.fi/wup-fin/wupfin2/ publications.htm

Ngoc T. A., Chinh L. V., Hiramatsu K. and Harada M., (2011a) Parameter identification for two conceptual hydrological models of upper Dautieng River Watershed in Vietnam, *J. Facul. Agric., Kyushu University* 56(1): 335-341.

Ngoc T. A., Hiramatsu K. and Harada M., (2011b) Optimization of Parameters for Two Conceptual Hydrological Models by Using a Genetic Algorithm. *Proceedings of the 5th International Symposium on the East Asian Environmental Problems 2011*, 241-246.

Ngoc T. A., Hiramatsu K. and Harada M., (2013a) Optimizing parameters for two conceptual hydrological models using a genetic algorithm, *JARQ* 47(1): 85-96.

Ngoc T. A., Hiramatsu K. and Harada M., (2014) Optimizing the Rule Curves of Multi-use Reservoir Operation using a Genetic Algorithm with a Penalty Strategy. *Paddy and Water Environment* **12**(1): 125-137.

Ngoc T. A., Nguyen D. D., Thu V. T. H. and Hiramatsu K., (2014) Framework For Flood Damage Assessment Considering Abnormal Conditions by Using The Hydraulic and GIS Modeling. *Proceedings of JSPS Core-to-Core Program*

SOWAC Project 2014 Fifth Joint Seminar between Water Resources University, Vietnam and Kyushu University, Japan: 80-86.

Ngoc T. A., Thanh Letrung, Hiramatsu K. and Quyet N. T., (2013b) The Effect of simulated sea level on the sedimentation of the Tien River Estuaries, Lower Mekong River, Southern Vietnam, *JARQ* 47(4): 405-415.

Ngoc T. A., Thu V. T. H., Khoa D. T. and Tinh. N. D., (2013c) Systematic Approach to Building Urban Resilience to Climate Change in Ho Chi Minh City. *Proceedings of JSPS Core-to-Core Program SOWAC Project 2013 Third Joint Seminar between Water Resources University, Vietnam and Kyushu University, Japan*: 202-211.

Nguyen Q. K., (2010) Report on "Study on appropriate water exploitation solutions to drought and salt intrusion mitigation in Mekong Delta to adapt with scenarios of hydraulic work development in the upstream". *Granted in Aids by Key Project of State KC.08.06.10.*

Nguyen T. V., (2007) Study on the Effect of Morphology Change on Salinity Distribution in the Dinh An Estuary, Lower Mekong River of Vietnam, *Journal of Coastal Research* 50: 268 – 272.

Nguyen V. L., Ta T. K. O. and Tateishi M., (2000) Late Holocene depositional environments and coastal evolution of the Mekong River Delta, Southern Vietnam, *Journal of Asian Earth Science* 18: 427– 439.

Nielsen S. A. and Hansen E., (1973) Numerical simulation of the rainfall runoff process on a daily basis, *Nordic Hydrology* 4: 171–190.

Pahl-Wostl C., (Ed.) (2006) Framework for Adaptive Water Management Regimes and for the Transition between Regimes. *NeWater project*, Report Series No.12.

Parchure T. M. and Mehta A. J., (1985) Erosion of soft cohesive sediment deposits. *Journal of Hydraulic Engineering*, ASCE 111: 1308-1326.

Parkinson J., and Mark O., (2005) Urban Stormwater Management in Developing Countries, *IWA Publishing*, London.

Rajurkar M. P., Kothyari U.C. and Chaube U.C., (2004) Modeling of the Daily Rainfall-Runoff Relationship with Artificial Neural Network, *J. Hydrol.* 285: 96-113.

Reznicek K. and Cheng T.C.E., (1991) Stochastic Modelling of Reservoir Operations, *European Journal of Operation Research* 50: 235-248.

Rose A. Z., (2004) Economic Principles, Issues, and Research Priorities in Natural Hazard Loss Estimation, In: Modeling the Spatial Economic Impacts of Natural Hazards Eds. Y. Okuyama and S. Chang, *Springer*:13-36.

Slobodan D., David B., Philippe G., Ole M. and Erik P., (2011) New policies to deal with climate change and other drivers impacting on resilience to flooding in urban areas: the CORFU approach, *Environmental Science and Policy* 14: 864-873.

Su M. D., Kang J. L., Chang L. F. and Chen A. S., 2005, A grid-based GIS approach to regional flood damage assessment, Journal of marine science and technology, Vol.13, No.3, pp.184-192.

Sugawara M., (1995) Tank model In "Computer Models of Watershed Hydrology" ed. by V. P. Singh, *Water Resources Publications*, Colorado: 165–214.

Ta T. K. O., Nguyen V. L., Tateishi M., Iwao K. and Saito Y., (2001) Sedimentary facies, diatom and foraminifer assemblages in a late Pleistocene–Holocene incised-valley sequence from the Mekong River Delta, Bentre Province, Southern Vietnam: the BT2 core. *Journal of Asian Earth Science* 20: 83–94.

Tamura T., Horaguchi K., Saito Y., Nguyen V. L., Tateishi M., Ta T. K. O., Nanayama K. and Watanabe K., (2010) Monsoon influenced variations in morphology and sediment of a mesotidal beach on the Mekong River delta coast, *Geomorphology* 116: 11–23.

Tawatchai T. and Gautam M. R., (2000) Application of Tank, NAM, ARMA and neural network models to flood forecasting, *Hydrological Processes* 14: 2473–2487.

Teisson C., (1991) "Cohesive suspended sediment transport: feasibility and limitations of numerical modelling", J. *Hydraul. Res.* 29(6): 755–769.

Thanh Letrung, Ngoc T. A. and Hiramatsu K., (2016) Effect of the interaction between monsoon currents and waves on the morphological processes in the Mekong River Delta Coast, *JARQ* **50**(2). (Accepted).

Thanh Letrung, Li Q., Li Y., Vukien T. and Quyet N. T., (2013), Morphology evolution of Cuadai Estuary, Mekong River, Southern Vietnam, *J. Hydrol. Eng*. 18(9): 1122–113.

The World Bank (WB) (2012) Tools for Building Urban Resilience: Intergrating Risk information into Investment Decisions – Pilot Cities Report – Jakarta and Can Tho.

Tung T-K (2002) Risk-based design of flood defense systems. In: Wu Y et al (Eds) Flood Defence. *Scence Press*, New York: 71–81.

Van Rijn L. C., (1984) Sediment transport, Part I: bed load transport, *The Journal of Hydraulic Engineering* 110(11): 1431-1456.

Vietnam Ministry of Natural Resources and Environment (MONRE) (2012) Climate change and sea-level rise for Vietnam, Hanoi.

Vietnam Ministry of Natural Resources and Environment (MONRE) (2009) "Climate change and sea level rise for Vietnam." Hanoi.

Wei C.C., and Hsu N.S., (2009) Optimal tree-based release rules for real-time flood control operations on a multipurpose multireservoir system, *Journal of Hydrology* 365: 213-224.

Wolanski E., Nguyen N. H. and Spagnol S., (1998) Sediment dynamics during low flow conditions in the Mekong River Estuary, Vietnam, *Journal of Coastal Research* 14: 472–482.

Wolanski E., Nguyen N. H., Le T. D., Nguyen H. N. and Nguyen N. T., (1996) Fine sediment dynamics in the Mekong River Estuary, Vietnam. *Estuarine, Coastal and Shelf Science* 43: 565– 582.

World Bank (WB) (2004) Involuntary Resettlement Sourcebook, *the World Bank*, Washington, DC.